Excitatory synaptic inputs onto parvalbumin-positive perisomatic region-targeting interneurons in the hippocampus

PhD Thesis

Orsolya Papp

János Szentágotai Doctoral School of Neurosciences
Semmelweis University

Supervisor: Norbert Hájos, D.Sc.

Official Reviewers: Tibor Zelles, Ph.D.
Gábor Molnár, Ph.D.

Chair of the Final Examination Board: Béla Halász, D.Sc.
Members of the Final Examination Board: Tibor Wenger, D.Sc.
István Tarnawa, Ph.D.

Budapest
2013

TABLE OF CONTENTS

LIST OF ABBREVIATIONS

2-AG: 2-arachidonoyl glycerol

AAC: axo-axonic cell

aCSF: artificial cerebrospinal fluid

AHP: afterhyperpolarization

AIS: axon initial segment

AM251: N-(Piperidin-1-yl)-5-(4-iodophenyl)-1-(2,4-dichlorophenyl)-4-methyl-1H-pyrazole-3-carboxamide, CB_1R antagonist

AMPA: α-amino-3-hydroxy-5-methylisoxazole-4-propionic acid

AP: action potential

BAPTA: 1,2-bis-(o-Aminophenoxy)-ethane-N,N,N',N'-tetraacetic acid tetrapotassium salt, Ca^{2+} chelator

CA: cornu ammonis

CB_1R: cannabinoid receptor type I

CB_1R KO: cannabinoid receptor type I knockout mouse

CCK: cholecystokinin

CP55,940: (-)-cis-3-[2-Hydroxy-4-(1,1-dimethylheptyl)phenyl]-trans-4-(3-hydroxypropyl)cyclohexanol, CB_1R agonist

DAG: diacylglycerol

DG: dentate gyrus

DGL-α: diacylglycerol lipase-α

DHPG: (S)-3,5-Dihydroxyphenylglycine

DL-AP5: DL-2-Amino-5-phosphonopentanoic acid, NMDA receptor antagonist

DMSO: Dimethyl sulfoxide, solvent

eCB: endocannabinoid

eCB-LTD: endocannabinoid-mediated long-term synaptic depression

eEPSP: evoked excitatory postsynaptic potential

eGFP: enhanced green fluorescent protein

eIPSC: evoked inhibitory postsynaptic current

EPSC: excitatory postsynaptic current

EPSP: excitatory postsynaptic potential

FS BC: fast-spiking basket cell

FS IN: fast-spiking interneuron

GABA: γ-aminobutyric acid

GAD67: glutamate decarboxylase-67

HFS: high frequency stimulation

i-LTD: long-term depression of inhibitory synapses

IPSC: inhibitory postsynaptic current

KA: kainic acid

LTD: long-term depression

LTP: long-term potentiation

LY367385: (S)-(+)-α-Amino-4-carboxy-2-methylbenzeneacetic acid, metabotropic glutamate receptor 1 antagonist

mAChR: muscarinic acetylcholine receptor

mGluR: metabotropic glutamate receptor

MPEP: Methyl-6-(phenylethynyl)-pyridine hydrochloride, metabotropic glutamate receptor 5 antagonist

mRNA: messenger ribonucleic acid

MS-DBB: medial septum-diagonal band of Broca

NBQX: 2,3-dihydroxy-6-nitro-7-sulfamoyl-benzo[f]quinoxaline-2,3-dione, AMPA/KA receptor antagonist

NGS: normal goat serum

NMDA: N-methyl-D-aspartate

O-LM cells: oriens lacunosum-moleculare cells

PB: Phosphate buffer

PV: parvalbumin

PV+ cells: parvalbumin-positive perisomatic region-targeting interneurons

sEPSC: spontaneous excitatory postsynaptic current

TBS: Tris-buffered saline

THL: N-Formyl-L-leucine (1S)-1-[[(2S,3S)-3-hexyl-4-oxo-2-oxetanyl]methyl]dodecyl ester, lipase blocker

tLTD: spike timing-dependent long-term depression

VGluT1: vesicular glutamate transporter 1

WIN55,212-2: (R)-(+)-[2,3-Dihydro-5-methyl-3-(4-morpholinylmethyl)pyrrolo[1,2,3-de]1,4-benzoxazin-6-yl]-1-naphthalenylmethanone mesylate, CB_1R agonist

WT: wild type

INTRODUCTION

The hippocampus is responsible for the computation of higher order cognitive functions such as memory formation and recall (Lisman & Idiart, 1995), memory consolidation (Buzsáki, 1986), or spatial navigation (O'Keefe & Recce, 1993). In this brain area, several rhythmic activities have been observed which were proved to have a tight link to cognitive processes (Vanderwolf, 1969; Leung, 1980; Buzsáki *et al.*, 1992; Chrobak & Buzsáki, 1994). During theta (4-8 Hz) and gamma (30-100 Hz) oscillations, acquisition and recall of memories can be achieved in hippocampal networks, whereas sharp-wave activity and embedded ripples (120-200 Hz) are suggested to underlie memory consolidation (Buzsáki, 1986; Skaggs & McNaughton, 1996). All of these network activities require an effective and temporarily precise inhibition to control the discharge of pyramidal cells (Buzsáki *et al.*, 1983; Cobb *et al.*, 1995; Ylinen *et al.*, 1995; Csicsvári *et al.*, 2003). The parvalbumin-positive perisomatic region-targeting interneurons (PV+ cells) are ideally suited to fulfill this function, due to their special features. Besides their strategically positioned synapses that provide effective inhibition, several single-cell features and input properties endow them to be a clockwork for network synchrony (Freund, 2003; Jonas *et al.*, 2004; Bartos *et al.*, 2007).

In terms of my PhD program, we studied the detailed anatomical and functional properties of the excitatory synaptic inputs engaged in driving PV+ cells in the hippocampus. We compared the excitatory synaptic inputs of the two types of PV+ cells, the axo-axonic and fast-spiking basket cells, with the aim to extend our knowledge about the distinguished function of these two cell types in orchestrating network activities.

In addition, we examined the possibility whether the afferent excitatory synaptic input of these cells is capable of performing long-term plasticity, and if so, what circumstances are required to change the reliable operation of these network-synchronizing GABAergic neurons. We particularly focused on long-term depression (LTD) and also mapped the underlying molecular pathway, uncovering a so far unknown metabotropic glutamate receptor- DAG lipase-α -CB_1 cannabinoid receptor-dependent LTD at excitatory synapses onto PV+ cells.

Being aware of the fact that the excitatory synaptic inputs onto PV+ cells could be readily modulated by cannabinoid compounds, we then investigated the mechanisms of the suppression of gamma oscillations upon CB_1 receptor (CB_1R) activation.

This thesis aims to summarize these findings and suggest a functional relevance for the excitatory synaptic inputs of PV+ cells in neurological diseases.

I. The hippocampus

The hippocampal formation is an archicortical structure of the brain. Its basic buildup is well conserved in mammals, although some subtle species specific differences can occur. As the experimental work described in the thesis was performed in mice, I would confine to introduce the organization of the rodent hippocampus.

In contrast to the six-layered structure of the neocortex, the cell bodies of hippocampal principal cells are rendered to one, densely packed layer. Due to the advantages of this seemingly simplified structure, the hippocampus is in the focus of neurobiological research. The cytoarchitectural similarity to other cortical regions may allow us to extrapolate to general rules of cortical computation.

The hippocampal formation comprises the *dentate gyrus* (DG), the hippocampus proper (or *Cornu Ammonis*, CA) and the subiculum. The neighboring areas that produce the direct input or output of the hippocampal formation, i.e. the entorhinal cortex, pre- and parasubiculum, together with the hippocampal formation, form a computational unit termed the hippocampal region (Andersen, 2007).

I.1. Cytoarchitecture

The principal cells of the hippocampal formation are glutamatergic cells, which comprise approximately 85% of the neurons (Andersen, 2007). The cell bodies of principal cells are confined to a single layer named as *granule cell layer (stratum granulosum)* in the DG or *pyramidal cell layer (stratum pyramidale)* in the CA regions. They form two enwreathing U-shape composing the special structure of this brain area (Figure 1). The remaining 15% of neurons in the hippocampus are GABAergic in nature, forming a highly heterogeneous cell population (Freund & Buzsáki, 1996).

I.1.1. Principal cells

In the DG, the main cell type is the granule cell possessing small somata (approximately 10 μm). These cells lack basal dendrites towards the *hilus*, the polymorphic cell layer enclosed by the *blades* of *stratum granulosum*. In the hilus, another type of glutamatergic cell is found, the mossy cell. The area occupied by the apical dendrites of the granule cells is named as *molecular layer (stratum moleculare)*. The *Cornu Ammonis* has three parts: the CA3 is the closest to the DG and composed of relatively large pyramidal cells (with approximately 20-30 μm of soma diameter). The CA3 region is further subdivided to three parts: a, b and c. The CA3c is next to the DG, while the CA3a is adjacent to the CA2. The *stratum lucidum*, formed by the axons of granule cells, can be found next to the pyramidal cell layer in the CA3 region. The CA2 region is a small group of cells inserted between CA3 and CA1. The cells in the CA1 region are smaller (with approximately 10-15 μm of soma diameter) and the most densely packed into a layer. The continuation of the *Cornu Ammonis* is the subiculum where the cell bodies become widely dispersed. The apical dendrites of pyramidal cells are present in the *stratum radiatum*; this layer is located superficial to the stratum lucidum in the CA3 region, and to the stratum pyramidale in the CA2 and CA1. The *stratum lacunosum-moleculare* is the most superficial layer of the hippocampus, and it is defined by the apical dendritic tufts of pyramidal cells and the inputs mainly from the entorhinal cortex. The layer located below the pyramidal cell layer is the *stratum oriens*, which contains the basal dendrites of pyramidal cells (Figure 1) (Andersen, 2007).

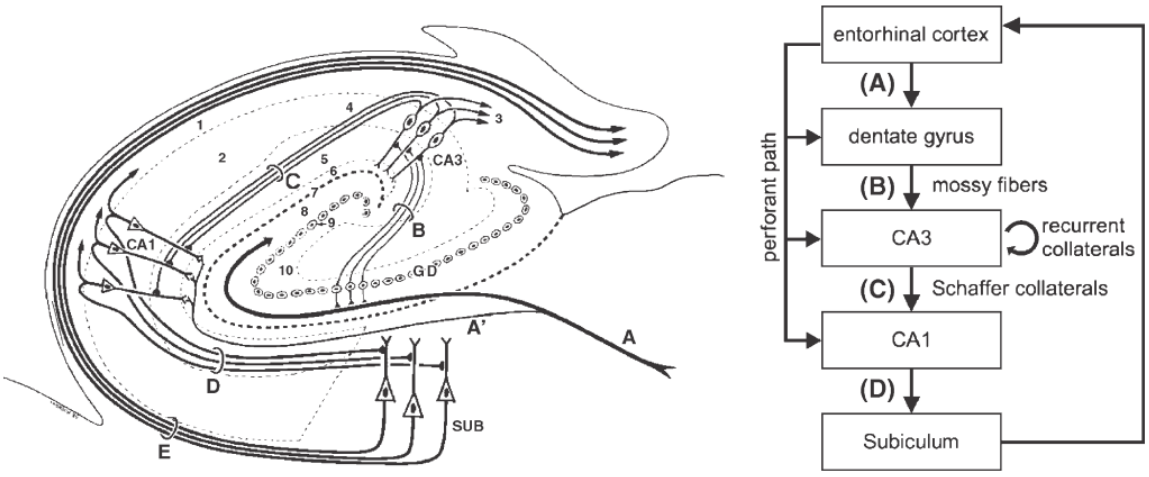

Figure 1. Cytoarchitecture of the hippocampal formation. *GD, dentate gyrus; CA3, CA1, fields of the Cornu Ammonis; SUB, subiculum. Cornu Ammonis: (1) alveus, (2) stratum pyramidale, (3) axon of pyramidal neurons, (4) Schaffer collateral, (5) stratum radiatum, (6) stratum lacunosum-moleculare, (7) hippocampal sulcus. Dentate gyrus: (8) stratum moleculare, (9) stratum granulosum, (10) hilus. Right: Internal connectivity of the hippocampal region. (A) Perforant path, (B) mossy fibers, (C) Schaffer collaterals, (D) connection from CA1 to the subiculum, (E) connection from the subiculum to deep layers of the entorhinal cortex. Adapted from Axmacher 2006.*

I.1.2. Intrahippocampal connectivity

Within the elements of the hippocampal formation, the flow of information is mostly unidirectional, giving rise to a trisynaptic loop (Andersen *et al.*, 1971). The first stage of the trisynaptic loop is the DG. The dendrites of the granule cells are the target of entorhinal afferents, which convey highly processed sensory information from the cortex. Granule cells are not interconnected with each other. The axons of the granule cells -known as mossy fibers- give rise to a few giant boutons (*mossy terminals*) and numerous small terminals (some of them locate on *filopodia*). The mossy terminals contact the hilar mossy cells, and also synapse on the complex spines of proximal dendrites of CA3 pyramidal cells called *thorny excrescences*. This is the second stage of the loop. The small filopodia which extrude from mossy terminals, contact the interneurons of the CA3 region. The CA3 pyramidal neurons have dense collateral system both ipsi- and contralaterally, giving rise to the excitatory inputs in the strata oriens and radiatum. The third element of the hippocampal trisynaptic loop is the projection of CA3 pyramidal cells to the CA1 region (the Schaffer collaterals), terminating in the strata oriens and radiatum. Similar to granule cells, excitatory CA1 neurons have sparse recurrent connectivity. Their axon innervates mostly GABAergic cells in the stratum oriens, and the main axon project to the subiculum and the entorhinal cortex. Although pyramidal cells in the CA3c region and the hilar mossy cells project back to the DG (Frotscher *et al.*, 1991; Li *et al.*, 1994), the main information flow within the hippocampus is unidirectional (Figure 1), which is significantly different from the other neocortical areas having characteristic reciprocal connectivity.

I.1.3. Afferent-efferent connectivity of the hippocampal formation

The afferent and efferent connectivity of the hippocampus is structured into three major fiber bundles. One of them is the angular bundle, which comprises the fibers of the entorhinal cortex, giving rise to the perforant path. Cells from layer II of the entorhinal cortex project to the outer two thirds of dentate molecular layer and to the stratum lacunosum-moleculare of the hippocampal CA2/3 region. The fibers from the lateral entorhinal area terminate more superficially, in the outer third of the stratum moleculare and in most distal parts of the stratum lacunosum moleculare, whereas the medial entorhinal area terminates in the middle of the stratum moleculare and in the proximal parts of the stratum lacunosum-moleculare. As the DG and the CA2/3 receive the entorhinal input from the same regions, it is possible that these areas receive similar information. However, the CA1 region is innervated by a different input. It receives axonal projection from layer III entorhinal cells showing a topographical organization: the cells from the lateral entorhinal cortex project to the CA1 located closer to the subiculum and the cells from the medial entorhinal cortex project to the part of the CA1 found near the CA2. Moreover, CA2 pyramidal cells receive convergent inputs from the layer II and layer III entorhinal cells (Chevaleyre & Siegelbaum, 2010). Only the CA1 projects back to the entorhinal cortical layers V and VI. The CA1 pyramidal cells tend to send their axons back to the same region of the entorhinal cortex, where they receive their input from. The angular bundle comprises other fibers that connect the hippocampus to few other cortical areas, as well. The CA1 has reciprocal connections with perirhinal and postrhinal cortices and with the basal parts of the amygdala (Andersen, 2007).

The second bundle is the fimbria-fornix fiber system, which is the major pathway for subcortical afferent and efferent connections. One of the major subcortical inputs to the hippocampus comes from the medial septum-diagonal band of Broca (MS-DBB), targeting the stratum oriens and -to a lesser extent- the stratum radiatum with GABAergic and cholinergic fibers. The GABAergic input selectively terminates on GABAergic cells (Freund & Antal, 1988). Some GABAergic cells from the CA and DG give rise to backprojections to the medial septal nuclei (Tóth & Freund, 1992). Concerning hypothalamic connections, the DG and the CA2 region receives prominent glutamatergic and also GABAergic input from the supramammillary and tuberomammillary nuclei terminating on proximal parts of the principal cells (Panula *et al.*, 1989; Maglóczky *et al.*, 1994; Soussi *et al.*, 2010). The nucleus reuniens of the thalamus densely innervates the stratum lacunosum-moleculare of the CA1, where it overlaps with fibers from the entorhinal cortex (Wouterlood *et al.*, 1990). The hippocampus

receives several types of monoaminergic inputs from ascendent pathways of the brainstem, such as noradrenergic fibers of the locus coeruleus, and serotonergic fibers from the raphe nuclei (Freund *et al.*, 1990). Besides diffuse serotonergic inputs, there is also evidence for direct glutamatergic input from the median raphe nucleus synapsing on interneurons (Varga *et al.*, 2009).

The third bundle is the commissural system connecting the hippocampi of the two hemispheres. The mossy cells from the hilus give rise to extensive projection to the ipsi- and contralateral DG, and the CA3 pyramidal cells have also extensive connections with the ipsi- and contralateral CA3 and CA1. Interestingly, the DG and CA1 principal cells do not project contralaterally.

I.1.4. GABAergic cells

While the principal cells of the hippocampus form relatively homogenous groups regarding their morphological and physiological features, the GABAergic cell population comprises a large variety of cell types. They influence temporal dynamics of synapses, organize network oscillations, participate in selecting cell assemblies and implementation of brain states (Klausberger & Somogyi, 2008). Most of the GABAergic cells in the hippocampus take part in local control of the circuit, so as termed interneurons; however some of them project out from the hippocampus, innervating subcortical and/or cortical areas (Figure 2).

Here the GABAergic cells will be classified based on their axonal and dendritic morphology. Generally, the dendritic location of neurons defines the inputs they receive, and the region targeted by their axons defines the specific domain in their target cells they can influence. We can dissect four major groups of interneurons in the hippocampus based on their axonal arborization. The *perisomatic region-targeting interneurons* innervate the perisomatic region of principal cells including the soma, proximal dendrites or axon initial segments. These synapses are in a strategic position to control the output of the pyramidal cells. The *dendritic layer-targeting interneurons* contact on several dendritic segments, often in a pathway-selective manner, thus they are able to influence a specific type of input. Most of the inhibitory cells (except axo-axonic neurons) innervate both pyramidal cells and interneurons; however, *interneuron-selective interneurons* target predominantly other

interneurons. The *long-range projecting GABAergic neurons*– besides giving rise to local collaterals– project out of the hippocampus with myelinated axons. They are supposed to regulate information flow between different areas (Freund & Buzsáki, 1996).

I.1.4.1. Perisomatic region-targeting interneurons

The soma and axons of perisomatic region-targeting interneurons can be found within or near the pyramidal cell layer. In most of the cases, their dendrites span all layers of the hippocampus.

The *axo-axonic cells* (AAC) provide the exclusive innervation of the axon initial segments of pyramidal cells (Somogyi, 1977). They release GABA and express the Ca^{2+}-binding protein parvalbumin (PV). The peculiarity of this cell type is that under certain circumstances it may depolarize its target cell due to the higher reversal potential of Cl^- present in the axon initial segments (Szabadics *et al.*, 2006; Khirug *et al.*, 2008). But generally, discharges of AACs seem to provide hyperpolarizing current (Glickfeld *et al.*, 2009). Additionally, modeling *in vivo*-like membrane potential fluctuations, the dominant postsynaptic effect of axo-axonic cells was shown to be inhibition (Woodruff *et al.*, 2011). Some of the axo-axonic cells have a dendritic tree confined to the stratum oriens (Ganter *et al.*, 2004).

The *basket cells* are named after their axons forming perisomatic "baskets" around the target cell bodies. There are two types of basket cells in the hippocampus that are markedly different despite their similar dendritic- and axonal morphology. They can be distinguished by neurochemical markers and firing pattern. One of the basket cells expresses a neuropeptide cholecystokinin (CCK) and has a regular-spiking firing pattern. The other basket cell expresses parvalbumin and has a fast-spiking firing property (FS BC). Their different synaptic input-output properties and *in vivo* behavior propose a distinguished function in the network (Freund, 2003; Klausberger *et al.*, 2003). For instance, the output of regular-spiking basket cells can be modulated by subcortical pathways (e.g. serotonin, acetylcholine), by retrograde signaling molecules (e.g. endocannabinoids) and by autoreceptors (such as $GABA_B$ receptors), thus, they are suggested to play a role in fine-tuning the network operation. The FS BCs are innervated extensively by glutamatergic inputs, and modulated by opioids. This type

of cell was proposed to be precisely timed device, which allows to control synchronous activities (Freund & Katona, 2007).

I.1.4.2. Dendritic layer-targeting interneurons

The *bistratified cells* share many features of PV+ cells. They also express PV and have fast-spiking characteristics (Buhl *et al.*, 1994; Klausberger *et al.*, 2004). Their soma is within or near the pyramidal cell layer; their dendrites arborize in the strata radiatum and oriens, but avoid the stratum lacunosum-moleculare (Halasy *et al.*, 1996). Their axons can be found in the strata oriens and radiatum. The somata and the horizontally-oriented spiny dendrites of *oriens lacunosum-moleculare cells* (O-LM cells) are located in the stratum oriens. Their axons arborize mainly in the stratum lacunosum-moleculare, suggested to control the entorhinal input of pyramidal cells (McBain *et al.*, 1994). O-LM cells express the neuropeptide somatostatin. The cell bodies of *Schaffer collateral-associated cells* are located in the stratum radiatum of the CA1, their dendrites project to all layers. Their axons target the oblique dendrites and, to a lesser extent, the basal dendrites of pyramidal cells. These interneurons contain CCK (Cope *et al.*, 2002; Pawelzik *et al.*, 2002). Their corresponding cell type is also present in the CA3 (Lasztóczi *et al.*, 2013). The *apical dendrite innervating cells* have very similar morphology to Schaffer collateral-associated cells, but instead of oblique dendrites they prefer to innervate the main apical shafts of the pyramidal cells (Klausberger *et al.*, 2005). The somata of the *perforant path-associated cells* can be found mainly at the border of strata radiatum and lacunosum-moleculare; their dendrites span all layers or remain in the stratum lacunosum-moleculare (Hájos & Mody, 1997; Klausberger *et al.*, 2005). The former three cell types are also immunopositive for CCK (Klausberger, 2009). A large group of subpopulations of hippocampal interneurons (approximately 30% of all GABAergic cells) have a characteristic feature that their local axon arbor is very dense. They are the *neurogliaform cells* (Price *et al.*, 2005) and *ivy cells* (Fuentealba *et al.*, 2008). Neurogliaform cells are confined to the stratum lacunosum moleculare, while ivy cells are located mainly close to the pyramidal cell layer. They can contact dendritic spines of pyramidal cells (Tamás *et al.*, 2003), but the majority of their axon endings do not form real synaptic contacts (Oláh *et al.*, 2009), thus, they could provide tonic inhibition of neighboring cells or regulate transmitter release via presynaptic $GABA_B$ receptors.

I.1.4.3. Interneuron-selective interneurons

Interneuron-selective interneurons have three subtypes (*I, II, III*), which can be distinguished based on their calretinin and vasoactive intestinal polypeptide content and axonal arborization pattern (Acsády *et al.*, 1996a; Acsády *et al.*, 1996b; Gulyás *et al.*, 1996). They can effectively control the firing output of other GABAergic cells (Chamberland *et al.*, 2010).

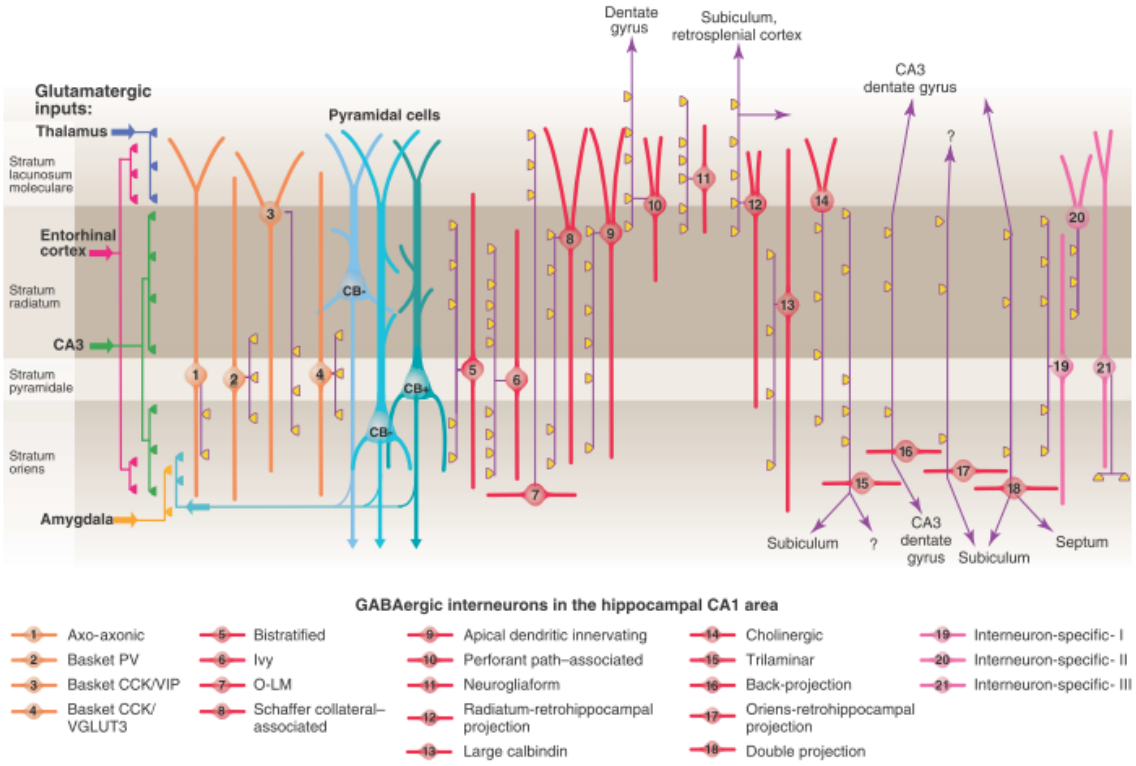

Figure 2. Diversity of interneurons in the CA1 region of the hippocampus. *Klausberger and Somogyi distinguished 21 types of interneurons in the CA1. The pyramidal cells are shown in blue, the somato-dendritic region of perisomatic region-targeting interneurons are orange. The dendritic layer-targeting interneurons are red, while interneuron-selective interneurons are shown in pink. Axons are purple; the main synaptic terminations are yellow. The distribution of the afferent glutamatergic inputs are indicated on the left. VIP, vasoactive intestinal polypeptide; VGluT, vesicular glutamate transporter; O-LM, oriens lacunosum moleculare. Adapted from Klausberger and Somogyi 2008.*

I.1.4.4. Long-range projecting GABAergic neurons

The GABAergic projection neurons are generally located in the stratum oriens, where they have horizontally oriented dendrites. The axon collaterals of *trilaminar cells* span three layers of the hippocampus (strata radiatum, pyramidale and oriens) and project toward the subiculum (Sík *et al.*, 1995; Ferraguti *et al.*, 2005). *Backprojecting cells* send axons backwards to CA3 or DG (Sík *et al.*, 1994), while the *double projection neurons* project to the medial septum and often also to the subiculum (Gulyás *et al.*, 2003; Jinno *et al.*, 2007). The *Oriens* or *radiatum retrohippocampal projection cells* can be found in the stratum oriens or radiatum, they project to the subiculum and retrohippocampal areas (Jinno *et al.*, 2007), as well as to the entorhinal cortex (Melzer *et al.*, 2012).

II. Long-term synaptic changes in hippocampal neurons

Experiences impact the brain function by affecting the activity of neural circuitries, which is manifested partly in changing synaptic weights. Long-lasting modification of synaptic strengths is tightly linked to the storage of new information and considered as the cellular basis of learning (Citri & Malenka, 2008). Long-lasting enhancement of synaptic inputs is termed long-term potentiation (LTP); long-lasting weakening is called long-term depression (LTD). The LTP of excitatory synapses was discovered first in the dentate gyrus (Bliss & Lomo, 1973), followed by the observation of LTD first in the cerebellum (Ito & Kano, 1982). These types of synaptic changes were then acknowledged as widespread phenomena expressed at excitatory synapses throughout the brain (Malenka & Bear, 2004). In these early years of discovery, the interneurons were considered to be rigid structures lacking any possibilities for potentiation or depression at their input or output synapses (McBain *et al.*, 1999). Indeed, most interneurons lack spines on their dendrites, a structure that provides compartmentalization for signaling cascades, which is necessary for altering synaptic strengths. Moreover the postsynaptic density, a protein matrix which contains the scaffolding proteins and signaling molecules necessary for plastic changes is much weaker at GABAergic synapses compared to excitatory synapses. After improving the recording conditions, it was shown that synapses onto interneurons (Buzsáki & Eidelberg, 1982; Laezza *et al.*, 1999), and also their GABAergic outputs (Chevaleyre & Castillo, 2003; Patenaude *et al.*, 2003) are

capable for long-term plasticity. Moreover, it has been clarified that interneurons might have dendritic compartments due to their fast receptor kinetics and activity of Na^+/Ca^{2+} exchanger (Goldberg *et al.*, 2003), which allow local changes in biochemical processes necessary for selective modification of synaptic operations.

Early studies have already established the basic properties of LTP: it exhibits cooperativity, associativity, and input specificity (Nicoll *et al.*, 1988). Cooperativity indicates that LTP can be induced by the simultaneous activation of a critical number of synapses or by coactivation of pre- and postsynaptic neurons. Associativity is the ability to potentiate a weak input when it is activated together with a strong input. Input specificity means that LTP is elicited only at activated synapses and not at adjacent synapses. These classic rules are, however, loosely interpreted in some forms of interneuron plasticity. Both LTP and LTD has early and late phase. In the early phase several second messenger cascades are activated, which are responsible for the induction period, this may last for a few minutes. During the late phase, new protein synthesis occurs (Citri & Malenka, 2008).

II.1. Induction mechanisms

LTP can be induced by several methods, for instance, by high frequency stimulation (HFS, up to 100 Hz) of presynaptic fibers. This approach might model a highly synchronized release of glutamate, e.g. during sharp waves (Buzsáki, 1989). Another way to induce LTP is theta-burst stimulation with or without coincident postsynaptic depolarization (pairing). In contrast, theta-burst stimulation combined with postsynaptic hyperpolarization induces LTD, which might be correlated with plastic changes occurring during theta oscillations (Huerta & Lisman, 1995; Hölscher *et al.*, 1997). Furthermore, LTD can also be triggered by low frequency (below 10 Hz) stimulation. Various receptor agonists or antagonists are also capable to induce long-term synaptic changes, referred as chemically-induced LTP or LTD. Another method for induction of long-term synaptic plasticity is the precise timing of single pre- and postsynaptic spikes, called spike-timing-dependent plasticity. LTP occurs, when the presynaptic spikes precede postsynaptic spikes by up to 0-20 ms, whereas LTD is observed when presynaptic spikes follow postsynaptic spikes by 0 to 20-50 ms interval (Feldman, 2009). This induction mechanism operates within a time window allowing coincident spiking of neurons during gamma oscillations (30-100 Hz).

II.2. Long-term plasticity of excitatory synapses onto principal cells

The common motif of the induction protocols to trigger long-term synaptic changes in principal cells is the necessity to raise Ca^{2+} concentration postsynaptically through N-methyl-D-aspartate (NMDA) receptors. This type of ionotropic glutamate receptors is permeable to Ca^{2+} and requires strong depolarization to become activated. If the increase in Ca^{2+} levels is fast enough, the cascade of the second messenger Ca^{2+}/calmodulin-dependent protein kinase II is activated, leading to an increase in the conductance of the fast, non-Ca^{2+}-permeable ionotropic receptor of glutamate, the α-amino-3-hydroxy-5-methyl-4-isoxazolepropionic acid (AMPA) receptor, and insertion of new AMPA receptors to the synapse. LTP is usually accompanied by enlargement of dendritic spines and formation of new ones. Conversely, a modest increase in postsynaptic calcium concentration induces LTD, by activating a pathway involving calcineurin phosphatase activation, consequent removal of AMPA receptors from the synapses and shrinkage of dendritic spines (Malenka & Bear, 2004; Citri & Malenka, 2008). The threshold level for generating LTP depends on the history of the synapse. If the synapse has previously undergone LTP, the threshold increases and a calcium influx will result LTD with a higher probability (Bear, 1995).

A special form of LTP occurs at mossy terminals in the hippocampus. The expression of this type of LTP is solely presynaptic (Nicoll & Malenka, 1995). As general mechanisms of presynaptic LTP, it requires the cAMP/PKA signaling pathway and the active zone protein RIM1α.

Another non-conventional type of LTD is mediated by retrograde messenger molecules, the endocannabinoids (eCB, eCB-LTD). It usually requires a coincident rise of Ca^{2+} and activation of metabotropic glutamate receptors (mGluR) postsynaptically, which triggers the subsequent release of eCBs from the postsynaptic neuron. These eCBs act on presynaptic CB_1Rs located at axon endings causing a decrease of transmitter release. This form of LTD is also widely distributed in the brain (Heifets & Castillo, 2009); although in some cases, mGluR-mediated LTD was shown to be independent of CB_1Rs (Rouach & Nicoll, 2003; Nosyreva & Huber, 2005). The role of astrocytes in eCB-LTD induction has also been recently revealed (Min & Nevian, 2012).

II.3. Long-term plasticity of excitatory synapses onto interneurons

In the past few years, numerous forms of long-term plasticity have been described in interneurons depending on cell type, brain region or stimulation protocols (Lamsa *et al.*, 2010; Kullmann & Lamsa, 2011; Laezza & Dingledine, 2011). A great drawback of early studies was the lack of proper identification of interneuron types. As a result of this, data are controversial and often not comparable to each other. Induction of plasticity in interneurons seems to have different rules than in pyramidal cells. In GABAergic cells, HFS often induces LTD instead of LTP (McMahon & Kauer, 1997b; Laezza *et al.*, 1999; Pelkey *et al.*, 2005). In interneurons located in the stratum radiatum, NMDA receptor-dependent LTP could be elicited (Lamsa *et al.*, 2005). However, other interneurons possess NMDA receptor-independent form of long-term plasticity, where Ca^{2+}-influx necessary for synaptic changes provided by Ca^{2+}-permeable AMPA (CP-AMPA) receptors (Nissen *et al.*, 2010), or L-type Ca^{2+}-channels (Galván *et al.*, 2008). A special type of LTP has been observed on interneurons equipped with CP-AMPA receptors: LTP was induced, when HFS was paired with postsynaptic hyperpolarization, named as *anti-Hebbian LTP* (Lamsa *et al.*, 2007; Oren *et al.*, 2009; Nissen *et al.*, 2010). A group of stratum oriens interneurons show postsynaptic $mGluR_{1/5}$ -dependent LTP (Lapointe *et al.*, 2004; Topolnik *et al.*, 2006). A series of studies implicated the role of presynaptic $mGluR_7$ receptors in the induction of LTD in CA3 interneurons (Laezza *et al.*, 1999; Pelkey *et al.*, 2005). The subcellular cascades underlying these types of plasticity are divergent and have not been precisely elucidated yet.

II.4. Endocannabinoid-dependent long-term plasticity

Endocannabinoid molecules are the most abundant retrograde messengers in the nervous system. Among eCBs, 2-arachidonoyl glycerol (2-AG) is the most prevalent in the brain (Kano *et al.*, 2009, Katona & Freund, 2012). The CB_1Rs are present at excitatory and inhibitory terminals and mediate either short- or long-term depression in the hippocampus (Ohno-Shosaku *et al.*, 2001; Wilson & Nicoll, 2001; Chevaleyre & Castillo, 2003), depending on stimulus type and length of transmitter release (Heifets & Castillo, 2009). The eCB-LTD is the most conventional form of LTD exhibited at GABAergic efferent synapses of CCK-positive interneurons (i-LTD), which was originally discovered in the amygdala (Marsicano *et*

al., 2002). This eCB-iLTD is heterosynaptic, because the presynaptic CB_1R-mediated reduction of GABA release requires activation of postsynaptic mGluRs by glutamatergic fibers (Chevaleyre & Castillo, 2003, Figure 3).

Despite the fact that CB_1Rs are usually present at glutamatergic terminals at lower levels compared to that found at GABAergic synapses (Kawamura *et al.*, 2006), homosynaptic eCB-LTD occurs in several glutamatergic synapses both in subcortical regions (Gerdeman *et al.*, 2002; Robbe *et al.*, 2002) and -using spike-timing dependent protocol- in the neocortex (Sjostrom *et al.*, 2003; Bender *et al.*, 2006; Lafourcade *et al.*, 2007). Whether this form of LTD is also present at glutamatergic terminals in the hippocampus have remained highly controversial. LTD at excitatory synapses induced by high concentrations of group I mGluR agonist dihydroxyphenylglycine (DHPG) seemed to be independent of CB_1Rs in pyramidal cells (Rouach & Nicoll, 2003; Le Duigou *et al.*, 2011) or in interneurons (Gibson *et al.*, 2008; Edwards *et al.*, 2012). In contrast, some studies detected CB_1R-dependent LTD in pyramidal cells (Xu *et al.*, 2010; Izumi & Zorumski, 2012).

II.5. Long-term plasticity at excitatory synapses onto PV+ interneurons

Lamsa and colleagues found anti-Hebbian LTP at excitatory synapses onto PV+ interneurons in response to HFS (Lamsa *et al.*, 2007). A recent study showed a persistent increase in intrinsic excitability of PV+ cells (Campanac *et al.*, 2013) in the CA1 region of the hippocampus. This type of potentiation occurred in response to HFS, induced by $mGluR_5$-mediated inactivation of Kv1 potassium channels. Investigations of spike-timing-dependent plasticity in the layer 2/3 of somatosensory cortex showed that fast-spiking (i.e. putative PV+) interneurons express postsynaptic mGluR-dependent LTD regardless of the timing of pre- and postsynaptic spiking (Lu *et al.*, 2007). However, it is still unclear whether eCBs are involved in mGluR-dependent LTD observed in PV+ interneurons.

Figure 3. Summary of the induction mechanism of endocannabinoid-mediated long-term depression (eCB-LTD). *Upon excess neuronal activity, group I mGluRs -located at the postsynaptic site, in the perisynaptic annulus- are activated and coupled to phospholipase C (PLC) through $G_{\alpha}q/11$ subunit and facilitate diacylglycerol (DAG) formation from*

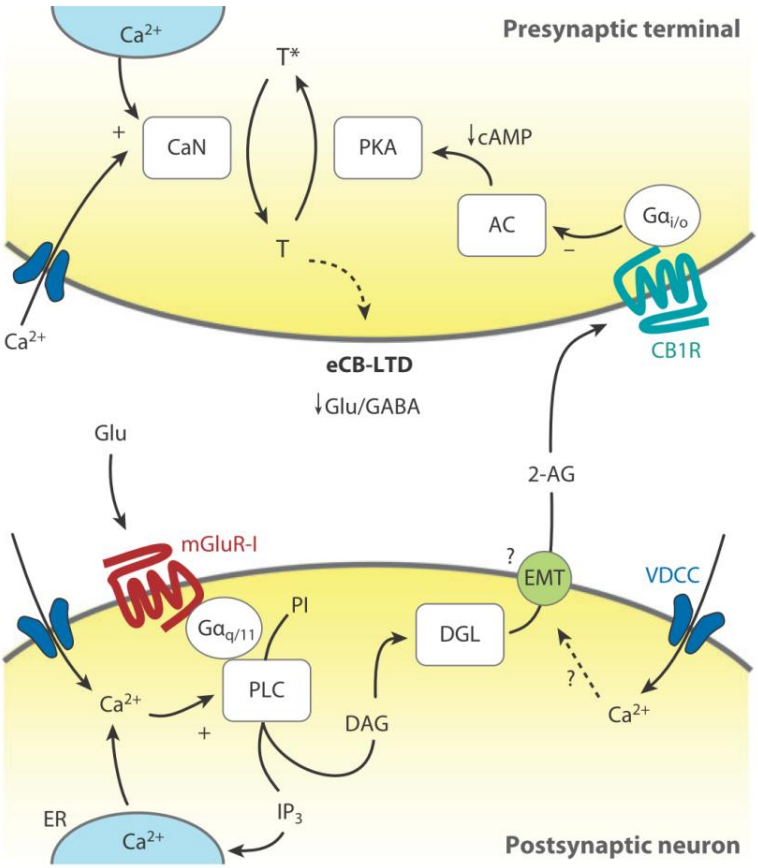

phosphatidylinositol (PI). DAG is further converted to 2-AG by diacylglycerol lipase-α (DGL-α). 2-AG is released from the postsynaptic neuron by presumable eCB membrane transporter (EMT) and binds CB_1Rs. In some forms of eCB-LTD, eCB mobilization requires postsynaptic Ca^{2+} rise probably to activate PLC. Postsynaptic action potentials (e.g., during spike timing–dependent protocols) may trigger this Ca^{2+} rise through voltage-gated Ca^{2+} channels (VGCC), NMDA receptors, or Ca^{2+} can be released from the endoplasmic reticulum (ER), by a product of PLC, inositol 1,4,5-trisphosphate (IP_3). At presynaptic terminals, CB_1R acts via G_αi/o through inhibition of adenylyl cyclase (AC), which reduces the activity of protein kinase A (PKA). This step may also require a presynaptic Ca^{2+} rise. The reduction of PKA activity leads to activation of the Ca^{2+}-sensitive phosphatase calcineurin (CaN), which shifts the kinase/phosphatase activity balance, thus, induces dephosphorylation of a yet unidentified presynaptic target (T), potentially RIM1α; resulting long-lasting reduction of transmitter release. Adapted from Heifets et al. 2009.

III. Oscillations in the hippocampus

In a cortical network, excitatory principal cells are designated for processing, storing and retrieving information, while inhibitory interneurons are responsible for spatial and temporal control of the firing of these cells, thereby enabling the synchronization of network activity. Oscillations emerge in brain regions where the recurrent excitatory connectivity of principal cells is prominent, including the neocortex, the CA3 region of the hippocampus or

the subiculum. Other brain areas lacking local recurrent collaterals can be entrained by extrinsic rhythmic inputs (Hájos & Paulsen, 2009). Several types of network activities related to memory acquisition have been observed in the hippocampus. For instance, theta (4-8 Hz) and gamma (30-100 Hz) oscillations are contributed to formation of new memory traces, whereas sharp waves and associated ripple (120-200 Hz) oscillations are suggested to play a role in memory consolidation (Buzsáki, 1986, Figure 4). These rhythmic events can be detected as fluctuation of the local field potential, which are proposed to be generated mainly by inhibitory conductances (Oren & Paulsen, 2010). Oscillations in networks can have a role in binding of assemblies coding several modalities of a cue (Singer, 1993) and/or arrange the timing of the discharge of connected cells promoting plasticity. During a network event, at least two features of a given cell activity might carry information: the timing of the cell's action potential relative to the network event (phase coding) or the frequency of the cell's spiking (rate coding). Lower frequency oscillations can involve more neurons in a larger brain volume and associated with larger voltage fluctuations, because a broader time window allows recruitment of larger number of cells. In contrast, fast oscillations are contributed to smaller, more localized cell assemblies, and are associated with smaller voltage fluctuations (Axmacher *et al.*, 2006; Buzsáki & Wang, 2012).

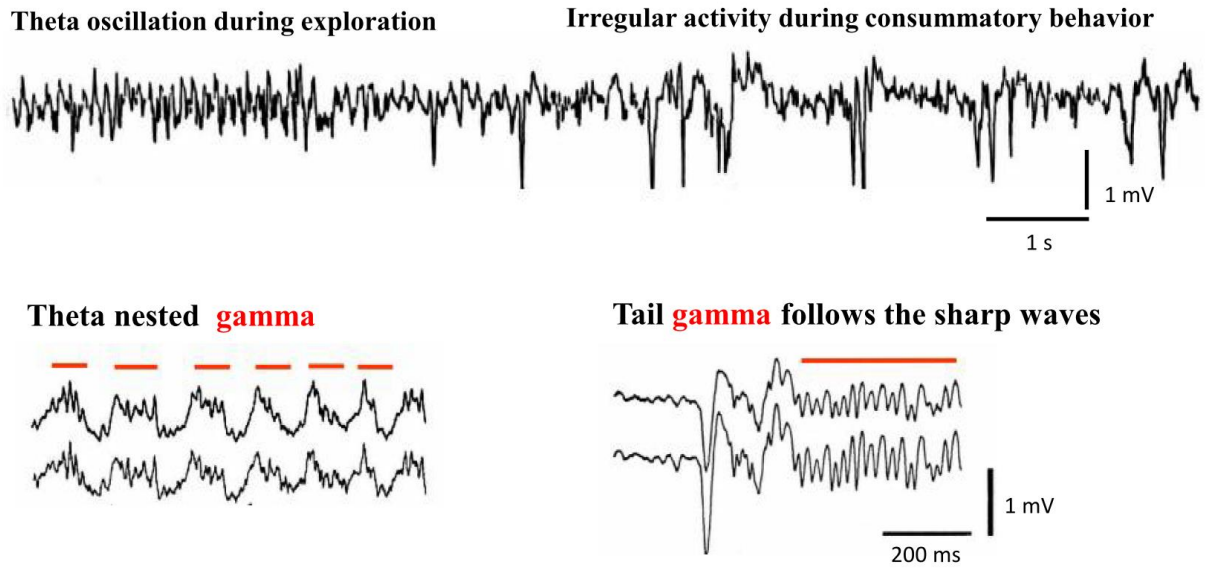

Figure 4. Activity patterns of the hippocampus recorded in vivo. *Top: Theta oscillation that occurs during exploratory behavior, whereas subsequent large irregular activity dominated by sharp waves which can be observed when the animal is in rest (Modified from Buzsáki,*

1989). Bottom: Gamma oscillations (indicated by red lines) can be found nested within theta activity (left) or following sharp waves (right). Modified from Buzsáki et al., 2003 (right) and Traub et al., 1996 (left).

III.1. Theta oscillations

Theta oscillations are characteristic activity patterns on the hippocampal EEG during exploratory behavior. The amplitude of theta oscillations is largest in the stratum lacunosum-moleculare of the CA1 region (Bullock *et al.*, 1990), and switches the polarity at stratum pyramidale (Leung & Yim, 1986; Fox, 1989). The MS-DBB and the supramammillary nucleus are the two critical subcortical structures involved in pacing the theta rhythm (Petsche *et al.*, 1962). According to the current theory, the theta rhythm is generated by pacemaker GABAergic neurons located in the MS-DBB (Hangya *et al.*, 2009) that project to the hippocampus and entorhinal cortex, providing a rhythmic inhibition on local inhibitory neurons (Miettinen & Freund, 1992). In addition, the hippocampal perisomatic region-targeting interneurons are tonically excited by acetylcholine released from septal cholinergic afferents. This cholinergic excitation together with the phasic inhibition can generate rhythmic discharges of GABAergic neurons synchronizing a large population of neuronal activities (Freund & Antal, 1988; Stewart & Fox, 1990). The glutamatergic input from the entorhinal cortex can also contribute to the rhythmic excitation, terminating in the stratum lacunosum-moleculare (Winson, 1974). Other non-subcortical mechanisms of theta generation can be also present in the hippocampal networks. For example, after lesioning of the entorhinal cortex, theta rhythm driven by the CA3 recurrent collateral system emerges (Kramis *et al.*, 1975; Lee *et al.*, 1994). Besides perisomatic region-targeting interneurons, at least three other types of GABAergic cells may also contribute to the maintenance of theta. The O-LM cells receive rhythmic excitation from pyramidal cells, thus they provide a rhythmic inhibition to the stratum lacunosum-moleculare. This rhythmic inhibition can prevent the discharge of weakly activated principal cells by entorhinal fibers, but can allow to spike neurons that code information. The perforant path-associated cells that are capable to discharge with theta frequency in response to cholinergic activation (Chapman & Lacaille, 1999) may also control the impact of the entorhinal input. The hippocampal GABAergic neurons with septal projection can provide rhythmic feedback to the medial septum (Alonso

& Kohler, 1982; Tóth *et al.*, 1993). Finally, pyramidal cells display subthreshold resonance in their membrane potential fluctuations, with a preferred frequency in the theta band. This single-cell feature of pyramidal cells can also actively contribute to their somatic and dendritic membrane potential oscillations during theta (Leung & Yim, 1991; Kamondi *et al.*, 1998; Strata, 1998).

III.1.1. Theta rhythm-related place coding

Remarkably, most pyramidal neurons are silent during theta rhythm. The few active cells discharge single spikes at the trough of theta measured in the pyramidal cell layer, when perisomatic inhibition is minimal. A prominent example of hippocampal information processing during theta rhythm is the representation of spatial location of the animal. Those pyramidal cells that are responsible for coding a single part of the territory are called place cells. The area where place cells fire is the cell's place field which corresponds to the physical environment where the animal is currently present (O'Keefe & Dostrovsky, 1971; O'Keefe & Recce, 1993). When the animal approaches the place field of a given cell, the cell increases its firing rate and its spikes display phase precession relative to the theta rhythm (Skaggs *et al.*, 1996). This change in the firing phase can reach 180° in the center of the place field (defined by the maximum discharge rate of the neuron). The coding of place fields occurs randomly. If a pyramidal cell is depolarized, e.g. when it receives input from perforant path fibers conveying the actual environmental cues, the synaptic connections between the pyramidal cell and its input can be strengthened, and then the cell can become responsive to a specific environmental input, overriding the rhythmic somatic hyperpolarization (Axmacher *et al.*, 2006).

III.2. Gamma oscillations

Gamma oscillations often occur embedded into theta oscillation (Buzsáki *et al.*, 2003) or following sharp wave activity (Traub *et al.*, 1996). During theta rhythm, perisomatic region-targeting interneurons fire bursts of spikes at the peak of the theta measured extracellularly in the stratum pyramidale, where the spikes in the burst episodes occur at

gamma frequency (Buzsáki *et al.*, 1983; Bragin *et al.*, 1995). Indeed, the inhibitory postsynaptic potential provided by these interneurons is known to be reflected in the gamma field (Oren *et al.*, 2010). Two mechanisms could underlie the generation of gamma oscillation: synchronization of interneuronal firing by mutual inhibition (Whittington *et al.*, 1995; Traub *et al.*, 1996; Wang & Buzsáki, 1996) or a reciprocal interaction between excitatory and inhibitory neurons (Csicsvári *et al.*, 2003; Mann *et al.*, 2005) is required (for review see Buzsáki & Wang, 2012). Again, as in the case of theta rhythm, only a small percentage of pyramidal cells are active during gamma oscillation (Csicsvári *et al.*, 2003; Senior *et al.*, 2008; Colgin *et al.*, 2009). This is in accordance with the theory that in a system linking cell ensembles by close coincident temporal activity, the spiking of most cells should be silenced in order to avoid their near-synchronous firing by chance (von der Malsburg, 1995).

In the hippocampus, at least two types of gamma oscillations can be distinguished. The slow gamma (30-50 Hz) is generated in the CA3 region, whereas the fast gamma (50-100 Hz) is driven by the rhythmic input from the entorhinal cortex (but see Buzsáki & Wang, 2012). These two types of transient oscillations may occur in different phases of the theta cycles. The slow gamma is preferentially present in the descending phase of theta cycles, while the fast gamma occurs at their trough. These two types of gamma oscillations might have distinguished roles in a learning task. The fast gamma may carry new information from the entorhinal cortex needed to be burnt in the network. For this purpose, the fast gamma provides a 10-15 ms long time window ideally suited to generate LTP. Thus, this type of oscillation may establish the basis for memory encoding. In case of retrieval, the slower gamma generated by the CA3 is suggested to play a role. The slow gamma could readily reactivate the cells representing a recent memory, but as the time window it provides (25-30 ms) is not optimal for potentiation, the retrieval process will avoid re-encoding of previously stored memories. A potential mechanism for a switch between the two types of gamma oscillations might be a strong excitation of the CA3 network or recruitment of distinct subpopulation of interneurons (Colgin & Moser, 2010).

III.2.1. Cooperative action of theta and gamma oscillations in the formation of working memory

A theory for the requirement of co-active theta and gamma oscillations was built by Lisman and colleagues. The 7+/-2 short-term memory items that humans can store is represented by the gamma cycles nested in each cycle of theta rhythm. Each item may be stored in one gamma cycle and the 7+/-2 items are always represented in the same order during theta cycles. In this concept, the theta rhythm provides an absolute phase reference to enable the preservation of the sequence. This coupling of theta and gamma oscillations can give rise to a working memory buffer and their frequency relationship is supposed to explain the limit of simultaneously storable memory items (Lisman & Idiart, 1995).

III.3. Sharp wave-ripples

Sharp waves are large amplitude events generated by population discharges. They are generated in the CA3 region during low arousal brain states, when recurrent collaterals of CA3 pyramidal cells are released from subcortical inhibition (Miles & Wong, 1983). They can be detected as a voltage deflection up to 1 mV lasting for 50-100 ms (Buzsáki, 1986). This field activity reflects the summated excitatory postsynaptic potential (EPSP) of Schaffer collaterals (Csicsvári *et al.*, 2000). The ascending phase and the peak of sharp waves are usually decorated by an embedded, fast oscillatory activity (120-200 Hz) called ripple (Buzsáki *et al.*, 1992; Ylinen *et al.*, 1995). Ripples are generated by the dynamic interaction of excitatory and inhibitory cells. The field potential during ripples may reflect synchronized somatic inhibitory postsynaptic potentials interrupted by synchronous spiking of pyramidal cells in every 5-6 milliseconds (Csicsvári *et al.*, 1999).

III.3.1. Sharp wave-ripples in memory consolidation

Sharp wave-ripples are considered to be the neural correlate of memory consolidation. During ripples, neuronal assemblies that participated in coding are re-activated in the same or reversed order on a compressed time scale (Skaggs & McNaughton, 1996; Nádasdy *et al.*,

1999; Diba & Buzsáki, 2007). Because sharp waves spread from the CA3 to the CA1, subiculum and then to layers V and VI of the entorhinal cortex (Chrobak & Buzsáki, 1996), they can mediate the transfer of recently acquired memories to their final place of storage in the neocortex. The strong excitation provided by recruitment of large cell assemblies during sharp waves might be able to initiate LTP in neurons which were weakly potentiated during the acquisition phase (Buzsáki, 1986).

III.4. *In vitro* oscillation models

Due to the lamellar structure of the hippocampus proper, the connectivity of the CA regions is well preserved in horizontal slices, which enables to investigate oscillations in acute slice preparations. These models allow the direct experimental study of the cellular and synaptic mechanisms underlying given network activities. As a corollary advantage, one can selectively target cell types under visual guidance, and pharmacological modifications are also possible. In case of sharp wave-ripples or slow gamma oscillations that emerge intrinsically in CA3 networks, detailed examination of the generation mechanisms becomes also available. While sharp wave-ripples emerge spontaneously in acute slices (Maier *et al.*, 2002), gamma oscillations require induction. They can be induced by activating mGluRs (Whittington *et al.*, 1995; Boddeke *et al.*, 1997), kainate receptors (Hájos *et al.*, 2000; Fisahn *et al.*, 2004; Gloveli *et al.*, 2005), or muscarinic acetylcholine receptors (mAChRs) (Fisahn *et al.*, 1998).

III.4.1. Carbachol-induced in vitro gamma oscillations

Our group studied the properties of *in vitro* gamma oscillations by activating mAChRs with bath application of an acetylcholine receptor agonist carbachol. This type of gamma oscillation can be maintained for hours, and intended to model *in vivo* gamma oscillation occurring at high cholinergic tone, that occur during exploratory behavior when gamma oscillation is embedded in theta rhythm (Marrosu *et al.*, 1995; Buzsáki *et al.*, 2003). Carbachol increases the excitability of CA3 pyramidal cells via $M_{1/3}$AChRs (Müller & Misgeld, 1986) and activate M_2AChRs on terminals of PV+ cells resulting in a decreased, but

sustained GABA release from their axon endings (Szabó *et al.*, 2010). These effects may contribute to the generation of gamma oscillations within the CA3, where the recurrent excitation of CA3 pyramidal cells drives the firing of inhibitory cells.

Carbachol-induced oscillation in the CA3 region shares many features of *in vivo* gamma oscillations observed in the same area. In accordance with *in vivo* observations, the phase of the local field potential also reverses in the stratum lucidum. *In vivo* and *in vitro* oscillations have identical current source density profiles. Pyramidal cells discharge with the highest probability at the trough of the oscillation both *in vivo* and *in vitro* when measured in the pyramidal layer, followed by the firing of interneurons with a monosynaptic delay. These similarities suggest that carbachol-induced gamma oscillations in slices are generated with a similar mechanism as *in vivo* occurring gamma oscillations and make this model suitable to study the underlying cellular processes (Hájos & Paulsen, 2009).

III.5. Parvalbumin-positive perisomatic region-targeting interneurons in oscillations

Perisomatic inhibition is considered to be the main current generator in multiple network oscillations synchronizing large assemblies of principal cells (Ellender & Paulsen, 2010). Thus, depending on brain state, PV+ cells seem to be the key elements of the rhythm of a wide range of cortical oscillations. Several studies show the crucial role of these cells in the generation of theta rhythm (4-8 Hz, Korotkova *et al.*, 2010) or gamma oscillations (30-100 Hz, Fuchs *et al.*, 2007; Cardin *et al.*, 2009; Sohal *et al.*, 2009), as well as in sharp wave-ripple activities (120-200 Hz, Rácz *et al.*, 2009; Ellender *et al.*, 2010).

III.5.1. Unique properties of PV+ cells that make them suitable to govern oscillations

Many different properties endow the PV+ cells to effectively control the output of principal cells (Bartos *et al.*, 2007). They strategically synapse on the somata and proximal dendrites (basket cells, Somogyi *et al.*, 1983; Kubota *et al.*, 2007) or axon initial segments (axo-axonic cells, Somogyi, 1977) of principal cells, where the action potentials are generated. The release of GABA from their axon terminals is precisely controlled by their action potentials, which is supported by the P/Q-type voltage-gated Ca^{2+}-channels in the

boutons and by the presence of parvalbumin. The P/Q-type Ca^{2+}-channels in the axon endings ensure an efficient rise of Ca^{2+} concentration in the close proximity of vesicles (Neher, 1998). The source of Ca^{2+} is tightly coupled to the Ca^{2+} sensor, estimated to be within 50 nm distances from the release sites (Hefft & Jonas, 2005). This structure can result in a fast, synchronized release of GABA-containing vesicles, precisely timed to the action potential invading the bouton. The fast and synchronous release of vesicles enables GABA receptors to be opened synchronously, producing a rapid rise time of synaptic currents. The parvalbumin-content of the cells (Katsumaru *et al.*, 1988) provides an efficient buffering of residual calcium, enabling a fast decay of GABA currents (Vreugdenhil *et al.*, 2003).

The membrane features of PV+ cells that determine their action potential generation also contribute to their effective inhibitory and synchronizing properties. The resting membrane potential of these interneurons is generally by 10-15 mV more depolarized (Fricker *et al.*, 1999; Verheugen *et al.*, 1999) than that of pyramidal neurons, which set them a ready-to-fire mode (Jonas *et al.*, 2004). Furthermore, the potassium current mediated via Kv3 channels is pivotal to the fast-spiking phenotype, making them well suited to fire action potentials with high frequency during sustained depolarization without distortion in the action potential shape (Doischer *et al.*, 2008; Goldberg *et al.*, 2011). Fast deactivation, high activation threshold and lack of inactivation of the Kv3 potassium channels are crucial for generating fast spiking (Lien & Jonas, 2003). The action potential of the PV+ cells has small half width, which may also participate in constraining fast decay of GABA release. Large afterhyperpolarization with fast kinetics is optimal for a maximal recovery of Na^{+} channels from inactivation and a minimal delay in the onset of the action potential initiation (Jonas *et al.*, 2004).

The excitatory synaptic input onto PV+ cells is also unique. They receive EPSPs with short latency and rapid kinetics (Miles, 1990). This is in part due to the fast synaptic currents mediated by AMPA receptors containing the GluA4 subunit (Jonas *et al.*, 1994; Geiger *et al.*, 1995) and to the fast clearance of glutamate from the synaptic cleft (Geiger *et al.*, 1997). PV+ interneurons receive relatively large excitatory inputs from each of their presynaptic pyramidal cells, which can even drive action potential generation (Galarreta & Hestrin, 2001; Woodruff *et al.*, 2011). Unique electrical properties of dendrites (Hu *et al.*, 2010; Nörenberg *et al.*, 2010) diminish filtering of EPSPs preserving the fast kinetics. The lack of active conductances on the dendrites endows them for precise monitoring of network excitation and generation of an inhibitory output appropriate for controlling the overall system.

PV+ cells form a highly interconnected network; they are synaptically (Bartos *et al.*, 2001) and electrically coupled with each other (Galarreta & Hestrin, 1999; Fukuda & Kosaka, 2000). Therefore, they can excite each other through fast electrical synapses (Tamás *et al.*, 2000). The kinetics of the mutual inhibition of these cells is faster than the inhibition received by the pyramidal cells (Bartos *et al.*, 2002), thus PV+ cells are capable to perfectly phase their spiking before synchronizing pyramidal cells throughout large areas.

Collectively, these features together provide PV+ interneurons a narrow time window for synaptic integration, ensuring fast and precisely timed spike generation (Glickfeld & Scanziani, 2006) and a resulting fast synchronous inhibition. These properties are pivotal for oscillogenesis at different frequencies (Freund & Katona, 2007; Fuchs *et al.*, 2007; Sohal *et al.*, 2009).

III.5.2. Emerging evidences for the role of PV+ cells in oscillations

Several findings indicate the role of PV+ cells in synchronous network operation. For instance, impairing PV+ cell function resulted in changes in the oscillations. In parvalbumin knockout mice, the power of *in vitro* gamma oscillation is increased, presumably due to an enhanced inhibition in the lack of the high affinity Ca^{2+}-binding protein (Vreugdenhil *et al.*, 2003). Similar increase in the gamma power was observed when Kv3.1 potassium channels responsible for the fast-spiking phenotype were ablated (Joho *et al.*, 1999). The loss of $GABA_A$ receptor-mediated synaptic inhibition onto PV+ cells reduced theta rhythm and coupling of theta and gamma oscillations, but left gamma oscillations intact (Wulff *et al.*, 2009). Manipulation of excitatory synaptic inputs onto PV+ cells also caused severe changes in synchrony and memory-related behavior. When either of their two major subunit types of AMPARs (GluA1 or GluA4) was deleted from PV+ cells, *in vitro* hippocampal gamma oscillations exhibited reduced power. In parallel, the animals showed impairments in hippocampus-dependent memory tasks (Fuchs *et al.*, 2007). *In vivo* recordings from the GluA1 knockout mice found increase of ripple amplitude, whereas theta and gamma oscillations remained intact (Rácz *et al.*, 2009). Removing the NR1 subunit of NMDA receptors from PV+ cells resulted in altered theta oscillations and damaged spatial navigation. Elevated power of gamma oscillations was also observed in $NR1^{PVCre-/-}$ mice, which was less modulated by theta (Korotkova *et al.*, 2010). Optogenetic stimulation in the neocortex showed

that the selective inhibition of PV+ cells suppressed gamma oscillations, while driving these neurons could generate gamma frequency rhythmicity (Sohal *et al.*, 2009). Although these elegant genetic studies all show the importance of PV+ cells in oscillatory activities, they still could not clarify the role of AACs and FS BCs separately, due of the lack of unequivocal distinguishing marker.

III.5.3. Distinct entrainment of AACs and FS BCs during oscillations

Recording the firing activity of cells and parallel measurement of field oscillations combined with *post hoc* anatomical identification could provide important details of how AACs and FS BCs behave during oscillations in the hippocampus. It was found that the spiking of the two cell types show differences during several types of network oscillations. For instance, AACs fire preferentially after the peak of theta rhythm measured in the stratum pyramidale, while FS BCs fire at the descending phase (Klausberger *et al.*, 2003; Lapray *et al.*, 2012; Varga *et al.*, 2012). Both AACs and FS BCs are entrained at the rising phase of the gamma cycles (measured with a field electrode placed in the stratum pyramidale), but AACs often skip the cycles in the carbachol-induced *in vitro* model (Gulyás *et al.*, 2010). In this model, FS BCs reliably discharge at each cycle and frequently (in about every 10^{th} cycle) fire doublets. Furthermore, selective reduction of GABA release from FS BCs provided direct evidence that the synaptic output of FS BCs is the major source of inhibition that generates oscillatory current producing the carbachol-induced gamma oscillation (Gulyás *et al.*, 2010). Intriguingly, *in vivo* studies reported weaker phase coupling of FS BCs during slow (30-80 Hz) or fast (90-130 Hz) gamma oscillations (Tukker *et al.*, 2007; Varga *et al.*, 2012). During sharp wave-ripples, both cell types increase their firing rate, but AACs cease their firing before the peak of sharp-waves, while FS BCs reliably follow ripples with high frequency discharges (Klausberger *et al.*, 2003; Lapray *et al.*, 2012; Varga *et al.*, 2012). Together, these observations suggest that the two cell types are recruited to network oscillations in a different manner.

Data from several other cortical areas also indicate distinguished recruitment of AACs and FS BCs. In the basolateral amygdala (Bienvenu *et al.*, 2012) and in the prefrontal cortex (Massi *et al.*, 2012), AACs, but not FS BCs were responsive (i.e. increased their firing) to painful stimuli. Moreover, in the somatosensory cortex, AACs have larger receptive field with

lower acuity upon whisker stimulation than that observed for FS BCs (Zhu & Zhu, 2004). When *in vitro* gamma oscillations in the CA3 were induced by local application of kainate to the border of strata radiatum and lacunosum-moleculare, spiking of AACs was continuous, lacking any gamma modulation that characterized FS BC firing (Dugladze *et al.*, 2012). Based on these data, it is tempting to speculate that excitatory synaptic inputs onto AACs and FS BCs exhibit different features, but the details are yet to be determined. Therefore, one of the aims of the thesis was to uncover the distinct properties of excitatory synaptic inputs onto AACs and FS BCs.

IV. Parvalbumin-positive interneurons in schizophrenia

Schizophrenia is a prevalent neuropsychiatric disorder usually developing during late adolescence. Besides its tremendous positive (hallucinations) and negative (anhedonia, social withdrawal) symptoms, the cognitive defects lie at the core of the disease preceding the development of the other symptoms (Inan *et al.*, 2013). The most important hallmarks of cognitive deficits are the failure in working memory and the lack of proper filtering of irrelevant sensory information (Javitt, 2009). For the proper functioning of both cognitive tasks, GABAergic inhibition is required at a crucial point of the processing (Freedman *et al.*, 1996; Rao *et al.*, 2000). This indicates that the timing of pyramidal cell firing by interneurons can play an important role in cognitive processes. Most of the studies investigating the neurobiological changes in schizophrenia have focused on the dorsolateral prefrontal cortex, a cortical area most tightly linked to the phenotype of observed symptoms, however, in some cases, severe changes in the hippocampus have also been revealed (Law *et al.*, 2006; Konradi *et al.*, 2011).

The role of PV+ interneurons in schizophrenia attracts widespread interest, since it was discovered that mRNA levels for the synthetizing enzyme of GABA, GAD67, which is highly abundant in PV+ cells, significantly decreases in tissues deriving from schizophrenic patients (Akbarian *et al.*, 1995). The decreased mRNA levels of PV (Hashimoto *et al.*, 2003; Hashimoto *et al.*, 2008b; Fung *et al.*, 2010) and the reduced number of PV+ neurons (Beasley & Reynolds, 1997) in samples from schizophrenic patients also support the hypothesis that impairment of PV+ cells may be characteristic in this illness. Another evidence for insufficient inhibition derived from PV+ cells is the decrease in the mRNA levels of

$GABA_A$ α1 receptors (Hashimoto *et al.*, 2008a; Hashimoto *et al.*, 2008b; Beneyto *et al.*, 2011) selectively in pyramidal cells (Glausier & Lewis, 2011). Furthermore, the increased abundance of chloride transporter, NKCC1 relative to the levels of another Cl^- regulator, KCC2 leads to elevated intracellular Cl^- concentration, which might further weaken the inhibition (Arion & Lewis, 2011). In parallel, gamma oscillation, which is thought to contribute to cognitive functions, is disrupted in schizophrenia (Cho *et al.*, 2006; Minzenberg *et al.*, 2010; Uhlhaas & Singer, 2010).

Recent studies indicated that impairment in the excitatory synaptic inputs onto PV+ cells might be responsible for their malfunction (Lewis *et al.*, 2012; Nakazawa *et al.*, 2012). Special attention was focused on the NMDA receptors expressed in PV+ cells deriving from the "NMDA theory" of schizophrenia (Javitt, 1987; Tamminga, 1998). This relies on the discovery that the psychotomimetic drug phencyclidine -a non-competitive antagonist of NMDA receptors (Lodge & Anis, 1982)- causes schizophrenic symptoms. Chronic application of NMDA receptor antagonists results in hyperactivation of cortical excitatory neurons (Krystal *et al.*, 1994; Suzuki *et al.*, 2002; Jackson *et al.*, 2004), and decreased expression of GAD67 and PV (Kinney *et al.*, 2006; Behrens *et al.*, 2007; Morrow *et al.*, 2007). Prolonged exposure of these antagonists reduces the amplitude of AMPA receptor-mediated synaptic currents in PV+ cells, while increases their amplitude in pyramidal cells (Wang & Gao, 2012). Ablating NR1 subunit of NMDA receptors in the majority of PV+ cells in mice triggered several behavioral symptoms of schizophrenia (Belforte *et al.*, 2010), including impairments of gamma oscillations and reduced performance in spatial- and working memory tasks (Korotkova *et al.*, 2010; Carlen *et al.*, 2012). When the NMDA receptor function was perturbed later than the second postnatal week, schizophrenia-like behavioral phenotype was not observed (Belforte *et al.*, 2010), highlighting the importance of changes during adolescence in the development of the disease.

Thus, these results collectively indicate that investigating the properties and operation of excitatory synaptic inputs onto PV+ cells might lead us to a better understanding of how these pivotal cells organize normal and abnormal cognitive functions in the brain.

AIMS OF THE THESIS

The main goal of the experiments during my graduate years was to investigate the excitatory synaptic inputs onto parvalbumin-positive perisomatic region-targeting interneurons (PV+ cells) in the hippocampus. Therefore, we focused on three objectives.

The first objective was to uncover the differences in the excitatory synaptic inputs of the two types of PV+ cells, the axo-axonic (AAC) and fast-spiking basket cells (FS BC), which may underlie the different recruitment of these two interneuron types during network oscillations in the CA3 region of the hippocampus. For this purpose, we asked the following questions:

- Are there any differences in the active and passive membrane properties of the two cell types that may contribute to their different entrainment during oscillations?
- How similarly can the two cell types be recruited by extracellular stimulation?
- Is there any dissimilarity in the kinetics of excitatory postsynaptic currents received by these interneurons?
- Do the two cell types have the same density of glutamatergic synaptic inputs? (This part was performed by Dr. Rita Karlócai)
- Is there any distinctive feature in their dendritic structures, which may underlie their different excitatory synaptic inputs?

The second objective was to reveal, whether the excitatory synaptic inputs onto PV+ interneurons are capable of undergoing long-term plastic changes. Based on the anatomical observations obtained by Dr. István Katona's group, that a synthetizing enzyme of the main endocannabinoid, 2-AG, is present at glutamatergic synapses of PV+ cells, we aimed to induce endocannabinoid-mediated long-term synaptic depression at the excitatory synapses in PV+ interneurons. (A larger part of these experiments was carried out by Dr. Zoltán Péterfi.) We investigated the following points:

- Is it possible to induce LTD in PV+ cells by post-pre pairing protocol or by pharmacological activation of mGluRs?
- Do pyramidal cells also exhibit LTD under similar circumstances?
- Are there any differences in the threshold of LTD induction in pyramidal cells and PV+ interneurons?

- What is the molecular cascade underlying these forms of LTD? Is it dependent on CB_1 cannabinoid receptors?

The third objective was to examine the contribution of changes in excitatory synaptic inputs onto FS BC in the cannabinoid-induced suppression of *in vitro* gamma oscillations (Dr. Noémi Holderith performed the majority of these experiments). We aimed to answer the following questions:

- Is the power of carbachol-induced gamma oscillation exhibit similar reduction in response to CB_1R agonists, as it was observed earlier in the kainate-induced oscillation model?
- How does cannabinoid administration affect the firing of pyramidal cells and FS BCs during gamma oscillation?
- Which type of inputs of these cells is affected by CB_1R agonists?
- The modification of glutamatergic or GABAergic input onto pyramidal cells/FS BCs is responsible for the observed changes in gamma oscillations?

MATERIALS AND METHODS

I. Animals

Experiments were approved by the Committee for the Scientific Ethics of Animal Research (22.1/4027/003/2009) and were performed according to the guidelines of the institutional ethical code and the Hungarian Act of Animal Care and Experimentation (1998. XXVIII. section 243/1998.). In the studies giving the basis of the thesis we used several mouse strains. Transgenic mice of the FVB strain expressing enhanced green fluorescent protein (eGFP) under the control of the PV promoter (Meyer *et al.*, 2002) were used in order to enhance the probability of targeting PV+ interneurons. Additionally, for investigation of CB_1R function during gamma oscillations and LTD, we used CB_1R knockout (CB_1R KO) mice (Zimmer *et al.*, 1999) and their wild type littermates of the C57BL/6 strain. For investigating gamma oscillations the CD1 mouse line was used.

II: Electrophysiological measurements

II.1. Slice preparation

Mice were deeply anaesthetized with isoflurane and decapitated. The brain was quickly removed from the skull and immersed into ice-cold solution containing (in mM): sucrose 252; KCl 2.5; $NaHCO_3$ 26; $CaCl_2$ 0.5; $MgCl_2$ 5; NaH_2PO_4 1.25; glucose 10; bubbled with 95% O_2 / 5% CO_2 (carbogen gas). Using a Leica VT1000S or VT1200S Vibratome (Wetzlar, Germany) we cut horizontal or coronal hippocampal slices of 150-200 μm thickness for studying postsynaptic currents or potentials and horizontal slices of 350-400 μm thickness for investigating gamma oscillations. Slices were placed into an interface-type holding chamber containing artificial cerebrospinal fluid (aCSF) which consists of (in mM): NaCl, 126; KCl, 2.5; $NaHCO_3$, 26; $CaCl_2$, 2; $MgCl_2$, 2; NaH_2PO_4 1.25; glucose 10, bubbled with carbogen gas at 36 ºC that gradually cooled down to room temperature (~1-1.5 hours).

II.2. Electrophysiological recordings

After incubation (at least an hour), the slices were transferred individually into a submerged-type recording chamber superfused with aCSF bubbled with carbogen gas at 30-32 °C. The cells were visualised using an Olympus BX61 or Nikon FN1 microscope equipped with differential interference contrast optics. The eGFP in cells were excited by a UV lamp, and the fluorescence was visualized by a CCD camera (C-7500; Hamamatsu Photonics, Japan). Patch pipettes were pulled from borosilicate glass capillaries with an inner filament (1.5 mm O.D.; 1.12 mm I.D., Hilgenberg, Germany) using a DMZ-Universal Puller (Zeitz-Instrumente GmbH, Germany). Data were recorded with a Multiclamp 700B amplifier (Axon Instruments, Foster City, CA, USA), low-pass filtered at 2 kHz and digitized at 10 kHz with a PCI-6024E A/D board (National Instruments, Austin, TX, USA) using EVAN 1.3 (courtesy of Professor Istvan Mody, Departments of Neurology and Physiology, UCLA, CA) or Stimulog software (courtesy of Prof. Zoltán Nusser, Institute of Experimental Medicine, Hungarian Academy of Sciences, Budapest, Hungary). During whole-cell recordings, access resistance was frequently monitored and recordings with access resistance larger than 15 MΩ and/or more than 20% change were discarded.

II.3. Investigation of single-cell and synaptic properties

To investigate the excitability, synaptic input features and membrane properties of the cells, we performed either loose-patch, whole-cell voltage-clamp and current-clamp recordings. During loose-patch recordings, we approached the cell membrane with glass pipettes (~3-5 MΩ) filled with aCSF thus we could detect discharges of individual cells extracellularly. The voltage- and current-clamp methods were suitable for detection of intracellular current- (excitatory postsynaptic current, EPSC) or potential deflections (excitatory postsynaptic potential, EPSP or action potential, AP). For whole-cell recordings, the intracellular solution contained (in mM): K-gluconate 110; NaCl 4; HEPES 20; EGTA 0.1; phosphocreatine-di-(tris) salt 10; Mg-ATP 2; Na-GTP 0.3; spermine 0.1; and 0.2 % biocytin (pH 7.3 adjusted with KOH; osmolarity 290 mOsm/l).

II.4. Comparison of axo-axonic cells and fast-spiking basket cells

Slices were superfused with aCSF containing 5 μM SR 95531 (gabazine) to block $GABA_A$ receptor-mediated conductance. Spontaneous EPSCs (sEPSC) were measured at -60 mV. Cells were stimulated with gradually increasing stimulus intensities near the firing threshold of the cells. The firing threshold of the cells was measured in loose-patch- and current clamp mode. Evoked EPSCs (eEPSC) and EPSPs (eEPSP) were recorded at the resting membrane potential of the cells, which was measured immediately after break-in. We recorded six responses at each stimulus intensity. The required stimulus intensity was generally 5-20 μA. Electrical stimulation of fibers was delivered via a Pt-Ir bipolar electrode (tip diameter of 10-20 μm, Neuronelektród Kft., Budapest, Hungary) every 10 s (0.1 Hz) using a Supertech timer and isolator (Supertech Ltd., Pécs, Hungary). The stimulating electrode was placed into the stratum oriens in the CA3 region in order to stimulate the CA3 recurrent collaterals, but avoid mossy fibers originating from granule cells located mainly in the stratum lucidum. The stimulation site was within 100 μm of the recorded cells.

To obtain a current-voltage (I-V) relationship for EPSCs, an intracellular solution containing (in mM): CsCl 80; Cs-gluconate 60; $MgCl_2 \times 6H_2O$ 1; Mg-ATP 2; HEPES 10; NaCl 3; QX-314Cl 5; spermine 0.1; and 0.2 % biocytin (pH 7.3 adjusted with KOH; osmolarity 290 mOsm/l) was used. We recorded eEPSCs at different holding potentials (at -60, -40, -20, +20 and +40 mV) under control conditions and in the presence of 10 μM NBQX, which is an antagonist of non-NMDA types of ionotropic glutamate receptors. AMPA/KA receptor-mediated synaptic currents were calculated by subtraction of responses measured in the presence of NBQX from control responses. Rectification index was taken as the ratio of AMPA/KA receptor-mediated conductances at -60 mV and +40 mV. The ratio of NMDA receptor-mediated current to all ionotropic receptor-mediated currents was calculated by dividing NMDA receptor-mediated conductances in the presence of NBQX with the size of control EPSCs measured at -40 mV. For isolating evoked inhibitory postsynaptic currents (eIPSCs), an excitatory amino acid receptor blocker kynurenic acid (2-3 mM) was added to the bath solution, while the pipette solution contained in mM: CsCl, 80; Cs-gluconate, 60; NaCl, 3; creatine phosphate, 10; $MgCl_2$, 1; HEPES, 10; ATP, 2 and QX-314Cl, 5 (pH 7.3, 290-300 mOsm/l).

To evaluate the changes in the peak amplitude of evoked postsynaptic currents upon CB_1R activation, control amplitudes in a 2-3 min time window were compared to those measured after 20 min-long drug application for the same period of time. Only those

experiments were included in the analysis that had stable amplitudes at least for 10 min before drug application.

To measure the membrane properties of the cells, we tested the voltage response to a series of hyperpolarizing and depolarizing square current pulses of 800 ms duration and amplitudes between -100 and 100 pA at 10 pA step intervals, then up to 300 pA at 50 pA step intervals and finally up to 600 pA at 100 pA step intervals from a holding potential of -60 mV in each cell. Using these voltage responses, we characterized active and passive membrane properties of AACs and FS BCs (for details, see (Antal *et al.*, 2006; Zemankovics *et al.*, 2010). For each cell, we selected the first response to which the cell was capable to discharge at least 3 APs, and we calculated the AP threshold, the afterhyperpolarization (AHP) amplitude and width at 25, 50 and 75%, and the rheobase. We defined AP threshold as the membrane potential where the velocity of membrane potential change reached 1 mV/ms. AHP is the negative deflection compared to steady state potential observed after APs. Rheobase was defined as the current step the cells required to fire at least 3 APs. The maximal current step was the highest current injection generating firing with lack of distortion. From this response we calculated the AP half width, the spike frequency, the accommodation ratio and the ratio of AP amplitude adaptation. The accommodation ratio was defined as the ratio of the interspike interval of the last two and the first two APs during the current step. The ratio of amplitude adaptation was the ratio of the last and the first AP amplitude. From responses to hyperpolarizing current steps, we calculated the input resistance, membrane time constant, membrane capacitance and relative sag amplitude of the cells. We analyzed the active membrane properties with SPIN software (Antal *et al.*, 2006) and the passive membrane properties with a Matlab script (Zemankovics *et al.*, 2010).

For comparison of the two cell types, data are presented as median and interquartile range. In all cases, the non-parametric Mann-Whitney test was applied, using STATISTICA 11 software (Statsoft, Inc., Tulsa, OK) or Origin 8.6 software (Northampton, MA). Before correlation tests for linear values, the normality of a distribution was tested by the Shapiro-Wilk and Kolmogorov-Smirnov tests. As the tests did not reject normality ($p>0.05$), the Pearson's correlation coefficient was used.

II.5. Investigation of LTD

In experiments studying long-term depression of synaptic inputs onto PV+ interneurons in the hippocampal CA1 region, we blocked $GABA_A$ receptor-mediated inhibitory postsynaptic currents with picrotoxin (70-100 μM) included in the aCSF. To avoid epileptic activity in the lack of inhibition, we used coronal slices, from which we trimmed the CA3 region, because this area is predisposed to generate large synchronous events.

For extracellular stimulation delivered at 0.1 Hz, a theta electrode was filled with aCSF and placed into the stratum radiatum in the CA1 region of the hippocampal slice within 100-200 μm of the recorded pyramidal cells and fast-spiking interneurons (FS INs). Two forms of LTD were studied at excitatory synapses onto CA1 pyramidal cells and FS INs which were identified as FS BCs, AACs or bistratified cells. Spike timing-dependent LTD was induced by a post-pre pairing protocol. Before the pairing, the strength of presynaptic stimulation (varying between 20 μA and 8 mA) was adjusted to evoke EPSCs with amplitudes that were consistently larger than 50 pA. During the pairing protocol, an AP in the postsynaptic neuron was evoked in current-clamp mode followed by stimulation of the excitatory inputs with a 10 ms delay. Altogether 600 pulses were given in six blocks of 100 pairings at a membrane potential between -50 and -58 mV. Pulse frequency was either 5 Hz or 10 Hz, interblock interval was 10 sec. In the second protocol, we induced LTD pharmacologically by perfusing the slices with 10 or 50 μM DHPG for 10 minutes. LTD was defined as the decrease in the amplitude of eEPSCs that could not recover after 20 mins of washout. In some of these chemical LTD experiments, a pair of EPSCs with an inter-stimulus interval of 50 ms was evoked.

All data for each experiment were normalized relative to baseline and reported as mean ± SEM. To evaluate whether the induction protocol readily induced LTD within a given experiment, we compared the peak amplitudes measured in a 10 min-long control, pre-induction period with those peak amplitudes that were determined in the last 5 min of the recordings after 25 min of the LTD using Student's t-test. Experiments involving pretreatments with an enzyme inhibitor (THL) or the receptor antagonists (MPEP, LY367385, AM251, DL-AP5) were analyzed in the same manner. To determine the efficacy of different treatments, EPSC amplitudes during the last 5 min after 25 min of the post-pre pairing or DHPG treatment were compared between the control and the treated groups using independent samples t-test. An alpha level of $p < 0.05$ was considered statistically significant.

Applied chemicals and their concentration: N-(Piperidin-1-yl)-5-(4-iodophenyl)-1-(2,4-dichlorophenyl)-4-methyl-1H-pyrazole-3-carboxamide (AM 251, 2 μM), N-Formyl-L-leucine (1S)-1-[[(2S,3S)-3-hexyl-4-oxo-2-oxetanyl]methyl]dodecyl ester (THL, 10 μM), 2-Methyl-6-(phenylethynyl)-pyridine hydrochloride (MPEP, 10 μM), (S)-(+)-α-Amino-4-carboxy-2-methylbenzeneacetic acid (LY 367385, 100 μM), (S)-3,5-Dihydroxyphenylglycine (DHPG, 10 or 50 μM), DL-2-Amino-5-phosphonopentanoic acid (DL-AP5, 100 μM) and 1,2-bis-(o-Aminophenoxy)-ethane-N,N,N',N'-tetraacetic acid tetrapotassium salt (BAPTA, 20 mM). From the lipofil chemicals we made up stock solutions in DMSO, in the final dilution, the concentration of DMSO was below 0.001%.

II.6. Studying gamma oscillation

To examine the cannabinoid effects on gamma oscillation, experiments were performed using a dual-superfusion recording chamber developed in the laboratory to improve oxygenation of slices (Hájos & Mody, 2009). Oscillatory activities at gamma frequency (25-40 Hz) were induced and maintained by bath application of 10 μM carbachol. Local field potentials and the spiking activity of cells were simultaneously recorded with two patch pipettes filled with aCSF. One pipette was placed within the pyramidal cell layer of the CA3b region at a depth of 100–200 μm to monitor local field oscillations. The other pipette was used under visual guidance to extracellularly detect APs from neurons.

For the analysis of gamma oscillation, power spectra density analysis was performed on 120-180 s epochs. Time windows of 1 s with 50 % overlap were multiplied by a Hanning window before a fast Fourier transform was performed. Peak power and peak frequency at that power value were used for comparison. A custom-written firing phase detection algorithm was used as described in details previously (Gulyás *et al.*, 2010). Spikes recorded in a loose-patch mode for 120-180 s were detected by manually setting the threshold on the unfiltered trace. The negative peak of the trough of the oscillation was considered as phase zero for field potentials band-pass filtered with an RC filter between 5 and 500 Hz. The phase of individual spikes was specified by calculating the position of the unit spikes in relation to two subsequent negative phase time points. The amplitude and the instantaneous frequency of the oscillation varied, and the detection algorithm often skipped one or more oscillation cycles. Therefore, our spike phase detection algorithm checked for the actual detected cycle length and assigned a phase to a spike only if the actual cycle length did not differ from the

mean of the average cycle length by more than a chosen fraction of 0.3 standard deviations of the cycle length. Phase values of individual cells were analyzed by circular statistical methods using Oriana 2.0 software (Kovach Computing Services, Anglesey, UK). Significant deviation from uniform (random) phase distribution along the circle indicated directionality. This was tested with Rao's spacing test and Rayleigh's uniformity test. To characterize a non-uniform distribution, two parameters of its mean vector (calculated from individual observations) were used, the mean angle and the length of the mean vector, i.e., the phase-coupling strength.

Applied chemicals and their concentration: (*R*)-(+)-[2,3-Dihydro-5-methyl-3-(4-morpholinylmethyl)pyrrolo[1,2,3-*de*]-1,4-benzoxazin-6-yl]-1-naphthalenylmethanone mesylate (WIN55,212-2, 1 μM), (-)-*cis*-3-[2-Hydroxy-4-(1,1-dimethylheptyl)phenyl]-*trans*-4-(3-hydroxypropyl)cyclohexanol (CP55,940, 1 μM) and 2,3-dihydroxy-6-nitro-7-sulfamoyl-benzo[f]quinoxaline-2,3-dione; (NBQX, 10 mM).

III. Anatomy

III.1. Identification of the cell types

After recordings, hippocampal slices were fixed overnight in 4% paraformaldehyde in 0.1 M phosphate buffer (PB), pH 7.4. Following fixation, slices were washed with 0.1 M PB several times. Biocytin-filled cells were visualized with Alexa 488- or Alexa 594-conjugated streptavidin (Alexa 488, 1:3000; Alexa 594, 1:1000; Invitrogen, Carlsbad, CA, USA). Neurons were identified based on their dendritic and axonal arborizations. The anatomical classification of CA1 pyramidal neurons and bistratified cells could unequivocally be achieved based on morphological criteria. At this stage we made high resolution 3D images from potential AACs and FS BCs of the CA3 region to reconstruct the dendritic trees with Neurolucida software. We used a FV 1000 Olympus confocal microscope (20x Objective, N.A. =0.75) in z-stack mode with 1-2 μm steps.

To distinguish between AAC and FS BCs, the close proximity of biocytin-labeled axon endings with axon initial segments (AISs) was inspected (Gulyás *et al.*, 2010). AISs were visualized by an immunostaining against the protein Ankyrin-G. Slices were embedded in 1% agar and re-sectioned to 40 μm thickness. The sections were then treated with 0.1 mg/ml pepsin (Cat. No. S3002; Dako, Glostrup, Denmark) in 1 N HCl at 37 °C for 15 min and were washed in 0.1 M PB. Sections were blocked in normal goat serum (NGS, 10%,

Vector Laboratories, Burlingame, CA) made up in Tris-buffered saline (TBS, pH 7.4) followed by incubation in mouse anti-Ankyrin-G (Santa Cruz Biotechnology, Santa Cruz, CA) diluted 1:100 in TBS containing 2% NGS and 0.05% Triton X-100. Following several washes in TBS, Alexa 594-conjugated goat anti-mouse (1:500) or Alexa 488-conjugated goat anti-mouse (1:500) was used to visualize the AISs, depending on the color of biocytin labeling. Maximum intensity z-projection images of 4 confocal stacks were taken using an A1R confocal laser scanning microscope (Nikon Europe, Amsterdam, The Netherlands) and a 60× (NA = 1.4) objective.

III.2. Reconstruction of cells with drawing tube

We reconstructed some representative cells with the aid of a drawing tube using a 40x objective. For this purpose, we performed an immunoperoxidase reaction using diamino-benzidine as chromogene. Slices were washed with 0.1 M PB several times, and incubated in a cryoprotecting solution (30% sucrose in 0.1 M PB; pH: 7.4) for 2 h. Slices were then freeze-thawed three times above liquid nitrogen and treated with 1% H_2O_2 in PB for 15 min to reduce endogenous peroxidase activity. For single biocytin staining, biocytin-filled cells were visualized using avidin-biotin complex with horseradish peroxidase activity (Vector Laboratories). Ammonium nickel sulfate hexahydrate ($(NH_4)_2(NiSO_4)_2x6H_2O$; Sigma) was added to intensify the color reaction of 3-3-diaminobenzidine tetrahydrochloride (0.05% solution in TBS, pH 7.4; Sigma) containing 0.015% H_2O_2.

III.3. Estimating the density of VGluT1-expressing synapses onto biocytin-labeled dendrites

After re-sectioning the slices to 40 μm thickness, sections were blocked in 5% NGS and 5% normal horse serum made up in TBS, pH 7.4, followed by incubation in guinea-pig anti-VGluT1 (1:10,000, Millipore, Billerica, MA) and mouse anti-Bassoon (1:3000, Abcam, Cambridge, UK) antibodies diluted in TBS containing 0.5% Triton X-100. Following several washes in TBS, the sections in which biocytin was developed with Alexa 594-conjugated streptavidin were treated with a mixture of Alexa 488-conjugated donkey anti-mouse and DyLight 405-conjugated donkey anti-guinea pig antibodies (1:500; Jackson ImmunoResearch, Bar Harbor, MA). If biocytin was visualized with Alexa 488-conjugated streptavidin, a

mixture of Cy3-conjugated goat anti-mouse (1:500; Invitrogen, Carlsbad, CA) and DyLight 405-conjugated donkey anti-guinea pig antibodies was applied to the sections. After several washes, sections were mounted on slides in Vectashield (Vector Laboratories). Images were taken using an A1R microscope and a 60× (NA = 1.4) objective. For high magnification images, single confocal images or maximum intensity z-projection images were used (2-3 confocal images at 0.3-3 μm). From 4 AACs, 9 dendritic segments in the stratum oriens, 10 in the strata pyramidale and lucidum and 11 in the stratum radiatum were imaged and investigated. For FS BCs, six dendritic segments were sampled in each layer from 4 FS BCs and analyzed. To improve the quality of the images, deconvolution was carried out with the Huygens Professional program (Hilversum, The Netherlands).

After deconvolution, the number of VGluT1-immunostained boutons forming close appositions with the biocytin-labeled dendrites, where Bassoon staining within the boutons was unequivocally present facing toward the dendrite, was counted using the NIS-viewer software (Nikon Europe). Dendritic surface was calculated by measuring the length, depth and radius of the dendrites with the aid of the NIH ImageJ image analyser software. Bassoon- or VGluT1-positive single stained elements were not counted. After calculating the surface of the dendritic segment, the Bassoon- and VGluT1-double-immunopositive inputs were quantified and normalized to 50 μm^2. Similar results were obtained with the two different mixtures of antibodies, and therefore the data were pooled.

III.4. Neurolucida analysis

Dendrites of biocytin-labeled AACs and FS BCs in the CA3 hippocampal region were reconstructed with Neurolucida 8.0 software using the 3D confocal images taken before re-sectioning. Values were corrected for shrinkage of the tissue. Branched Structure, Convex Hull and Sholl Analyses were performed on the reconstructed dendrites. For Sholl analysis, concentric spheres at 50 μm radius intervals were drawn around the cell, centered at the cell body, and several dendritic parameters were measured independently for each shell. For correlating sEPSC rate with dendrite length in cells, dendrite length at different distances from the soma was calculated as the sum of data in shells obtained in Sholl analysis until the given sphere border.

RESULTS

Differentiation between parvalbumin-positive axo-axonic and fast-spiking basket cells using Ankyrin-G immunostaining

To investigate the properties of PV+ interneurons in hippocampal slices, we used a mouse line expressing eGFP under the control of the PV promoter (Meyer *et al.*, 2002). After whole-cell recordings, the slices were fixed and the biocytin content of interneurons was revealed. The recorded cells were *post hoc* identified based on their proper axonal arborization. The vast majority of PV+ cells were AACs, FS BCs and bistratified cells; however, especially in the CA1 region we observed PV+ O-LM cells as well (Figure 5).

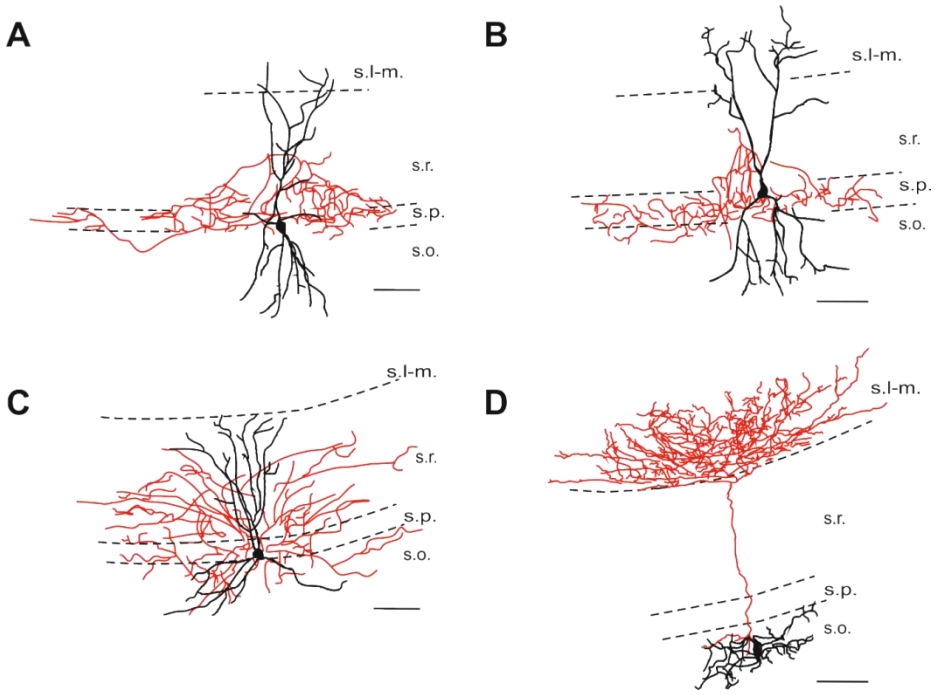

Figure 5. Light microscopic reconstructions of the parvalbumin-positive interneuron types in the CA1 region of the hippocampus. *Representative members of the four morphologically distinct interneuron types showing a FS BC (**A**); an AAC (**B**); a bistratified cell (**C**) and an O-LM cell (**D**). Dendrites are represented in black and axons are visualized in red. Scale bar, 100 µm. s.l-m., stratum lacunosum-moleculare; s.r., stratum radiatum; s.p., stratum pyramidale; s.o., stratum oriens.*

Bistratified cells had axon collaterals in the strata radiatum and oriens, and only sparsely arborized in the pyramidal cell layer (Figure 5C). O-LM cells innervated the stratum lacunosum-moleculare (Figure 5D). FS BCs targeted mainly stratum pyramidale, but their axon collaterals could be traced to the proximal strata oriens, and radiatum in CA1 and also in stratum lucidum in CA3. In the case of AACs, the axon arbor was shifted towards the border of strata pyramidale and oriens, where most of the AISs of pyramidal cells are located (Figure 5A, B, Figure 6A, B). Based on these morphological properties, AACs and FS BCs could not be exactly identified. To unequivocally distinguish AACs and FS BCs, we performed double immunolabeling for biocytin and Ankyrin-G in each case. Ankyrin-G is an anchoring protein (Jenkins & Bennett, 2001) accumulating predominantly in the AIS (Boiko *et al.*, 2007). Interneurons were identified as AACs if the axon terminals of labeled cells formed close appositions with AISs, or as BCs if their axons avoided the Ankyrin-G immunoreactive elements (Figure 6C-E).

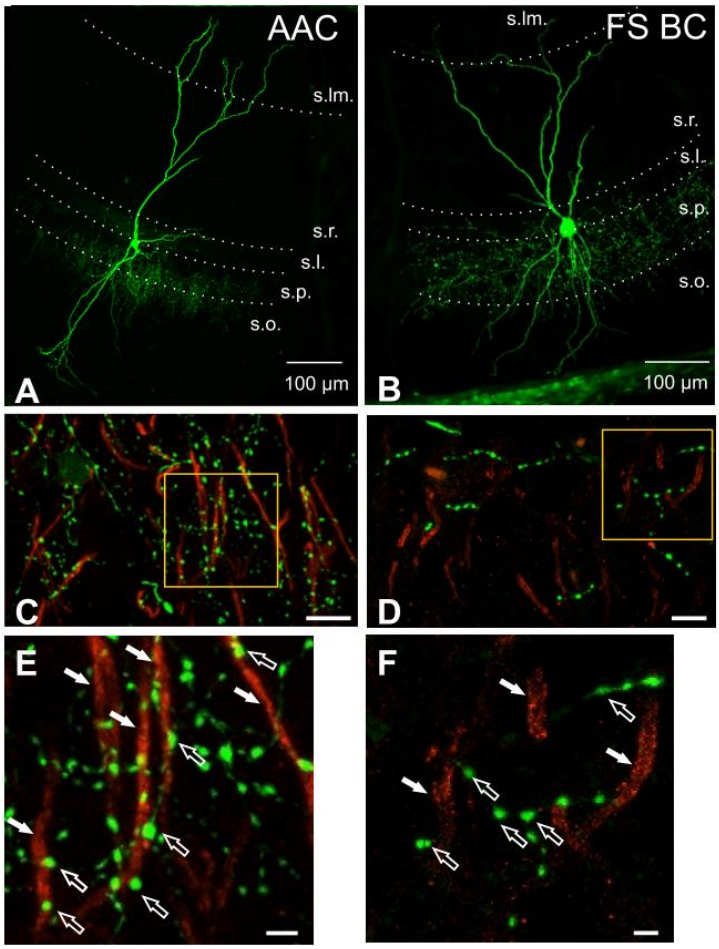

Figure 6. Distinguishing AACs and BCs with Ankyrin-G staining. *Maximum intensity projection of confocal images of a representative AAC,* ***A*** *and a FS BC,* ***B*** *filled with biocytin. Borders of hippocampal layers are indicated with dashed lines. s.o., stratum oriens, s.p., stratum pyramidale, s.l., stratum lucidum, s.r., stratum radiatum, s.lm. stratum lacunosum-moleculare.* ***C,*** *Double immunofluorescent labeling for Ankyrin-G (red) and biocytin (green) shows close appositions of biocytin-filled boutons with axon initial segments (AIS), a characteristic of AACs.* ***D,*** *Same staining as in* ***C,*** *but in this case the biocytin-filled axon terminals avoid the Ankyrin-G-labeled AISs, which characterize FS BCs. Scale bars are 10 µm.* ***E, F,*** *Enlarged pictures of*

*the parts labeled by yellow boxes in **C** and **D,** respectively. Open arrows indicate biocytin-labeled boutons, filled arrows mark Ankyrin-G-stained AIS. Scale bars are 2.5 µm.*

I. Quantitative differences in the convergence of local pyramidal cells onto parvalbumin-positive axo-axonic- and basket cells in the hippocampal CA3 subfield

I.1. Membrane properties of AACs and FS BCs in the hippocampal CA3 region

From the voltage responses upon the injection of a series of hyperpolarizing and depolarizing square current pulses into the interneurons, we first determined the active and passive membrane properties of AACs and FS BCs (Figure 7A-C, Table 1).

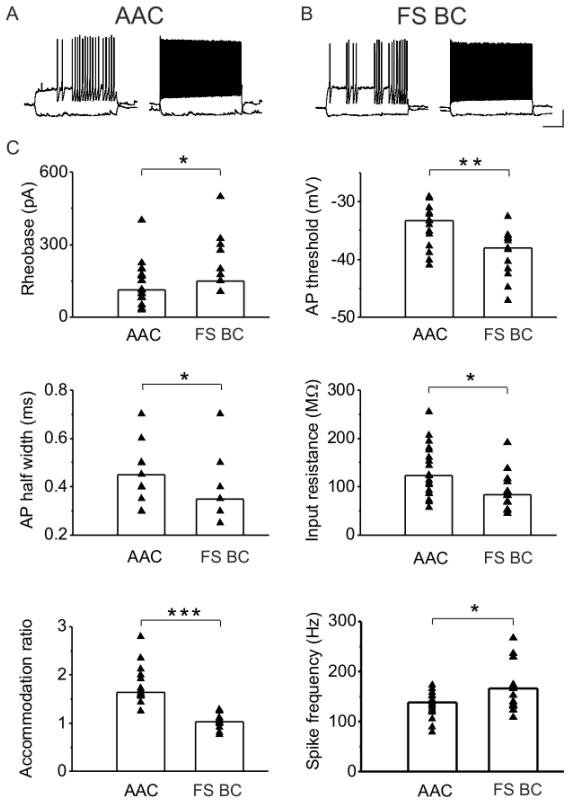

Figure 7. The single-cell properties of AACs and FS BCs are distinct in the CA3 region of mouse hippocampus. A, B, *Voltage responses to hyperpolarizing (100 pA) or depolarizing (200 pA and 600 pA) current steps, in AAC (**A**) and FS BC (**B**). Calibrations, 200 ms and 20 mV. **C**, Single-cell properties that were found to be distinct in the two cell types. Here on the graphs and in Figures 8-13 each triangle represents a value from an individual cell, bars show the median of values in each group and asterisks indicate significant differences. Comparison of rheobase (p=0.036) action potential (AP) threshold (p=0.0015), AP half-width (p=0.044), input resistance (p=0.019) accommodation ratio (p<0.001) and spike frequency (p=0.028) are shown. Significance levels here and in and in Figures 8-13: *: p<0.05, **: p<0.01, ***: p<0.001.*

Table 1. Membrane properties of PV+ interneurons innervating the perisomatic region of pyramidal cells in the CA3 region of the hippocampus. *Data are presented as the median with the first and third quartiles in parentheses. Significant differences ($p<0.05$) shown in bold were determined with the Mann-Whitney test.*

	AAC	n	FS BC	n	p
Rheobase (pA)	**113 (80-188)**	**20**	**150 (150-275)**	**13**	**0.036**
AP threshold (mV)	**-33.3 (-37.7--31.95)**	**15**	**-38 (-41.6--36.3)**	**13**	**0.0015**
AHP ampl. (mV)	19.95 (15.3-21.3)	15	19.6 (16.7-21.4)	13	0.765
AHP 25% decay (ms)	**10.65 (7.03-18.8)**	**20**	**5.8 (4.6-6.85)**	**13**	**0.019**
AHP 50% decay (ms)	**20.75 (14.03-40)**	**20**	**9.7 (7.75-11.2)**	**13**	**0.016**
AHP 75% decay (ms)	**30.15 (16.58-69.65)**	**20**	**13.5 (10.7-17.3)**	**13**	**0.020**
AP half-width (ms)	**0.45 (0.4-0.5)**	**20**	**0.35 (0.3-0.4)**	**13**	**0.044**
Spike frequency (Hz)	**138 (120-148)**	**20**	**166 (134-174)**	**13**	**0.028**
Accommodation ratio	**1.64 (1.58-2.00)**	**15**	**1.03 (0.99-1.11)**	**13**	**$1.2*10^{-5}$**
Ratio of AP amplitude adaptation	0.69 (0.52-0.8)	15	0.65 (0.62-0.73)	13	0.596
Resting membrane potential (mV)	-46.5 (-50--43)	36	-45 (-50--40)	24	0.154
Input resistance (MOhm)	**122.7 (86.5-175.6)**	**19**	**82.7 (67.1-111)**	**8**	**0.019**
Membrane time constant (ms)	13.71 (10.04-16.38)	15	13.15 (10.71-14.13)	13	0.674
Membrane capacitance (pF)	103.9 (72.7-148.7)	15	151.4 (86-204.4)	13	0.322
Relative sag amplitude	0.227 (0.130-0.258)	15	0.280 (0.091-0.336)	13	0.512

We found that the rheobase of FS BCs was significantly higher, whereas their AP threshold was lower than that of AACs in response to rheobase current steps. The AHP shape of FS BCs was narrower, as indicated by significantly shorter AHP widths at 25, 50 and 75% of the amplitude. In contrast, we found no differences in the AHP amplitude. At maximal current injection, the half width of APs in FS BCs was significantly shorter, and these cells displayed significantly higher AP frequency with lower accommodation than AACs.

Adaptation in the amplitude of APs was not different between cell types. The resting membrane potential of AACs and FS BCs was identical. The membrane time constant, capacitance and relative sag amplitude of the two cell types were similar, but FS BCs had a significantly lower input resistance (Table 1).

As AACs had a higher AP threshold than FS BCs in response to near-threshold current steps, we sought to find a possible difference in the structural organization of the AIS. We examined the length of the Ankyrin-G-immunopositive segment and the distance of its beginning from the soma, since previous studies have shown that these features could correlate with the variability in AP threshold (Grubb & Burrone, 2010; Kuba *et al.*, 2010). The investigation revealed that the length of the Ankyrin-G-immunopositive segment in the AISs and the distance of its beginning from the soma were not different between AACs and FS BCs, suggesting that these structural properties of the AIS are not responsible for the difference observed in the AP threshold (Table 3).

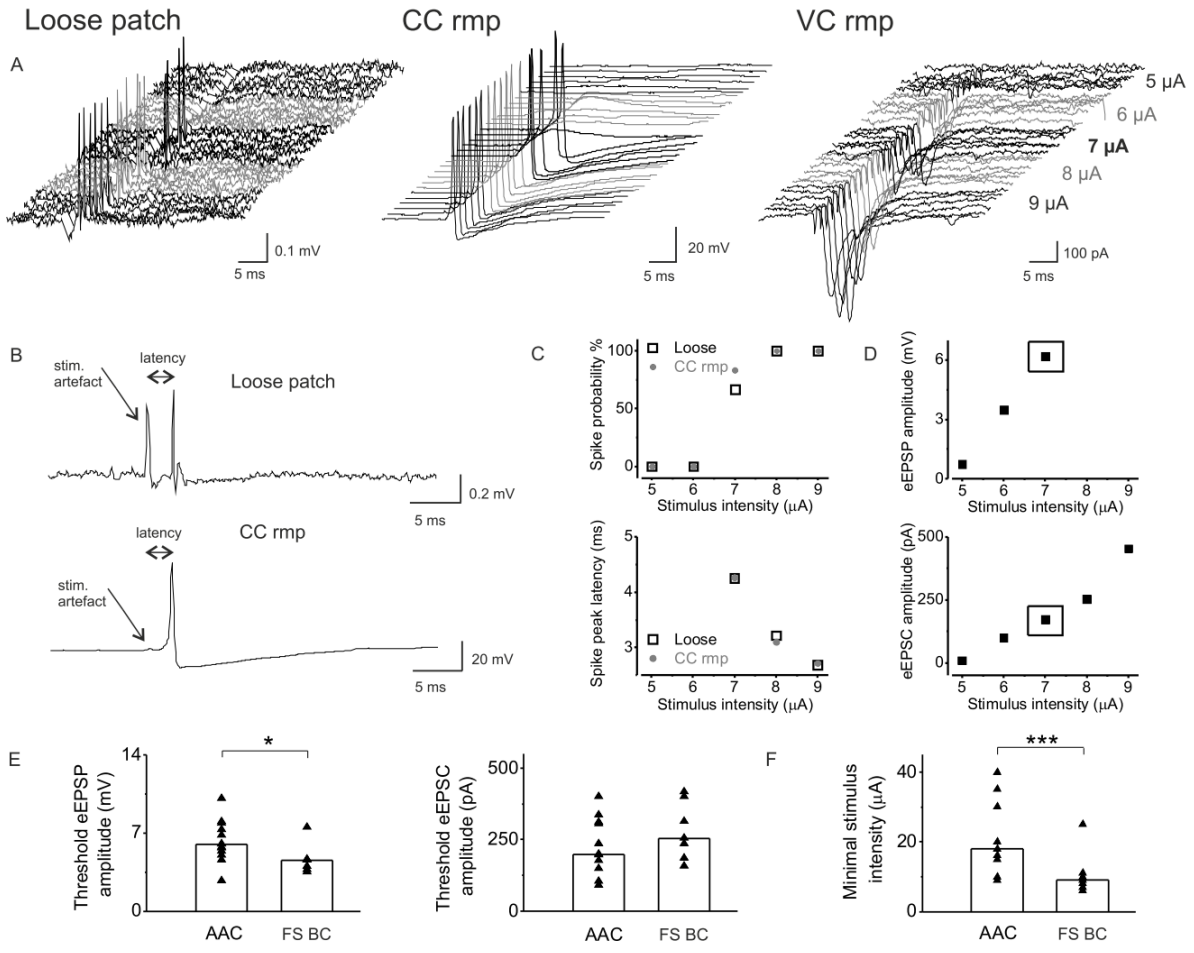

Figure 8. Determining the magnitude of excitatory synaptic inputs at spiking threshold in AACs and FS BCs. A*, Family of responses obtained in a representative cell upon focal stimulation of fibers with increasing stimulus intensities in loose-patch, current-clamp or voltage-clamp mode. Rmp, resting membrane potential.* ***B****, Examples of discharging a cell in loose-patch and current-clamp mode. AP latencies (i.e. spike peak latency) detected extra- or intracellularly were calculated as the time between the beginning of the stimulus artifact and the AP peak.* ***C****, Comparison of the probability and the peak latency of spikes recorded extra- and intracellularly in the same cell in response to equivalent, gradually increasing stimulus intensities. Open squares show average values of six consecutive loose-patch measurements at each stimulus intensity, while filled gray circles indicate corresponding current-clamp data.* ***D****, The amplitude of evoked EPSPs and EPSCs linearly increased as a function of stimulus intensity. We determined the size of EPSP/Cs and stimulus intensities needed to discharge the cells (7μA, outlined with square frames) from the EPSP/C amplitude vs. stimulus intensity curves* ***E****, Comparison of the amplitude of EPSPs (p=0.027) and EPSCs (p=0.257) at spike threshold in AACs and FS BCs. F, Lower stimulus intensities were needed to discharge FS BCs compared to AACs (p=0.001).*

I.2. FS BCs receive a higher number of proximal excitatory synaptic inputs than AACs

Next, we aimed to establish the magnitude of excitatory synaptic inputs necessary to evoke an AP in AACs and FS BCs. To this end, we stimulated CA3 recurrent collaterals in the stratum oriens with gradually increasing stimulus intensities and recorded first in loose-patch mode, followed by measurements obtained in current-clamp and voltage-clamp mode (Figure 8A, B). The stimulus intensity necessary to induce spiking in cells using extra- or intracellular recordings showed a strong correlation (minimal stimulus intensity for AACs, r^2=0.977, p<0.001, n=7; for FS BCs, r^2=0.8, p=0.004, n=7; maximal stimulus intensity for AACs: r^2=0.682, p=0.013, n=7; for FS BCs, r^2=0.965, p<0.001, n=6; Figure 8C), suggesting that whole-cell recordings did not significantly perturb spiking properties or excitatory synaptic transmission. This allowed us to determine the EPSP and EPSC amplitude at AP threshold. Thus, by measuring the size of synaptic inputs in whole-cell mode at those stimulus intensities that were needed to evoke AP firing, we could compare the properties of excitatory synaptic inputs at spiking threshold in AACs and FS BCs (Figure 8D).

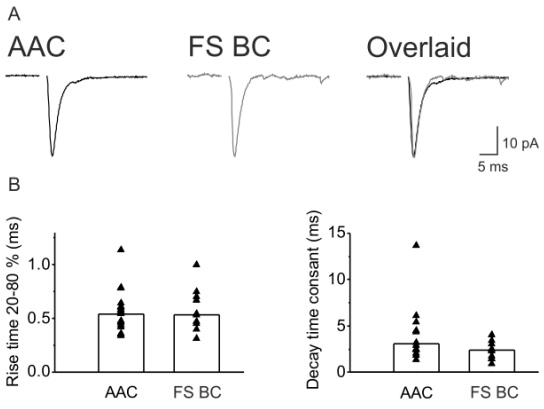

Figure 9. Kinetic properties of EPSCs evoked by focal stimulation of fibers in the stratum oriens in AACs and FS BCs are similar. A, *Representative EPSCs at spike threshold in an AAC and a FS BC averaged from 6 consecutive traces.* ***B,*** *20-80% rise time (p=0.780) and decay time constant (p=0.101) of evoked EPSCs in AACs and FS BCs were not different.*

We found that the magnitude of the electrically evoked EPSPs necessary to discharge the cell at the resting membrane potential was smaller in FS BCs than in AACs (Figure 8E, Table 2). In contrast, the EPSC amplitudes evoked under the same conditions in both interneuron types were similar. Importantly, evoking APs in FS BCs required significantly lower stimulus intensities than in AACs (Figure 8F), but the maximal values for EPSPs and EPSCs, which could be triggered by focal stimulation, were comparable (Table 2). These data suggest that there are some differences in the excitatory synaptic inputs to these two types of PV+ interneurons.

In the next set of experiments, our goal was to clarify the kinetics of evoked EPSCs eEPSCs and the ratio of AMPA and NMDA receptor-mediated currents in PV+ interneurons. Our analysis revealed that the 20-80 % rise time and decay time constant of EPSCs evoked in AACs and FS BCs at the membrane potential of -60 mV was similar (Figure 9, Table 2). In addition, we obtained the I-V curves for AMPA receptor-mediated synaptic currents by measuring the EPSC amplitudes in the absence and presence of NBQX (5 μM; Figure 10A, B), and subtracting the NMDA receptor-mediated component from the averaged traces obtained under drug-free conditions. In both interneuron types, the AMPA receptor-mediated synaptic currents showed strong inward rectification in a similar manner (Figure 10B, C Table 2), indicating that AMPA receptors with high Ca^{2+} permeability should mediate fast EPSCs (Geiger *et al.*, 1995). Furthermore, we also compared the proportion of NMDA receptor-mediated currents in the evoked synaptic responses and found no difference between the two cell types (Figure 10C, Table 2). These results propose that EPSCs in AACs and FS BCs are mediated via ionotropic glutamate receptors with similar properties.

Table 2. Properties of excitatory synaptic inputs recorded in AACs and FS BCs. *Data are presented as the median with the first and third quartiles in parentheses. Significant differences ($p<0.05$) shown in bold were determined with the Mann-Whitney test.*

	AAC	n	FS BC	n	p
Amplitude of threshold eEPSP (mV)	**6 (5.21-7.6)**	**13**	**4.58 (3.74-4.64)**	**7**	**0.027**
Amplitude of threshold eEPSC (pA)	199 (149-312)	11	255 (186-402)	7	0.257
Amplitude of maximal eEPSC (pA)	350 (205-800)	27	475 (360-650)	18	0.701
Stimulus intensity at AP threshold (μA)	**18 (15-32.5)**	**16**	**9 (7-11)**	**10**	**0.001**
20-80 % rise time of eEPSC (ms)	0.54 (0.44-0.61)	19	0.53 (0.4-0.7)	11	0.780
Decay time constant of eEPSC (ms)	3.06 (2.43-4.47)	14	2.38 (1.46-3.07)	10	0.101
Rectification index of AMPA rec.-mediated currents	0.195 (0.1-0.3)	18	0.105 (0.01-0.35)	6	0.424
Ratio of NMDA/AMPA currents	0.105 (0.067-0.2)	18	0.215 (0.086-0.49)	6	0.257
Peak amplitude of sEPSC (pA)	23.61 (19.34-28.03)	6	27.65 (19.88-30.85)	6	0.689
Interevent interval of sEPSC (ms)	**0.056 (0.038-0.134)**	**6**	**0.023 (0.016-0.030)**	**6**	**0.013**
20-80 % rise time of sEPSC (ms)	0.347 (0.253-0.447)	6	0.369 (0.353-0.374)	6	0.575
Decay time constant of sEPSC (ms)	1.83 (1.67-2.14)	6	2.07 (1.99-2.34)	6	0.171

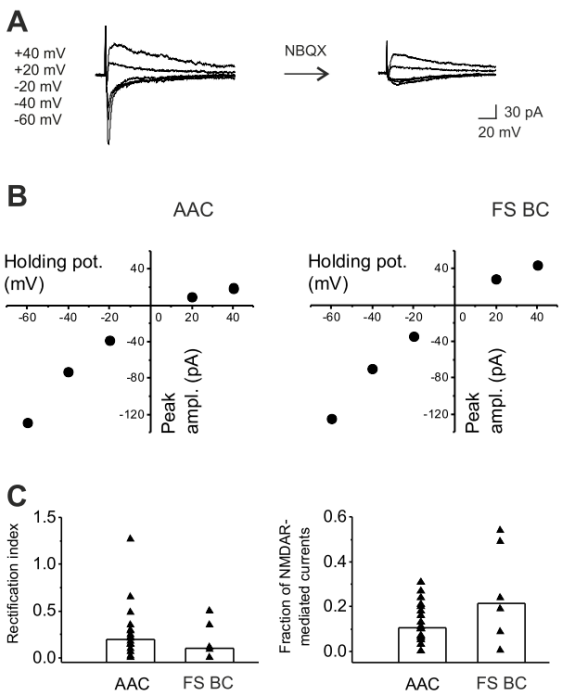

Figure 10. AMPA and NMDA receptor-mediated synaptic currents in AACs and FS BCs are comparable. A, *EPSCs evoked by focal stimulation in a cell at different holding potentials in the absence or presence of 5 μM NBQX. Traces are averages of 6 consecutive sweeps.* ***B,*** *Examples of I-V curves obtained in an AAC and a FS BC.* ***C,*** *Rectification indices for AMPA receptor-mediated synaptic currents (p=0.424) and the fraction of NMDA receptor-mediated synaptic currents in the evoked synaptic responses (p=0.257) in AACs and FS BCs were similar.*

To further examine the features of excitatory synaptic inputs received by PV+ cells, we recorded spontaneously occurring EPSCs (sEPSCs) in AACs and FS BCs (Figure 11A). In agreement with our eEPSC parameter data, the peak amplitude, 20-80% rise time and decay time constant of sEPSC were comparable in both interneuron types (Figure 11B, Table 2). In contrast, the interevent interval of sEPSCs measured in FS BCs was significantly lower, and thus the sEPSC rate was higher, compared to that recorded in AACs (Figure 11B, Table 2). These observations indicate a higher number of excitatory synaptic inputs in FS BCs compared to AACs.

I.3. The density of excitatory synapses on the proximal dendrites of AACs and FS BCs is similar

The higher sEPSC rate and the lower stimulus intensity required for AP generation by focal stimulation in FS BCs propose that the number of excitatory synaptic inputs received by the proximal parts of FS BCs might be higher compared to AACs. This difference can be due to the fact that the dendrites of FS BCs might be covered with excitatory synapses more densely, but the length of proximal dendrites is similar in both cell types. Alternatively, the

density of excitatory synaptic inputs can be similar for both cell types, but the proximal dendrites of FS BCs may be longer or more numerous than of AACs. To distinguish between these two possibilities, we estimated the density of excitatory synapses received by the dendrites of both cell types. We calculated the number of VGluT1- and Bassoon-double-immunopositive axon endings forming close appositions with the biocytin-labeled dendrites of PV+ cells. VGluT1 is a marker for cortical excitatory synapses (Kaneko & Fujiyama, 2002; Fremeau *et al.*, 2004), while Bassoon is present at the presynaptic active zone (tom Dieck *et al.*, 1998; Richter *et al.*, 1999), allowing us to determine whether synapses in the axon endings are indeed closely apposed to the biocytin-filled dendrites or face unlabeled profiles (Figure 12A, B). We randomly sampled biocytin-positive dendritic segments in three different layers (stratum oriens, proximal region -including strata pyramidale and lucidum- and stratum radiatum) and found a similar number of excitatory axon endings apposed to both cell types (Figure 12G, Table 3). In conclusion, our data show that the density of VGluT1-immunopositive axon endings on the proximal dendrites of both AACs and FS BCs is similar.

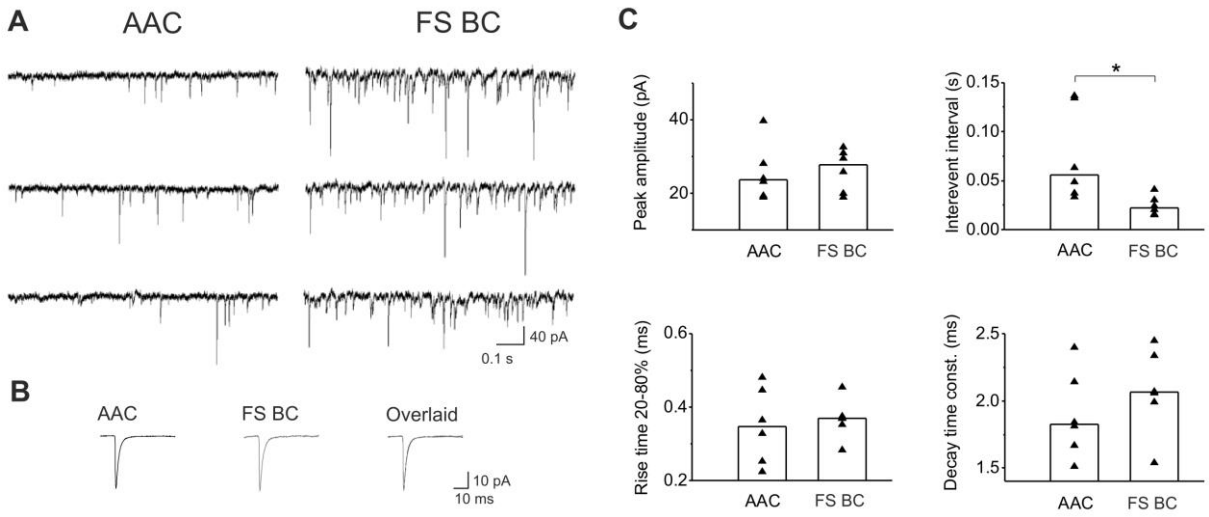

Figure 11. Comparison of sEPSC properties. A, *Representative sEPSC recordings obtained in AACs and FS BCs.* ***B,*** *Averages of 600 consecutive sEPSC events from the same recordings as in* ***A****.* ***C,*** *Peak amplitude (p=0.689), interevent interval (p=0.013), 20-80% rise time (p=0.575) and decay time constant (p=0.171) of sEPSCs in AACs and FS BCs are plotted.*

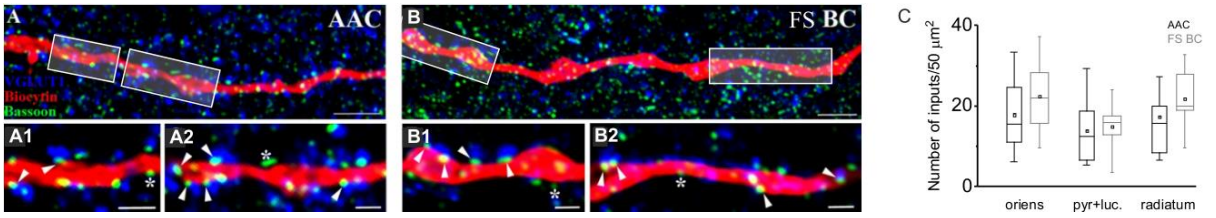

Figure 12. Excitatory synapse density on the proximal dendrites of AACs and FS BCs is similar. A, B, *Triple immunofluorescent labeling for VGluT1 (blue), Bassoon (green) and biocytin (red). Scale bars are 6 µm.* ***A1, A2, B1, B2*** *Contact sites on dendrites at higher magnification. Scale bars are 2 µm. Arrowheads indicate putative excitatory terminals expressing VGluT1 together with Bassoon labeling, which faces toward the labeled dendrites, indicating the presence of synaptic contacts. Asterisks mark VGluT1-immunonegative (putative inhibitory or subcortical) axon endings terminating on the labeled dendrites.* ***C,*** *Glutamatergic input density on the labeled dendrites in stratum oriens (p=0.377), strata pyramidale and lucidum (p=0.786), and stratum radiatum (p=0.092) obtained from 4 AACs and 4 FS BCs. Values derived from AACs are indicated in black, while those from FS BCs are gray. Here on the box charts and in Figure 13, the mean (small open square), the median (midline of the big box), the interquartile range (large box), and the 5/95% values (end of the whiskers) are shown.*

I.4. FS BCs have significantly longer dendrites with a more extensive proximal arborization compared to AACs

Since we have not observed any difference in the density of excitatory synapses received by the dendrites of the two interneuron types, we next investigated the structure of the dendritic trees of AACs and FS BCs to clarify the possible reasons underlying the difference in sEPSC rate and the stimulus intensities needed to discharge them (Table 3). We reconstructed the dendritic arbor of biocytin-filled cells with the Neurolucida software using the 3D confocal images taken from the recorded neurons (Figure 13A). We measured several dendritic parameters including total dendritic length, dendritic length in each hippocampal layer (Figure 13B) or as a function of dendritic order, number of dendrites, number of nodes (Figure 13C), soma surface, and the highest order dendritic segment with Branched Structure Analysis. The volume occupied by the cells was measured with Convex Hull Analysis and the

number of apical and basal intersections as a function of distance from the soma was analyzed using Sholl Analysis (Figure 13D). We found that the soma surface of AACs and FS BCs was similar (Figure 13B). In contrast, the dendrites of FS BCs were longer by 50% compared to that observed for AACs, which was due to significantly longer dendrites in strata oriens and radiatum (Table 3). In addition, the 3rd and 5th order dendrites of FS BCs were longer and more numerous, while their 2nd and 4th order dendrites had more nodes than AACs (Figure 13C). These observations are in accordance with the Sholl Analysis, which also revealed a higher number of dendrite: shell intersections in FS BC proximal regions, both in the strata radiatum and oriens. Median values of apical and basal intersections for the two PV+ cell types indicated that in FS BCs, both the apical and basal parts of the dendrites exhibited more extensive arborization closer to the cell body. In contrast, the distal dendrites of AACs in the apical part, closer to or within the stratum lacunosum-moleculare ramified more intensely than that of FS BCs. This was supported by the significantly higher ratio of distal versus proximal intersections in AACs (i.e. at 300/150, 350/150, 300/200, 350/200 μm; Table 3). We found no difference in the highest order of dendritic segments, indicating that the total branching number is similar, but the structure of branching is different. Consistently, Convex Hull Analysis showed that the occupied volume of the two cell types is equal. Thus, FS BCs tend to be more ramified and more symmetric, while AACs are more polarized with a characteristic tuft in the apical part of their dendrites. This structural difference observed for FS BCs, especially the longer dendrites and denser proximal arborization could explain the higher rate in sEPSC occurrence and the lower stimulus intensities necessary to evoke APs in them by focal stimulation of fibers in the stratum oriens.

If this assumption is valid, then the number and/or length of proximal dendrites should correlate with the rate of sEPSCs. Indeed, we found positive correlation between the sEPSC rate and the dendritic length at distances of 50 and 100 μm from the soma (at 50 μm, $r=0.82$, $p=0.014$; at 100 μm, $r=0.75$, $p=0.03$; Figure 14A, B). Up to 300 μm, the correlation was less strong (at 150 μm, $r=0.68$, $p=0.061$; Figure 14C, at 200 μm, $r=0.66$, $p=0.075$; at 250 μm, $r=0.67$, $p=0.067$), but was also significant at 300 μm ($r=0.73$, $p=0.039$). At 350 μm from the soma, there was no correlation between dendritic length and sEPSC rate ($r=0.54$, $p=0.169$; Figure 14D). These results raise the possibility that the larger number of excitatory synaptic inputs received by FS BCs is due to their longer dendritic tree.

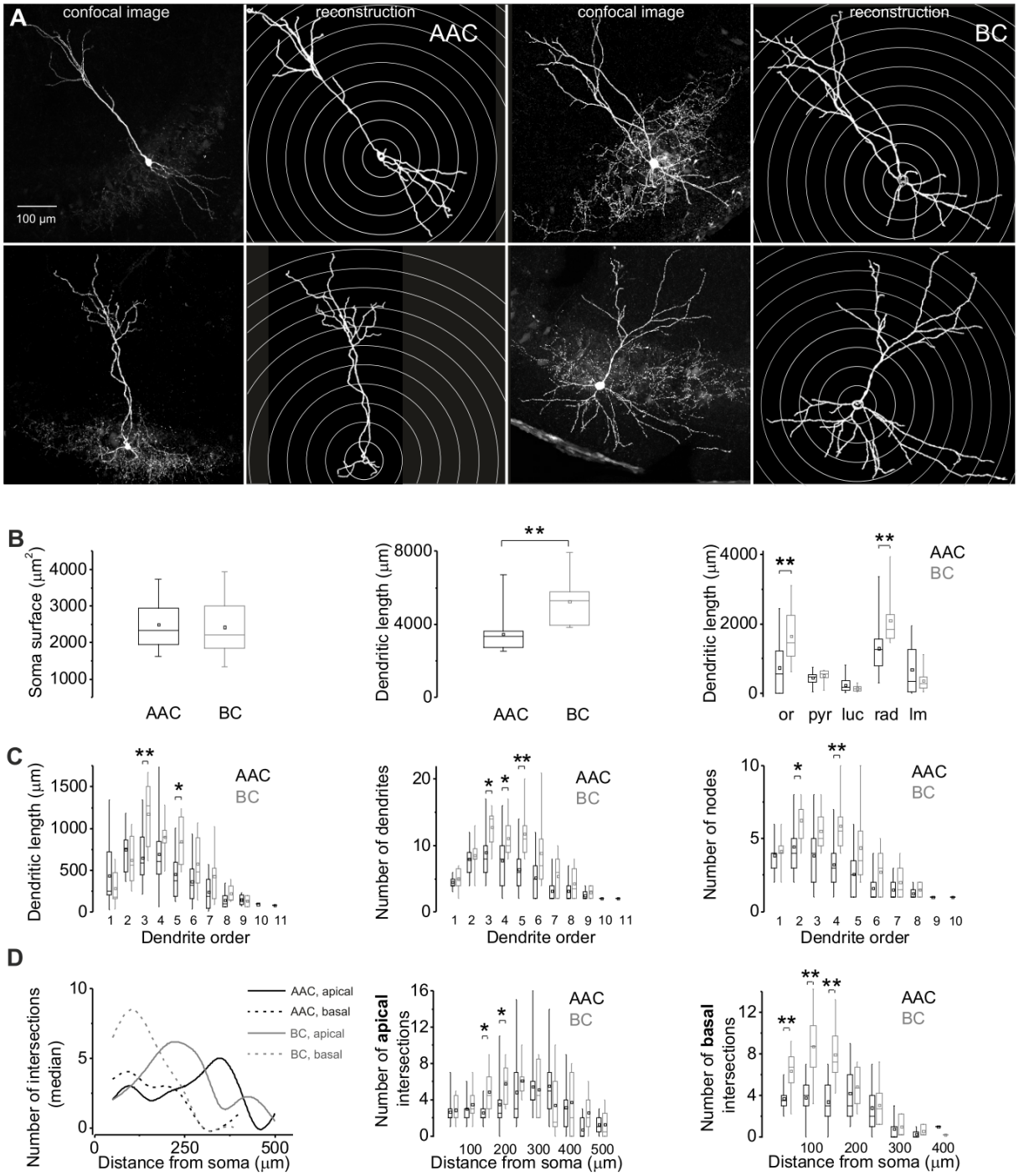

Figure 13. Dendritic arborization of AACs and FS BCs are distinct. A, *Maximal intensity projection confocal images of two AACs and two FS BCs and their dendrites reconstructed with Neurolucida software. Concentric spheres drawn on the reconstructions illustrate the radii used for Sholl Analysis.* ***B,*** *Box chart comparison of soma surface (p=0.061), total dendritic length (p=0.004), and dendritic length in different hippocampal layers obtained from 15 AACs and 8 FS BCs (or, stratum oriens: p=0.010, rad, stratum radiatum: p=0.007).*

C, *Comparison of the dendritic length, the number of dendrites and the number of nodes between the two PV-positive interneuron types as a function of dendritic order.* ***D,*** *Results of Sholl Analysis. Left: a summary graph of the number of the intersections on the apical or basal dendrites as a function of radial distance from the soma; middle and right: the number of intersections on the apical or basal dendrites is shown separately as a function of distance from the soma.*

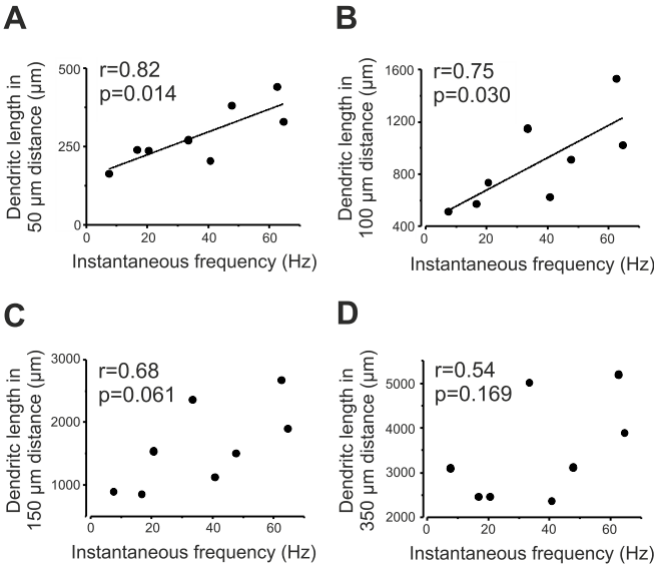

Figure 14. Relationship between the sEPSC rate recorded in individual cells and their dendritic length in different distances (50, 100, 150 and 350 µm) from the soma. *Lines in graphs indicate significant correlations.*

Table 3. Morphological analysis of AACs and FS BCs. *Data are presented as the median with the first and third quartiles in parentheses. Significant differences (p<0.05) shown in bold were determined with the Mann-Whitney test.*

	AAC	n	FS BC	n	p
AIS length (µm)	29.05 (22.45-38.75)	8	28.45 (24.6-33.3)	6	0.746
Dist. of AIS from soma (µm)	4.35 (3.35-11.3)	8	6.8 (2.8-9.8)	6	1
# of inputs/50 µm^2 in str. oriens	15.40 (11.01-24.59)	9	21.95 (15.77-28.19)	6	0.377
# of inputs/50 µm^2 at prox. region	12.44 (6.51-18.76)	10	15.80 (12.78-17.47)	6	0.786
# of inputs/50 µm^2 in str. radiatum	15.66 (8.45-19.99)	11	19.92 (18.99-27.9)	5	0.257
Surface of soma (µm^2)	2329 (1957-2940)	9	3428 (2686-4990)	8	0.061

Total dendritic length (μm)	**3325 (2743-3614)**	**15**	**4978 (3656-5480)**	**8**	**0.004**
Dendritic length in str. oriens(μm)	**570 (0.1-1222)**	**15**	**1493 (1025-2358)**	**8**	**0.010**
Dendritic length in str. pyr. (μm)	480 (333-541)	15	565 (455-675)	8	0.186
Dendritic length in str. luc. (μm)	179 (97-374)	15	132 (78-219)	8	0.420
Dendritic length in str. rad. (μm)	**1259 (805-1571)**	**15**	**1877 (1563-2363)**	**8**	**0.007**
Dendritic length in str. lm. (μm)	337 (40-1259)	15	292 (113-581)	8	0.457
Dendritic length at 3rd order (μm)	**587 (448-896)**	**15**	**1271 (764-1561)**	**8**	**0.006**
Dendritic length at 4th order (μm)	601 (405-920)	14	895 (810-995)	8	0.094
Dendritic length at 5th order(μm)	**376 (179-649)**	**14**	**829 (546-1171)**	**8**	**0.013**
# of dendrites at 3rd order	**8 (6-10)**	**15**	**14 (9.75-14.75)**	**8**	**0.017**
# of dendrites at 4th order	**8 (4-10)**	**14**	**10 (8.5-13.5)**	**8**	**0.047**
# of dendrites at 5th order	**6 (4-8)**	**14**	**11 (8.5-13.5)**	**8**	**0.004**
# of nodes at 2nd order	**4 (3-5)**	**15**	**7 (4.5-7)**	**8**	**0.027**
# of nodes at 3rd order	4 (2-5)	14	5 (4.25-6.75)	8	0.051
# of nodes at 4th order	**3 (2-4)**	**14**	**5.5 (4.25-6.75)**	**8**	**0.004**
The highest order of dendr. segments	7 (6-9)	15	7.5 (7-8.75)	8	0.575
# of apical inters. at 150 μm	**2 (1.75-3.25)**	**14**	**4.5 (3-7.25)**	**8**	**0.020**
# of apical inters. at 200 μm	**2.5 (2-4.25)**	**14**	**6 (3.25-7.75)**	**8**	**0.033**
# of basal inters. at 50 μm	**3.5 (3-4.25)**	**14**	**6.5 (5-7.75)**	**8**	**0.009**
# of basal inters. at 100 μm	**4 (3-5)**	**14**	**8.5 (6.25-10.75)**	**8**	**0.003**
# of basal inters. at 150 μm	**3 (1.5-5.5)**	**13**	**7 (5.5-10.25)**	**8**	**0.004**
convex hull volume (μm^3)	$1.24*10^7$ (10^7-$1.8*10^7$)	15	$2.11*10^7$ ($1.33*10^7$-$2.67*10^7$)	8	0.165
Ratio of apical intersections, 300/150 μm	**2 (1.46-3)**	**14**	**0.95 (0.51-2.06)**	**10**	**0.049**
Ratio of apical intersections, 350/150 μm	**2.5 (1.19-3.75)**	**14**	**0.5 (0.16-1.83)**	**9**	**0.025**

Ratio of apical intersections, 300/200 μm	**1.73 (1.4-2)**	**14**	**0.94 (0.45-1.5)**	**10**	**0.021**
Ratio of apical intersections, 350/200 μm	**1.93 (0.79-3.13)**	**14**	**0.33 (0.15-1.21)**	**9**	**0.037**

II.: Investigating long-term depression of excitatory synaptic inputs onto parvalbumin-positive interneurons

In the next set of experiments, we investigated whether the excitatory synaptic inputs onto PV+ cells can undergo long-term changes, focusing specially on long-term depression of synaptic transmission. LTD of excitatory synaptic inputs in pyramidal cells has been established formerly (Dunwiddie & Lynch, 1978; Dudek & Bear, 1992; Mulkey & Malenka, 1992; Bashir *et al.*, 1993), and various types of LTD has been described in hippocampal interneurons (McMahon & Kauer, 1997b; Laezza *et al.*, 1999; Gibson *et al.*, 2008; Le Duigou *et al.*, 2011; Edwards *et al.*, 2012). However, the existence of LTD in fast-spiking PV+ interneurons is still debated (Lu *et al.*, 2007; Nissen *et al.*, 2010).

We conducted these experiments in the CA1 region of the hippocampus, where -as I mentioned above- we found numerous fast-spiking bistratified cells and a few O-LM cells among PV+ interneurons expressing eGFP. As recordings obtained in AACs, FS BCs and bistratified cells were statistically not different, in this study we pooled the results and we refer them as those measured in fast-spiking interneurons (FS INs). Results recorded in O-LM cells are not presented in this thesis.

II.1. Spike timing-dependent LTD at excitatory synapses has higher induction threshold in FS INs compared to pyramidal cells

We evoked LTD at synapses formed by Schaffer collaterals stimulating in the stratum radiatum of the hippocampal CA1 region. We applied a post-pre pairing protocol when a postsynaptic spike was followed by a presynaptic input with a delay, repeated several times. We first evoked excitatory currents in the postsynaptic neuron by focal electrical stimulation. After a 10 min-long baseline period, we switched to current-clamp mode and evoked APs in the postsynaptic neuron, which were followed by extracellularly evoked EPSPs. To monitor potential changes in the EPSC amplitude after pairing of the neuronal firing with the presynaptic excitatory input, we then switched back to voltage-clamp mode and continued recording for another 20-30 min. EPSC amplitudes recorded during the last 5 minutes of this

recording period were compared with amplitudes during the pre-stimulation period (for details, see Figure 15A and Materials and Methods).

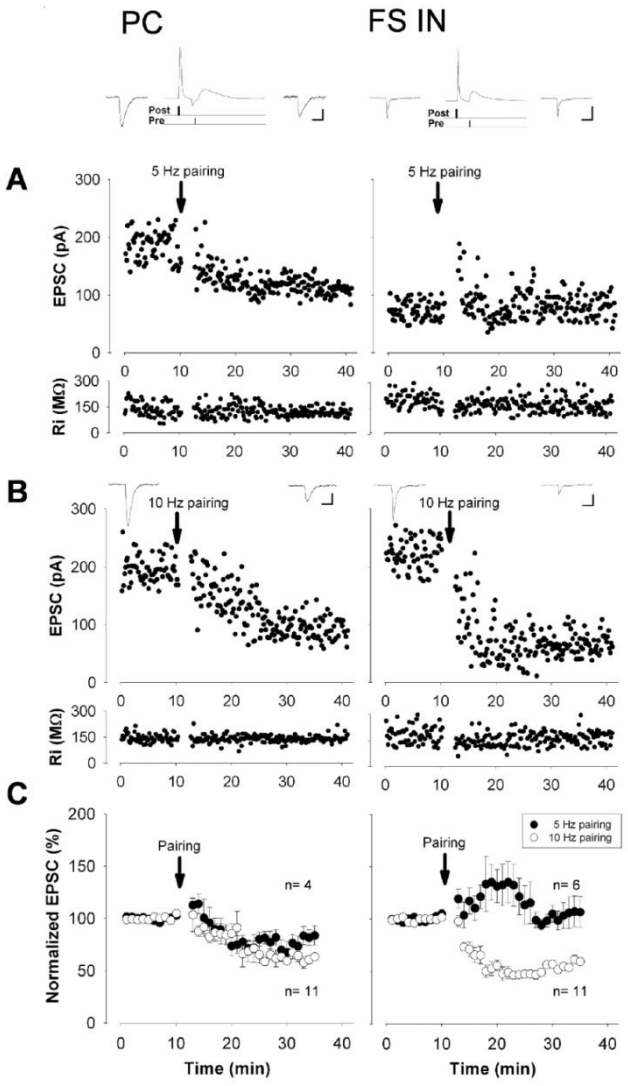

Figure 15. Differences of tLTD induction at excitatory synapses onto pyramidal cells (PC) and FS INs in the CA1 subfield of the hippocampus. A, *Representative experiments showing the presence or absence of long-lasting changes in EPSC amplitude after pairing of action potential discharge with stimulation of excitatory fibers at 5 Hz. Time graphs of EPSC amplitude and input resistance recorded in different cell types. Inserts above the graphs depict the averaged records of five consecutive EPSCs taken just before and 25 min after the pairing, respectively. In between, the schematic drawings of the post-pre pairing protocol together with the corresponding responses are also presented.* ***B,*** *If the postsynaptic cell firing was paired with the presynaptic input at 10 Hz, tLTD was induced in each cell type.* ***C,*** *Summary graphs of percent change of EPSC amplitude after pairing the postsynaptic firing with the presynaptic stimulation at 5 or 10 Hz is illustrated in comparison with baseline values before pairing. In pyramidal cells, both protocols induced tLTD. In contrast, only the 10 Hz, but not the 5 Hz pairing protocol induced tLTD in interneurons. For details see Table 4. All data points on the plots represent a mean ± SEM of six consecutive events. Differences in baseline values in case of individual cells are likely due to their different inputs. Scale bars, 10 ms and 60 pA.*

Postsynaptic APs paired with EPSPs arriving at a time delay of 10 ms at 5 Hz readily induced spike timing-dependent LTD (tLTD) reflected by a 30 % decrease in the amplitude of eEPSCs in CA1 pyramidal cells. However, the same protocol failed to evoke tLTD in FS INs (Figure 15A, Table 4). To investigate whether interneurons may have a higher threshold for LTD induction, pairing of the postsynaptic AP discharge with EPSPs was also performed at 10 Hz. Remarkably, robust tLTD of similar magnitude (30-40% decrease of eEPSC amplitude) could be detected both in pyramidal cells and FS INs (p=0.128, Figure 15B, Table 4). The pairing protocol delivered at 5 Hz or 10 Hz in pyramidal cells produced comparable tLTD in magnitude (p=0.325, Figure 15C, Table 4).

Table 4. Effects of the pairing protocol on EPSC amplitude in distinct cell types and the outcome of different drug treatments or genetic inactivation of CB_1Rs on the magnitude of tLTD. *Student's paired t-test was used to evaluate the significant changes in post-pre pairing experiments compared to baseline values at different frequencies. In the drug treatment experiments, independent samples t-test was used for the statistical comparison between data obtained with 10 Hz pairing in the absence or the presence of different drugs, or in the measurements conducted in slices prepared from wild-type or CB_1R knockout (KO) mice. Data are expressed as mean ± SEM.*

	Pyramidal cell			**FS IN**		
	%	**n**	**p**	**%**	**n**	**p**
Pairing at 5 Hz	0.735±0.028	4	0.046	1.049±0.060	6	0.55
Pairing at 10 Hz	0.582±0.023	11	<0.001	0.591±0.015	11	<0.001
+ DL-AP5	0.642±0.031	4	0.982	0.426±0.082	4	0.060
+ MPEP	0.999±0.033	7	< 0.001	1.002±0.015	10	< 0.001
+ BAPTA	0.926±0.018	4	< 0.001	0.975±0.028	3	< 0.001
+ THL	0.991±0.010	8	< 0.001	0.957±0.032	7	< 0.001
CB_1R KO	0.990±0.022	10	< 0.001	0.980±0.019	8	< 0.001

These findings demonstrate that tLTD can be induced at excitatory synapses on both pyramidal cells and FS INs, but the threshold for tLTD induction is higher in FS INs compared to pyramidal cells in the CA1 hippocampal region.

II.2. Properties of spike timing-dependent LTD at excitatory synapses onto pyramidal cells and FS INs

Postsynaptic spiking alone (i.e. without pairing with EPSPs) delivered at 10 Hz did not alter the amplitude of synaptic currents (pyramidal cells, 97.7±1.4% of control, n=4, p=0.13; FS INs, 101±4% of control, n=4, p=0.96), indicating the associative nature of this form of LTD in all cell types. Next, we tested the magnitude of LTD as a function of the time delay of EPSPs following the APs. Pairing of the APs with EPSPs with a time delay of 30 ms at 10 Hz induced a smaller change in the EPSC amplitude than the pairing with the time delay of 10 ms (pyramidal cells, 81.4±9.8% of control, n=4, p=0.15; FS INs, 67.9±5.2% of control, n=4, p=0.01). In contrast, no change in the amplitude of EPSCs was observed, when EPSPs were evoked 50 ms after the AP discharge (pyramidal cells, 99.7±3.7% of control, n=5, p=0.98; FS INs, 99.5±2.7% of control, n=4, p=0.78), suggesting the importance of the precise timing of postsynaptic cell activity in relation to the arrival of presynaptic inputs.

Previous studies established that somewhat similar forms of tLTD (although induced with different stimulation frequencies and pairing protocols) at excitatory synapses of cortical principal cells require the activation of presynaptic ionotropic NMDA receptors (Sjostrom *et al.*, 2003; Rodriguez-Moreno & Paulsen, 2008; Min & Nevian, 2012). Therefore, we first repeated the 10 Hz pairing protocol using the 10 ms delay in the presence of 100 μM DL-AP5, an NMDA receptor antagonist. Bath application of this antagonist caused no change in tLTD either in pyramidal cells or in FS INs (Table 4). These data indicate that NMDA receptor activation is not necessary for inducing this form of tLTD in pyramidal cells and FS INs.

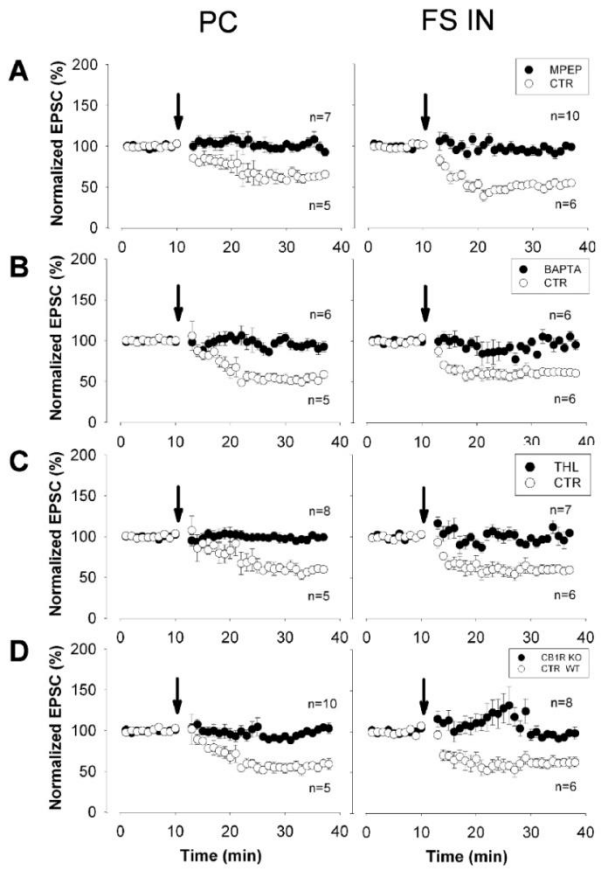

Figure 16. Pharmacological and genetic approaches identify the molecular elements involved in the induction of 10 Hz tLTD. A, *The tLTD phenomenon is blocked in both pyramidal cells and interneurons during the perfusion of the mGluR$_5$ antagonist MPEP (10 μM);* ***B,*** *using an intrapipette solution containing 20 mM BAPTA or* ***C,*** *during the perfusion of the DAG lipase blocker THL (10 μM).* ***D,*** *The tLTD phenomenon is not present in slices prepared from CB$_1$R KO mice. The results are plotted and compared with data obtained from their wild-type littermates. For all other numerical details and respective statistical analysis see Table 4. All data points on the plots represent mean ± SEM of six consecutive events.*

II.3. Spike timing-dependent LTD at excitatory synapses onto both pyramidal cells and FS INs is mediated by endocannabinoid signaling

In the next set of experiments, we sought to determine the molecular cascade mediating tLTD in CA1 neurons using the post-pre pairing protocol with the time delay of 10 ms at 10 Hz. First we recorded neurons in the presence of 10 μM MPEP, an antagonist of mGluR$_5$, and found that tLTD could not be induced in CA1 pyramidal cells or in FS INs (Figure 16A, Table 4). Next, we tested whether the intracellular elevation of Ca^{2+} in the postsynaptic neuron is necessary for tLTD. Including the Ca^{2+} chelator BAPTA (20 mM) in the intrapipette solution indeed fully eliminated tLTD in all tested neuron types (Figure 16B, Table 4). In the hippocampus, group I mGluR-stimulation leads to the biosynthesis of DAG, the precursor of the endocannabinoid 2-AG in a Ca^{2+}-dependent manner, which requires DGL-α activity (Jung *et al.*, 2005; Jung *et al.*, 2007). However, contribution of

endocannabinoids mediating the mGluR-dependent LTD has been highly controversial (Rouach & Nicoll, 2003; Gibson *et al.*, 2008; Le Duigou *et al.*, 2011; Edwards *et al.*, 2012; Izumi & Zorumski, 2012). Hence, we aimed to clarify the potential role of DGL-α in tLTD. In the presence of the DAG lipase blocker, THL (10 μM), tLTD could not be induced in pyramidal cells or in FS INs (Figure 16C, Table 4). Given the recent genetic evidence indicating that DGL-β, a related isoform of DGL-α, does not contribute to 2-AG synthesis in the hippocampus (Tanimura *et al.*, 2010), our results therefore suggest that DGL-α is required for tLTD in pyramidal cells and FS INs in the hippocampus. Finally, we investigated the potential contribution of 2-AG's receptor, the CB_1R to tLTD using hippocampal slices prepared from wild-type or CB_1R KO mice. While robust tLTD was observed in CA1 neurons in wild-type mice, the same pairing protocol did not evoke changes in the EPSC amplitude in pyramidal cells or in FS INs recorded in slices derived from CB_1R KO littermates (Figure 16D, Table 4).

Together these results provide direct evidence for the requirement of retrograde endocannabinoid signaling in tLTD at excitatory synapses in pyramidal cells and FS INs.

II.4. Chemical LTD at excitatory synapses also requires endocannabinoid signaling

The involvement of $mGluR_5$ in endocannabinoid-mediated tLTD in the hippocampus raises the question whether the activation of group I mGluRs *per se* is sufficient to induce LTD at excitatory synapses in both pyramidal cells and hippocampal interneurons. To address this issue, we pharmacologically activated group I mGluRs by bath application of DHPG. We found that 10 μM DHPG induced significant LTD only in pyramidal cells, but not in FS INs (Figure 17A, B, Table 5). In contrast, DHPG at a higher concentration (50 μM) readily induced LTD in both pyramidal cells and in interneurons (Figure 17A, B, Table 5). Thus, these observations are in accordance with the finding obtained with our post-pre pairing protocol demonstrating that a higher threshold is necessary for the induction of LTD in interneurons compared to pyramidal cells.

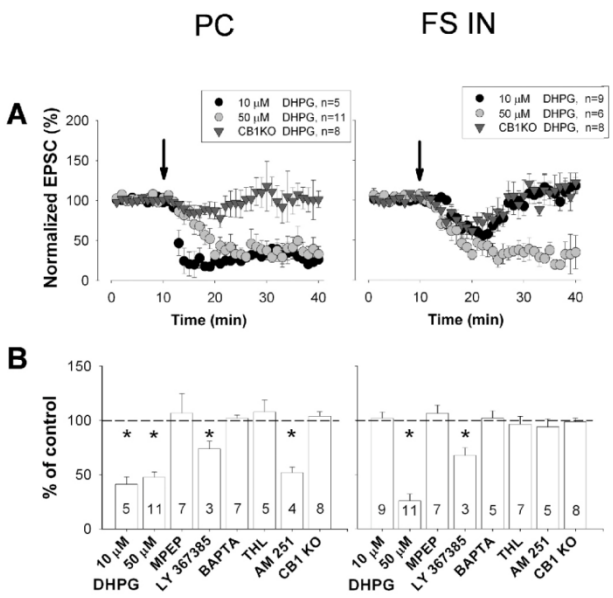

Figure 17. The group I mGluR agonist DHPG induces LTD of excitatory synapses onto PCs and FS INs via triggering retrograde endocannabinoid signaling. A, *Concentration-dependence of chemical LTD induction in pyramidal cells and in interneurons by DHPG. The summary plots of the EPSC amplitudes show that a higher concentration of DHPG is necessary to induce LTD in interneurons compared to pyramidal cells. However, even this higher concentration of DHPG was unable to induce LTD in slices prepared from CB_1R KO animals.* ***B,*** *Summary of the effects of pharmacological and genetic manipulations on the magnitude of 50 μM DHPG-induced LTD. All data are expressed as percent change relative to control values (mean ± SEM). The number of cells in different conditions is shown inside the bars. *, $p<0.05$.*

We examined the pharmacological profile of chemical LTD in pyramidal cells and interneurons. We observed that application of DHPG (50 μM) did not evoke LTD in the studied cell types in the presence of MPEP (Figure 17B, Table 5). In contrast, LY367385, a specific antagonist of $mGluR_1$ significantly reduced, but did not eliminate LTD in pyramidal cells and FS INs. The inclusion of BAPTA (20 mM) into the intrapipette solution prevented changes in the amplitude of EPSCs after 50 μM DHPG treatment in both pyramidal cells and FS INs (Figure 17A, B, Table 5). Similarly to tLTD, group I mGluR-dependent LTD could not be detected in slices pre-incubated with 10 μM THL (Figure 17B, Table 5) indicating the involvement of 2-AG in this chemical form of LTD. However, variable effects were observed in the presence of 2 μM AM 251, a CB_1R antagonist. While this antagonist did not affect chemical LTD in pyramidal cells, it could prevent LTD in FS INs (Table 5). In contrast to the controversial results obtained with this widely used CB_1R antagonist, the same DHPG treatment did not result in LTD in slices prepared from CB_1R KO mice, but induced robust LTD in slices derived from their wild-type littermates (Figure 17A, B, Table 5).

Table 5. Effects of DHPG on EPSC amplitudes in distinct cell types and the outcome of different drug treatments or genetic inactivation of CB_1Rs on the magnitude of chemical LTD. *Student's paired t-test was used to evaluate the significant changes upon 10 μM or 50 μM DHPG treatments. In all other cases, independent samples t-test was used for statistical comparison. The p values are the results of the comparisons between the data obtained upon 50 μM DHPG application in the absence and the presence of different drugs, or in the measurements conducted in slices prepared from wild-type or CB_1R KO mice. Data are expressed as mean ± SEM.*

	Pyramidal cell			**FS IN**		
		n	**p**		**n**	**p**
10 μM DHPG	0.346±0.071	5	<0.001	1.019±0.049	9	0.165
50 μM DHPG	0.483±0.049	11	<0.001	0.258±0.064	11	<0.001
+ MPEP	1.006±0.177	7	0.011	1.064±0.075	7	<0.001
+ LY 367385	0.738±0.070	3	0.007	0.676±0.069	3	0.013
+ BAPTA	0.870±0.026	5	< 0.001	1.027±0.066	3	0.001
+ THL	1.079±0.105	5	0.003	0.962±0.073	7	0.002
+ AM 251	0.519±0.051	4	0.143	0.930±0.073	5	<0.001
CB_1R KO	1.038±0.043	8	< 0.001	0.985±0.035	8	<0.001

To evaluate whether the changes in EPSC amplitudes in chemical LTD experiments are due to mechanisms occurring at presynaptic or postsynaptic sites, a pair of EPSCs with an inter-stimulus interval of 50 ms was evoked, which allowed us to monitor the alterations in paired-pulse ratios of synaptic currents. In pyramidal cells, we observed that the paired-pulse ratio is significantly increased in parallel with LTD induction upon DHPG treatment (control: 1.83±0.11, in 10 μM DHPG: 2.37±0.25, n=5, p=0.035; control: 1.67±0.12, in 50 μM DHPG: 2.86.1±0.46, n=11, p=0.031), but no change was detected in CB_1R KO mice (control: 1.59±0.24, in 50 μM DHPG: 2.057±0.37, n=8, p=0.24). Similarly, when LTD was induced by 50 μM DHPG application in FS INs, significant increase in paired-pulse ratio was revealed (control: 2.96±0.48, in 50 μM DHPG: 6.9±1.92, n=11, p=0.049). In contrast, but comparable to that found in pyramidal cells, when LTD could not be observed in these interneurons, the

paired-pulse ratio was not altered either (control: 2.11±0.12, in 10 μM DHPG: 1.95±0.14, n=9, p=0.35; KO mice control: 2.45±0.11, after 50 μM DHPG: 3.18±0.81, n=8, p=0.33).

These results highlight that group I mGluR activation with DHPG is sufficient to induce strong LTD at excitatory synapses onto CA1 pyramidal cells and FS INs. This form of synaptic plasticity has comparable molecular mechanisms to the tLTD triggered with a post-pre pairing protocol, and its expression is accompanied with changes at the presynaptic site. Finally, these experiments demonstrate that retrograde 2-AG signaling is necessary for both forms of LTD in both pyramidal cells and FS INs.

III. The role of excitatory synaptic inputs onto fast-spiking basket cells in cannabinoid-mediated suppression of gamma oscillations

PV+ fast-spiking inhibitory neurons provide precisely timed synchronous inhibition onto the output regions of pyramidal cells, which is capable to phase their discharges (Bartos *et al.*, 2007). Thus, these cells could have a pivotal role in synchronous network activity (Fuchs *et al.*, 2007; Cardin *et al.*, 2009; Rácz *et al.*, 2009; Sohal *et al.*, 2009; Ellender *et al.*, 2010). Reducing the excitatory synaptic input onto PV+ cells results in a decrease in the power of gamma oscillation (Fuchs *et al.*, 2007). Previously, it was shown that cannabinoid compounds were able reduce the amplitude of gamma oscillations (Hájos *et al.*, 2000). As we observed that the excitatory synaptic input onto FS INs could be modulated by endocannabinoids in a CB_1R-dependent manner, a question raises whether the same input onto fast-spiking cells is affected during the CB_1R-mediated suppression of gamma oscillations. Among PV+ cells, FS BCs are the prior candidates to govern gamma oscillation (Gulyás *et al.*, 2010) thus here, we examine exclusively this type of cells.

III.1. Effect of CB_1R activation on cholinergically-induced oscillations in the hippocampus

We induced gamma oscillation in mouse hippocampal slices by bath application of the acetylcholine receptor agonist carbachol (10 μM). Synchronous network activities at 30-32 ºC could be detected as oscillations in local field potentials recorded in the pyramidal cell layer of the hippocampal CA3 region (Figure 18A). The average peak frequency (30.1 ± 1.5 Hz, n=13) and mean peak power (87.9 ± 20.3 μV^2, n=13) of these oscillations calculated from the power spectral density function were comparable to results reported previously in studies using slices prepared from the rat hippocampus (Fisahn *et al.*, 1998; Hájos *et al.*, 2004; Oren *et al.*, 2006). First, we asked whether cholinergically-induced oscillations could be controlled by CB_1R activation, similarly to that we observed for kainate-induced network oscillations (Hájos *et al.*, 2000). Indeed, addition of CB_1R agonists CP55,940 or WIN55,212-2 to the bath solution (1 μM) significantly decreased the power of the oscillations (Figure 18A, B left panels). After 20 min of bath application of these agonists, the peak power of oscillatory activities was significantly reduced to 62.1 ± 6.3 % of control and 54.7 ± 15.2 % of control

for CP55,940 and WIN55,212-2, respectively (Figure 18C, D, left panels, Table 6) without a substantial change in the frequency (Figure 18C, D right panels, Table 6).

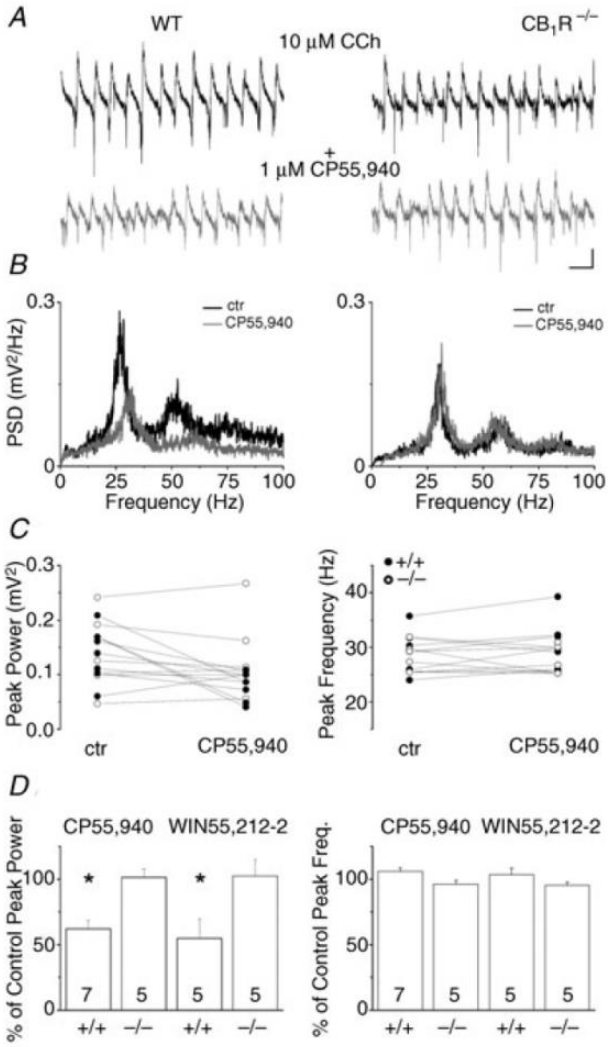

Figure 18. CB_1R activation reduces the power of the cholinergically-induced gamma oscillations in the CA3 region of the hippocampus. A, *Example traces of extracellular field recordings of cholinergically-induced oscillations (10 µM carbachol) in the pyramidal cell layer of CA3 in a wild type animal (WT, left traces) and in a CB_1R KO mouse (right traces) before (upper black traces) and after bath application of the cannabinoid receptor agonist CP55,940 (1 µM, lower grey traces).* ***B,*** *Power spectra calculated from the power spectral density function (PSD) of the traces in* ***A*** *showing peaks between 25-30 Hz (black), with harmonics both in the WT and in the CB_1R KO animals. CB_1R agonist application reduced the peak power and is accompanied by a modest shift in the peak frequency (grey). No change was detected in the CB_1R KO animals (right).* ***C,*** *Comparison of the peak power (left) and peak frequency (right) change in wild type (filled black circles) and CB_1R KO (empty circles) animals.* ***D,*** *Summary graphs showing the reduction in peak power (left) due to the bath application of either CP55,940 or WIN55,212-2 (1 µM, asterisks indicates $p<0.05$) without substantial changes in the peak frequency (right). Scale bars, 0.1 mV and 50 ms.*

The reduction in the peak power caused by CP55,940 (control: 98.1 ± 16.2 μV^2; in CP55,940: 61.8 ± 11.8 μV^2; n=3; p=0.024) could be fully reversed by subsequent co-application of the

CB_1R antagonist SR141716A (1 μM; in CP55,940 + SR141716A: 90.1 ± 12.9 μV^2; n=3; p=0.019). Moreover, the pre-treatment of slices with SR141716A for one hour prevented the CP55,940-induced drop in oscillation power (in SR141716A: 67.4 ± 9.3 μV^2; in SR141716A+CP55,940: 64.9 ± 8.8 μV^2; p=0.23; n=3). Importantly, SR141716A alone did not change the parameters of the oscillation (control: 69.8 ± 10.4 μV^2 and 34.3 ± 2.2 Hz; in SR141716A: 67.4 ± 9.3 μV^2, and 31.8 ± 2.4 Hz; p=0.15 and p=0.19, respectively, n=3), suggesting the lack of tonic CB_1R activation in our slice preparations that could interfere with oscillogenesis. To further confirm that cannabinoids acted exclusively via CB_1Rs, we tested the specificity of these agonists using CB_1R KO mice (Figure 18A, B right panels). The properties of carbachol-induced oscillations in slices prepared from CB_1R KO mice were not different from those observed in their wild type littermates (peak frequency: 31.1 ± 1.1 Hz, n=10, p=0.64; peak gamma power: 103.6 ± 21.5 μV^2, n=10, p=0.6). Bath application of CB_1R agonists for 20 min did not change the peak power (Figure 18C, D left panel, Table 6) or frequency (Figure 18C, D, right panels, Table 6) of the oscillations. These results indicated that both synthetic cannabinoids could significantly reduce the peak power of cholinergically-induced oscillations in the CA3 subfield via activation of CB_1Rs.

Table 6. Basic properties of cholinergically-induced network oscillations in the CA3 region of the hippocampus under control conditions and 20 min after drug application. *Data were compared using the Student's paired t-test: significant differences are indicated in bold. Data are presented as mean ± SEM.*

Genotype	Property	Control	CP55,940	P value	Number
WT	Peak frequency (Hz)	28.9±1.5	30.6±1.7	0.097	7
	Peak power (μV^2)	136±18.5	80.4±10.4	**0.0098**	7
CB_1R KO	Peak frequency (Hz)	28.7±1.1	27.8±1.0	0.32	5
	Peak power (μV^2)	140.8±34.3	153.3±85.9	0.11	5
Genotype	**Property**	**Control**	**WIN55,212-2**	**P value**	**Number**
WT	Peak frequency (Hz)	30.1±2.2	30.7±1.2	0.69	5
	Peak power (μV^2)	70.3±17.5	45.2±13.7	**0.027**	5
CB_1R KO	Peak frequency (Hz)	33.4±1.1	31.8±0.7	0.12	5
	Peak power (μV^2)	66.5±14.8	67.5±12.9	0.91	5

III.2. CB_1R activation suppresses the firing rate of CA3 pyramidal cells and fast-spiking basket cells during gamma oscillations

What might be the mechanism underlying the reduction of the oscillation power as a consequence of the cannabinoid agonist treatment? In the *in vitro* model of gamma oscillations induced by carbachol, the rhythmic inhibitory currents originating from the periodic discharge of parvalbumin-containing FS BCs generate the majority of field potential oscillations (Mann *et al.*, 2005; Atallah & Scanziani, 2009; Sohal *et al.*, 2009; Gulyás *et al.*, 2010; Oren *et al.*, 2010).

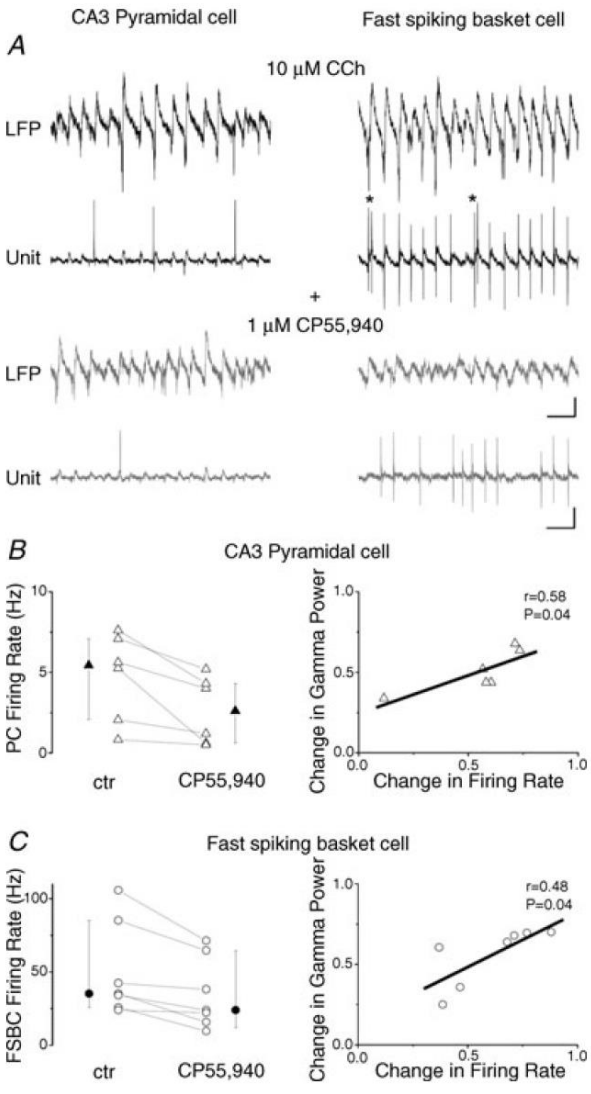

Figure 19. Effect of CB_1R activation on the firing frequency of CA3 PCs and FS BC during carbachol-induced gamma oscillations. A, *Simultaneous extracellular recordings of field potentials in the stratum pyramidale of CA3 (top black traces) during carbachol-induced oscillations and spike trains recorded in a loose-patch mode (bottom black traces) from a post hoc anatomically identified CA3 PC (left) and a FS BC (right). The CB_1R agonist CP55,940 (1 μM) reduces the firing frequency of both cell types (lower grey traces) along with the power of the oscillation (upper grey traces). CCh, carbachol. Scale bars, 0.1 mV (field potentials) or 0.2 mV (spike recordings) and 50 ms.* ***B, C, left****, Summary of the effect of the CP55,940 application on the firing rate of each measured CA3 PC (triangles) and FS BC (circles) showing a clear reduction in all cases. The vertical bars adjacent to the pairwise comparisons indicate medians and interquartile ranges of the corresponding data (filled symbols).* ***B, C, right,*** *A linear relationship was found between the*

change in the peak power of the oscillation and the change in the firing rate of the recorded cells, both normalized to control.

Hence, we hypothesized that perisomatic inhibition should be suppressed by cannabinoids in order to reduce the power of gamma oscillations. Since FS BCs do not express CB_1Rs at their axon terminals (Katona *et al.*, 1999; Hájos *et al.*, 2000), cannabinoids cannot directly control their synaptic output (Hájos *et al.*, 2000; Ohno-Shosaku *et al.*, 2002). Thus the reduction of synchronized GABA release during gamma oscillations can only be achieved either by a decrease in the firing frequency of FS BCs or by the de-synchronization of their spiking activity without a change in the mean frequency (Andersson *et al.*, 2010; Gulyás *et al.*, 2010).

Table 7. Firing properties of CA3 PCs and FS BCs during carbachol-induced oscillations under control conditions and 20 min after drug application. *Data are presented as the median with interquartile range in parentheses, except for phase values, which are given as the mean phase ± circular SD. Significant changes are indicated in bold.*

	CA3 pyramidal cells (n=6)		
	Control	**CP55,940**	**P value**
Firing frequency (Hz)	5.4 (1.7-7.2)	2.6 (0.6-4.5)	**0.031**
Spikes/oscillation cycle	0.19 (0.07-0.26)	0.08 (0.02-0.17)	**0.031**
Phase (°)	7.7±6.3	10±7.8	0.62
Phase-coupling strength	0.69 (0.67-0.72)	0.58 (0.44-0.69)	**0.031**

	CA3 fast-spiking basket cells (n=7)		
	Control	**CP55,940**	**P value**
Firing frequency (Hz)	35.1 (25.7-85.1)	23.8 (12.1-64.6)	**0.015**
Spikes/oscillation cycle	1.07 (0.75-2.46)	0.74 (0.43-1.82)	**0.015**
Phase (°)	23±13.3	33.1±22.6	0.358
Phase-coupling strength	0.83 (0.8-0.85)	0.78 (0.73-0.79)	**0.015**

To reveal which scenario might be responsible for the CB_1R-mediated reduction in oscillations, we simultaneously recorded local field potentials and the spiking activity of individual neurons, which were *post hoc* anatomically identified. In this set of experiments, we first monitored the discharge of CA3 pyramidal cells using a loose-patch mode in parallel with the field oscillation. As Figure 19 shows, bath application of CP55,940 resulted in a significant decrease in the firing rate of pyramidal cells to 55.2 ± 9.2 % of control (Figure 19A left panel and B, Table 7) along with a change in the power of the oscillation (50.2 ± 5.3 % of control, control: 146.5 ± 16.7 μV^2, in CP55,940: 72.2 ± 8.1 μV^2, n=6, p=0.002). In addition to the spiking activity, the phase-coupling strength of spiking was also found to be reduced after drug treatment without any change in the mean phase (Table 7). Under identical conditions, we next investigated the firing behavior of FS BCs, which discharged in almost every oscillation cycle and often fired doublets of APs (Figure 19A right panel and C). In addition to the substantial dampening of the field oscillation upon CB_1R activation (53.3 ± 7.1 % of control, control: 117.3 ± 25.6 μV^2, CP55,940: 58.4 ± 13.2 μV^2, n=7, p=0.028), the spiking activity of FS BCs was also suppressed to 62.2 ± 7.1 % of control (Figure 19, Table 7). The reduced firing rate was complemented by a decrease in the phase-coupling strength, but not in the mean phase (Table 7). When comparing the change in the peak power of the oscillation and the change in the firing rate of the recorded cells, we found a linear relationship both in the case of pyramidal cells (r=0.58, n=6, p=0.04; Figure 19B right panel) and of FS BCs (r=0.48, n=7, p=0.04, Figure 19C right panel). Thus, larger reductions in the peak power of gamma oscillations caused by CB_1R activation were accompanied by a more suppressed and less precise firing activity in CA3 neurons.

III.3. CB_1R activation suppresses monosynaptically evoked EPSCs in CA3 pyramidal cells and fast-spiking basket cells in the presence of carbachol

The microcircuits comprising pyramidal cells and FS BCs generate the cholinergically induced gamma oscillation in hippocampal slices, but at which synapses do cannabinoids control the neurotransmission? A recent study elucidated that synaptic communication between CA3 pyramidal cells is regulated by CB_1R activation (Hofmann *et al.*, 2008), similar to that observed in other hippocampal subfields (Misner & Sullivan, 1999; Chiu & Castillo, 2008; Xu *et al.*, 2010). To test whether excitatory synaptic transmission between CA3

pyramidal cells would be sensitive to cannabinoids under the conditions used to induce oscillations in this study, we performed the following experiments in the presence of 10 μM carbachol. EPSCs were evoked by stimulation of fibers in the stratum radiatum. In CA3 pyramidal cells, both CP55,940 and WIN55,212-2 (bath applied at 1 μM) significantly reduced the peak amplitude of the evoked currents (68.9 ± 5.1 % and 76.4 ± 9.1 % of control respectively, Table 8; Figure 20A and D).

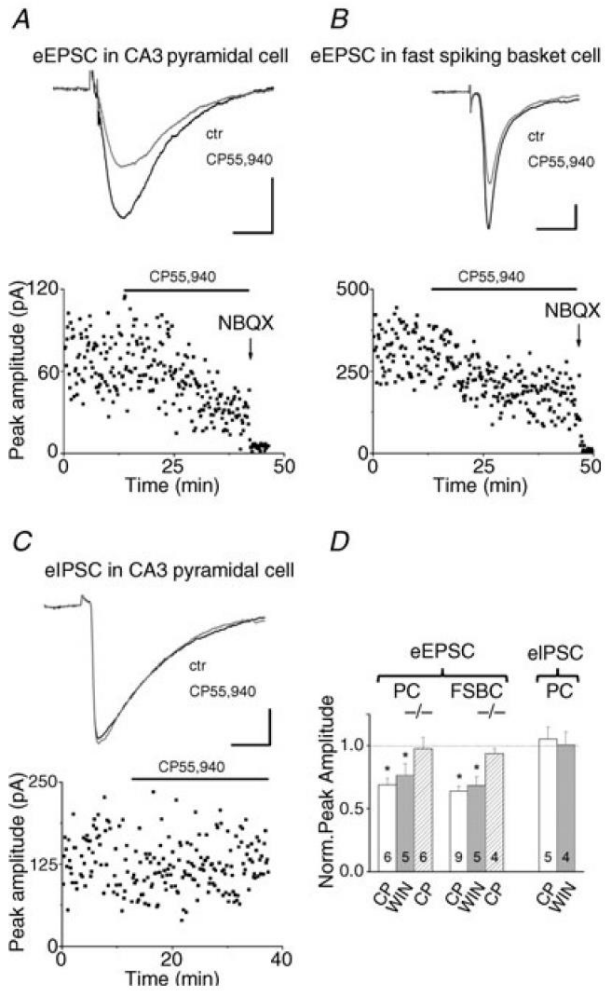

Figure 20. Cannabinoid agonists reduce the monosynaptically-evoked EPSCs recorded in CA3 PCs and FS BCs, but have no effect on IPSCs measured in CA3 PCs in the presence of carbachol. A, B, *Upper traces show typical mean EPSCs evoked in the stratum radiatum of CA3 recorded in a CA3 PC (**A**) or in a FS BC (**B**) in control (black) and after CP55,940 (1 μM, grey) application. Plots (lower panels) of the peak amplitude of eEPSCs show a reduction upon CP55,940 application (black lines indicate the wash-in period of the drug). NBQX, an antagonist of AMPA/KA receptors, was applied in each case at the end of the recording to verify that EPSCs were recorded.* ***C,*** *Typical mean IPSC (upper panel) recorded in a CA3 pyramidal cell before (black trace) and after (grey trace) application of CP55,940 (1 μM). Lower panel shows the amplitude plot of eIPSCs. No change in the peak amplitude can be detected after the application of the CB_1R agonist (black line).* ***D,*** *Graph summarizing the effect of CP55,940 (CP, white columns) and WIN55,212-2 (WIN, grey columns) application on the eEPSCs and eIPSCs. The normalized peak amplitudes after drug application compared to control (dashed line) are shown. Dashed columns represent the results obtained in CB_1R KO animals. Scale bars, 30 pA and 10 ms.*

Next, we examined the sensitivity of EPSCs in FS BCs measured under identical conditions. Similar to the findings obtained in CA3 pyramidal cells, but in contrast to previous data (Hoffman *et al.*, 2003), application of both cannabinoid agonists substantially suppressed the amplitude of evoked events in FS BCs (CP55,940: 63.9 ± 3.8 %; WIN55,212-2: 68.3 ± 7.2 %, Table 8, Figure 20B and D). After 20 min of cannabinoid treatment, 1 µl of 10 mM NBQX applied directly to the recording chamber (volume of 1 ml) readily eliminated all evoked currents recorded in both cell types, confirming that primarily AMPA/KA receptor-mediated synaptic currents were evoked (Figure 20A, B). In addition, the specificity of the effects of cannabinoids was also tested in CB_1R KO animals. No significant effect was found in the case of CP55,940 application on evoked EPSCs in CA3 pyramidal cells (97.4 ± 8.9 % of control Table 8, Figure 20D) or in FS BCs (93.6 ± 4.3 % of control, Table 8, Figure 20D), verifying the selective activation of CB_1Rs by CP55,940. These observations suggest that excitatory synaptic transmission received by both CA3 pyramidal cells and FS BCs could be substantially reduced by cannabinoids in a CB_1R dependent manner during cholinergic receptor activation.

Table 8. *Effect of cannabinoid receptor agonists on the peak amplitude of electrically-evoked postsynaptic currents (PSC) recorded in CA3 neurons. Data were compared using the Student's paired t-test: significant differences are indicated in bold. Data are presented as mean ± SEM.*

Geno-type	Cell type	PSC type	Control (pA)	CP55,940 (pA)	P value	Number
WT	PC	EPSC	114.8±40.4	79.2±37.7	**0.041**	6
	FS BC	EPSC	343.9±59.2	220.4±42.8	**0.0007**	9
	PC	IPSC	141.1±11.9	148.6±21.1	0.29	5
CB_1R KO	PC	EPSC	106.1±57.1	98.2±53.8	0.16	6
	FS BC	EPSC	109.3±21.7	101.3±20.1	0.53	4

Geno-type	Cell type	PSC type	Control (pA)	WIN55,212-2 (pA)	P value	Number
WT	PC	EPSC	110.5±61.2	84.5±62.3	**0.047**	5
	FS BC	EPSC	242.5±48.5	164±39. 9	**0.025**	5
	PC	IPSC	100.7±61.5	101.5±76.2	0.56	4

III.4. CB_1R activation has no effect on monosynaptically-evoked IPSCs recorded in CA3 pyramidal cells in the presence of carbachol

Next, we checked the cannabinoid sensitivity of synaptic inhibitory transmission under the present recording conditions. Pharmacologically-isolated IPSCs evoked by stimulation of fibers in the stratum pyramidale were recorded in CA3 pyramidal cells in the presence of carbachol. Bath application of CB_1R agonists (CP55,940 and WIN55,212-2) did not produce any effect on the IPSC amplitude (101.59 ± 9.32 % and 100.87 ± 9.85 % of control, respectively; Table 8, Figure 20C, D). These data are in line with earlier findings showing that perisomatic inhibition, which is critical for gamma oscillations, predominantly originates from cannabinoid-insensitive GABAergic terminals (Fukudome *et al.*, 2004; Neu *et al.*, 2007; Szabó *et al.*, 2010), because GABA release from the axon endings of CB_1R-expressing interneurons is almost completely muted in the presence of carbachol at a concentration higher than 5 μM (Gulyás *et al.*, 2010). Moreover, our results are also consistent with the hypothesis that cannabinoids do not suppress gamma oscillations through the direct reduction of phasic inhibitory input onto CA3 pyramidal cells, but rather act by decreasing the excitatory drive in the hippocampal network. The reduced excitatory synaptic input onto FS BCs alone may account for a significant drop in the oscillation power upon CB_1R activation

Next we attempted to differentiate the relative roles of CA3 pyramidal cells and FS BCs in mediating the cannabinoid effect on gamma oscillations. To address this question, we took advantage of the distinct temporal efficacy of CP55,940 on the suppression of EPSC amplitudes observed in the two cell types. As Figure 20A and B indicated, this cannabinoid receptor ligand seemed to reduce the EPSC amplitude recorded in FS BCs faster than in pyramidal neurons.

To quantify this difference, we calculated the changes in the peak amplitude every 5 minutes from the beginning of the drug superfusion. EPSC amplitudes evoked in FS BCs showed a significant decrease at 5 and 10 minutes compared to control, but no change in the EPSC amplitudes recorded in CA3 pyramidal cells could be observed (Figure 21A, Table 9). This significant difference in the changes of the peak amplitudes between the two cell types upon the beginning of CP55,940 treatment (5 min and 10 min $p<0.001$) could not be observed at the second half of the 20 minute period (15 min: $p=0.52$; 20 min: $p=0.48$), as the peak amplitude of EPSCs recorded in CA3 pyramidal cells started to decrease gradually from 15 minutes onwards (Figure 21A). Examination of the effect of CP55,940 on the spiking activity of individual neurons as well as on the oscillation power at the same time points showed that

at 5 minutes pyramidal cell spiking was not significantly different from the control (90.8 ± 2.5 % of control, n=6, p=0.09), whereas the firing frequency of FS BCs was already significantly suppressed (73.9 ± 6.7 % of control, n=7, p=0.01). The peak power of gamma oscillations decreased in parallel with the FS BC firing (Figure 21B, C; peak power in slices where pyramidal cells were recorded: 75.9 ± 3.4 % of control, n=6, p=0.001; peak power in slices where FS BCs were recorded: 69.1 ± 7.9 % of control, n=7, p=0.047). At the 10, 15 and 20 minute time points no significant difference could be detected in the changes of spiking activity and oscillation power (Figure 21B, C, p>0.1). Figure 21C demonstrates that there was no significant difference in the kinetics of the power decrease between the two slice populations, where the CA3 pyramidal cells and the FS BCs were measured. Similarly, the peak power of the oscillations in control conditions did not differ either (peak power in slices where pyramidal cells were recorded: 146.5 ± 16.7 μV^2, n=6; peak power in slices where FS BCs were recorded: 117.3 ± 25.6 μV^2, n=7, p=0.45).

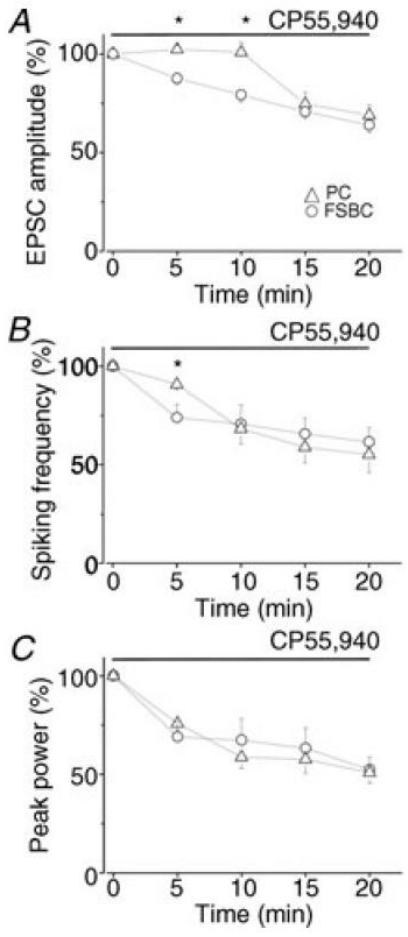

Figure 21. The reduced spiking frequency of FS BCs is already accompanied by a significant drop in the oscillation power, while PC firing is still unaltered. A, *Time course of the decrease of EPSC amplitudes recorded in CA3 PC and in FS BC during CP55,940 wash-in. Note that in the first 10 min no change in the EPSC amplitude measured in pyramidal cells could be detected, whereas EPSCs in FS BCs were already depressed even after 5 min of drug application. Asterisks indicate the significant difference between the two cell types.* ***B,*** *Superfusion of CP55,940 caused a gradual decrease in spiking frequency of PCs and FS BCs during ongoing gamma oscillations. At 5 min, however, there was no substantial change in the spiking frequency of PCs, but the discharge rate of FS BCs was significantly suppressed (asterisk). At later time points no significant difference in the magnitude of the reduction in firing rate could be noticed between the two cell types.* ***C,*** *In the same experiments as in* ***B,*** *the oscillation power was significantly*

reduced already 5 min after drug application, a reduction that further developed as CP55,940 was perfused. Circuit and triangle symbols represent data obtained in two populations of slices, where CA3 PCs and FS BCs, respectively were measured. Data are presented as mean ± SEM.

Table 9. *Change in the peak amplitude of electrically-evoked EPSCs recorded in CA3 neurons at different time points from the beginning of CP55,940 application. Data were compared using the Student's paired t-test: significant differences are indicated in bold. Data are presented as mean ± SEM.*

Time points	% of control amplitude in PC (N=6)	P value	% of control amplitude in FS BC (N=9)	P value
5 min	102.4 ± 2.1	0.27	87.6 ± 2.7	**0.031**
10 min	100.9 ± 4.9	0.85	79.3 ± 3.6	**0.009**
15 min	74.6 ± 5.9	**0.03**	70.7 ± 3.3	**0.008**
20 min	68.9 ± 5.1	**0.041**	63.9 ±3.8	**0.0007**

The coincidence of the drop in oscillation power with the decrease in the excitatory synaptic input and the resulting firing activity of FS BCs, but not of pyramidal cells at the beginning of CP55,940 treatment suggests that cannabinoid effects on gamma oscillations could primarily be mediated by the suppression of FS BC function by decreasing the excitatory input on them. This produces less perisomatic inhibitory current and thus smaller oscillations (Gulyás *et al.*, 2010; Oren *et al.*, 2010). However, upon longer cannabinoid application the reduced activity of pyramidal cells, causing even less excitatory drive onto FS BCs, can also contribute to the full reduction in the oscillation power.

DISCUSSION

In our studies presented in this thesis, we investigated the properties of excitatory synaptic inputs of PV+ interneurons in the CA3 and CA1 region of the hippocampus.

In the first part, we explored the membrane features of PV+ cells that can influence the computation of inputs and determine the transformation of inputs to output signals. In addition, we investigated the basic characteristics of excitatory synaptic inputs and the relative density of excitatory boutons on the dendrites of PV+ cells. We also studied the dendritic structure of these cells, which may influence the input properties by affecting the distribution of excitatory synapses. Since we separated AACs from FS BCs using an immunofluorescent method, we could compare and contrast their properties. These two cell types are often considered to be identical in many single-sell properties, however, the target region they innervate, and presumably, their role in network activity are quite different. We found quantitative anatomical and physiological differences in the excitatory input characteristics of these two cells types, which further strengthen their divergent role in neuronal computation.

In the second part, we aimed to uncover the properties of long-term depression of excitatory synaptic inputs onto these cells. We proved the presence of a type of LTD in the CA1 region of the hippocampus, which is mediated by endocannabinoids. We induced this type of LTD by both pairing protocol and chemical stimulation of receptors. We have shown that excitatory synaptic inputs onto both principal cells and interneurons have the ability to produce the endocannabinoid-mediated long-term depression, but the induction threshold of this LTD is markedly different in the two cell types.

The main goal of the third part was to understand the role of the excitatory synaptic inputs onto PV+ basket cells in the suppression of gamma oscillation mediated by exogenously applied cannabinoids in the CA3 region of the hippocampus. As it was known earlier (Gulyás 2010), FS BCs are key players in the generation of gamma oscillations. Since both excitatory synaptic inputs onto pyramidal cells and FS BCs can be modulated by endocannabinoids, we inquired whether the dampening of activity in pyramidal cells underlies the reduced firing of FS BCs, or the suppressed activity of FS BCs results in the silencing of principal cells. We found that the cannabinoid-mediated decrease of excitatory synaptic inputs onto FS BCs occurred earlier than onto pyramidal cells, proposing that the reduction of excitatory synaptic inputs solely onto FS BCs might be sufficient to suppress *in vitro* gamma oscillations.

I. Quantitative differences underlie the different properties of excitatory synaptic inputs received by axo-axonic and fast-spiking basket cells

In this study, we have investigated the single-cell properties, excitatory synaptic input features and the morphological characteristics of AACs and FS BCs in the CA3 region of the hippocampus. We found that, in comparison to AACs, FS BCs have a lower AP threshold and input resistance, a narrower AP and AHP, and a higher spike frequency with no accommodation. EPSC properties in both cell types were comparable, except we recorded a higher rate of sEPSCs in FS BCs. The stimulus intensity needed to evoke spiking in FS BCs was lower, although the EPSC magnitude necessary for AP generation was similar in both interneuron types. In addition, we revealed that the density of excitatory synapses at proximal dendrites was similar in both PV+ cell types, but FS BCs have significantly longer dendrites, which ramify more extensively in the strata oriens and radiatum compared to AACs. These structural differences might explain, at least in part, the observed differences in sEPSC rate and lower stimulus intensity necessary to evoke EPSCs at AP threshold in FS BCs by stimulating recurrent collaterals in the stratum oriens.

I.1. Single-cell properties of PV+ interneurons targeting the perisomatic region in cortical areas

In accord with previous findings in cortical structures (Buhl *et al.*, 1994; Kawaguchi, 1995; Cauli *et al.*, 1997; Kawaguchi & Kubota, 1997; Pawelzik *et al.*, 2002), we observed that the perisomatic region-targeting PV+ interneurons have fast-spiking properties with moderate accommodation, low input resistance and narrow APs with large and fast AHPs compared to that characterized in other types of GABAergic cells (Freund & Buzsáki, 1996; Ascoli *et al.*, 2008). These features in AACs and FS BCs, however, were found to be distinct both in CA3 and somatosensory cortex (present study, Woodruff *et al.*, 2009; Xu & Callaway, 2009), indicating that pooling data of comparable, but not identical, interneuron types can mask differences that might be important to understand the function of these interneurons in neuronal networks. We also observed that FS BCs exhibited significantly higher spike frequency and a lower accommodation ratio than AACs, implying a potential difference in Kv3 potassium conductance, which is pivotal for the fast-spiking phenotype (Lien & Jonas,

2003, Goldberg *et al*., 2011). The threshold for AP generation was higher in AACs than in FS BCs, although the Ankyrin-G staining in AISs, which was shown to correlate with the location of voltage-gated Na^+ channels (Jenkins & Bennett, 2001; Grubb & Burrone, 2010), was similar in both cell types. This observation suggests that the difference in AP threshold cannot be explained simply by a structural discrepancy in AIS organization, in contrast to what was found in other cell types (Grubb & Burrone, 2010; Kuba *et al.*, 2010). Interestingly, we revealed that the same EPSC amplitude was necessary to evoke an AP in both cell types, in spite of the fact that AACs had a higher AP threshold. A plausible explanation for this contradiction can be that AACs have a larger input resistance, giving rise to larger voltage change in these interneurons when equal synaptic current is evoked in FS BCs and AACs. Indeed, the magnitude of EPSPs near AP threshold was significantly larger in AACs than in FS BCs. Thus, the higher AP threshold and input resistance in AACs ensures that the same synaptic current is needed to discharge both PV+ interneuron types. Since in the thin slices used here sEPSCs correspond mostly to unitary events with a similar amplitude in both interneuron types (Table 2), and PV+ interneurons in CA3 are innervated mainly via single synaptic contacts (Sík *et al.*, 1993), we conclude that the spiking of AACs and FS BCs in this hippocampal region should be driven to fire APs by a similar number of excitatory neurons.

I.2. Distinct innervation of AACs and FS BCs by glutamatergic afferents

The morphological analysis of the dendritic trees of intracellularly-labeled interneurons in CA3 showed that FS BCs had longer and more arborized dendrites in the strata oriens and radiatum than AACs. In contrast, the density of excitatory synapses received by the proximal dendrites of both interneuron types was estimated to be comparable. These data together could explain our electrophysiological observations, namely that a lower intensity of focal stimulation was necessary to evoke EPSCs with the similar amplitudes in FS BCs compared to AACs, and the sEPSC rate was higher in FS BCs than in AACs. The strong relationship found between the sEPSC rates recorded in individual interneurons and the number of their dendritic branches also strengthens this conclusion (Figure 14). Since CA3 pyramidal cells innervate PV+ interneurons mainly via single release sites localized predominantly in the strata oriens and radiatum (Gulyás *et al.*, 1993b; Sík *et al.*, 1993), our results suggest that more numerous excitatory neurons can excite FS BCs than AACs in this

hippocampal region. Knowing that individual FS BCs inhibit a larger number of pyramidal cells than AACs (Gulyás *et al.*, 1993a), FS BCs and AACs should be embedded quite differently into intrahippocampal networks.

Another difference in their excitatory afferentation is the proportion of the synaptic inputs with extrahippocampal origin. Comparable to what was observed in CA1 (Li *et al.*, 1992; Klausberger *et al.*, 2003), we also found that the distal dendrites of AACs in CA3 have a tufted appearance, allowing them to receive a higher fraction of glutamatergic inputs from cortical or subcortical structures compared to FS BCs. Similarly to the cortex, AACs also have more polarized dendritic trees than FS BCs (Woodruff *et al.*, 2011). These morphological data strongly argue for the distinct function of AACs and FS BCs in cortical operation (Dugladze *et al.*, 2012).

Intriguingly, recent study (Tukker *et al.*, 2013) found in the dorsal hippocampus that CA2/3, but not CA1 FS BCs have large dendritic arborization in stratum lacunosum-moleculare. As we obtained our results from the ventral hippocampus, we presume differences in the excitatory innervation of FS BCs according to functional diversity along the dorsoventral axis (Kheirbek *et al.*, 2013). As the ventral hippocampus is much more implemented in emotional and motivational responses, AACs might monitor emotionally-charged inputs in the stratum lacunosum-moleculare, whereas from the same layer, FS BCs in the dorsal hippocampal region may receive heavier inputs that convey spatial information. To evaluate this suggestion, further investigation of the dendritic structure of AACs in the dorsal CA3 would be beneficial. Furthermore, species differences (rat *versus* mouse) should also be considered.

I.3. Firing behavior of AACs and FS BCs during different network states

AACs and FS BCs were found to discharge distinctly during characteristic network activities in the hippocampus. For instance, FS BCs fired more APs than AACs during gamma oscillations or sharp wave-ripple oscillations (Klausberger *et al.*, 2003; Tukker *et al.*, 2007; Gulyás *et al.*, 2010), and they fired at different phases of the hippocampal theta rhythm. Additionally, recent studies have shown that the spiking response of AACs and FS BCs to a given external stimulus varies. In the basolateral amygdala (Bienvenu *et al.*, 2012) or in the prefrontal cortex (Massi *et al.*, 2012), AACs begin to fire at high frequencies in response to

painful stimuli, whereas FS BCs discharge at a rather lower rate. In the somatosensory cortex, in response to whisker stimulation, AACs were found to have a larger receptive field with a lower acuity compared to other fast-spiking neurons (Zhu & Zhu, 2004). Together these observations may propose that AACs can be more responsible for stimuli arriving from the external world, adjusting the significance of direct sensory inputs or their processed forms, while FS BCs could monitor and more faithfully control the activity of intracortical communication.

II. Endocannabinoid-mediated long-term depression of excitatory synapses onto fast-spiking interneurons require higher induction threshold compared to pyramidal cells

In the present study, we observed two forms of LTD mediated via retrograde endocannabinoid signaling at Schaffer collaterals synapsing onto FS BCs or principal cells in the CA1 region of the hippocampus. The excitatory synaptic inputs of these interneurons and pyramidal cells readily undergo spike timing-dependent LTD. This form of LTD is absent, when DGL-α or CB_1R function is blocked. The same synapses exhibit robust LTD induced by DHPG, an agonist of group I mGluRs known to mobilize 2-AG (Jung *et al.*, 2005), and this chemical form of LTD is mechanistically similar to tLTD. Both forms of LTD have higher induction thresholds in these hippocampal interneurons than in pyramidal neurons.

II.1. Endocannabinoid-mediated LTD in hippocampal pyramidal neurons

Recent advances led to the appreciation that induction and expression of LTD is mechanistically diverse and may require several independent molecular signaling cascades (Feldman, 2009; Collingridge *et al.*, 2010). One of these cascades utilizes endocannabinoids to signal backwards across synapses and permanently silence presynaptic activity (Sjostrom *et al.*, 2003; Bender *et al.*, 2006; Nevian & Sakmann, 2006), but several other forms of LTD do not require endocannabinoid signaling (Collingridge *et al.*, 2010). This mechanistic and molecular heterogeneity is apparent using similar induction protocols in a synapse-specific

manner (Crozier *et al.*, 2007) or at different developmental stages (Yasuda *et al.*, 2008). For example, tLTD in excitatory cells is dependent on CB_1R function at certain neocortical excitatory synapses (Sjostrom *et al.*, 2003; Bender *et al.*, 2006; Nevian & Sakmann, 2006; Crozier *et al.*, 2007), but not in others (Crozier *et al.*, 2007; Banerjee *et al.*, 2009). However, despite the widespread expression of group I mGluRs, DGL-α and CB_1Rs at hippocampal excitatory synapses (Luján *et al.*, 1996; Katona *et al.*, 2006; Yoshida *et al.*, 2006), and the reliable inducibility of tLTD at excitatory synapses onto principal cells (Debanne *et al.*, 1994; Niehusmann *et al.*, 2010), involvement of retrograde endocannabinoid signaling in a spike timing-dependent form of synaptic plasticity has not previously been demonstrated in hippocampal neurons. Moreover, despite the consistent manifestation of mGluR-LTD (Palmer *et al.*, 1997; Huber *et al.*, 2001), and the presence of a somewhat similar form of LTD at GABAergic synapses (Chevaleyre & Castillo, 2003), conflicting reports were available to date, whether this chemical form of LTD requires retrograde endocannabinoid signaling at excitatory synapses on hippocampal principal cells. While pharmacological blockade of CB_1Rs did not prevent DHPG-induced LTD at excitatory synapses according to earlier studies and in the present study (Rouach & Nicoll, 2003; Nosyreva & Huber, 2005; Lanté *et al.*, 2006; Izumi & Zorumski, 2012), we demonstrated by using a genetic inactivation approach that DHPG-LTD in fact requires CB_1Rs, in agreement with a recent report using higher concentrations of DHPG (Xu *et al.*, 2010). Our study further extends this conclusion by uncovering the indispensable role of DGL-α activity in DHPG-LTD, and reveals the participation of the endocannabinoid 2-AG in long-term depression at excitatory synaptic inputs received by hippocampal excitatory cells.

A potential explanation for these contradicting results may be the observation that CB_1R antagonists are less capable to antagonize CB_1R-dependent depression of excitatory synaptic transmission than of inhibitory synaptic transmission in the hippocampus (Hájos & Freund, 2002), implicating that synapse-specific differences may exist in the molecular organization of CB_1Rs. An experimental preparation-dependent variability in the contribution of astrocytic CB_1Rs to synaptic plasticity is also emerging and may underlie some of the discrepancies in the magnitude and direction of synaptic plasticity (Navarrete & Araque, 2010; Han *et al.*, 2012; Min & Nevian, 2012). Finally, the ratio of $mGluR_1/mGlu_5$ contribution to DHPG-induced LTD may also differ between experimental paradigms (Izumi & Zorumski, 2012). Nevertheless, the $mGluR_5$-specific antagonist MPEP fully eliminated the spike timing-dependent and chemical forms of LTD, and both required endocannabinoid signaling based on genetic evidence. Thus, together with another form of autaptic LTD

observed in hippocampal cultures (Kellogg *et al.*, 2009), these observations clearly demonstrate that at least three forms of endocannabinoid-mediated LTD are possible at hippocampal excitatory connections onto pyramidal neurons.

II.2. Endocannabinoid-mediated LTD in fast-spiking interneurons

Long-term depression of glutamatergic synaptic inputs onto hippocampal interneurons can also be triggered by several induction protocols (McMahon & Kauer, 1997a; Laezza *et al.*, 1999; Gibson *et al.*, 2008; Nissen *et al.*, 2010; Le Duigou *et al.*, 2011; Edwards *et al.*, 2012). When tested, LTD in cortical GABAergic interneurons was found to be insensitive to treatment with CB_1R antagonists (Lu *et al.*, 2007; Gibson *et al.*, 2008; Le Duigou *et al.*, 2011; Edwards *et al.*, 2012), which was surprising, because synthetic cannabinoid ligands effectively suppress excitatory synaptic inputs onto hippocampal interneurons including FS BCs (Gibson *et al.*, 2008). Here we found that LTD could not be induced in FS INs in the presence of the CB_1R antagonist or in animals lacking CB_1Rs. In contrast, robust LTD was observed upon both induction protocols in three types of FS INs (FS BCs, AACs and bistratified cells) in wild-type animals indicating that parvalbumin-containing interneurons are also able to control the weights of their glutamatergic inputs via endocannabinoid mobilization. Moreover, the group of Dr. István Katona in our institute showed that parvalbumin-positive interneurons also express DGL-α, which especially accumulates in a perisynaptic annulus around excitatory synapses on aspiny parvalbumin-positive dendrites (Péterfi *et al.*, 2012). Indeed, we found that treatment with either MPEP or THL completely eliminated both forms of LTD in FS INs arguing for the functional operation of the retrograde endocannabinoid-mediated signaling pathway in these cell types. Thus, the evidence presented here suggests that at least three types of interneurons can control the strength of their excitatory synapses via endocannabinoids.

III. Cannabinoid effects on gamma oscillations is primarily mediated by the reduction of excitatory synaptic inputs onto fast-spiking basket cells

Studying the effect of CB_1R antagonists on cholinergically-induced hippocampal gamma oscillations, we found that exogenous cannabinoids reduce the power of gamma oscillations in a CB_1R-dependent manner. Decreased peak oscillatory power upon CB_1R activation is accompanied by reduced and less precise firing activity in CA3 pyramidal cells and FS BCs, neuron types that are critically involved in the generation of field oscillations in this model. In the presence of carbachol, CB_1R activation can significantly suppress excitatory synaptic transmission recorded in CA3 pyramidal cells and FS BCs, whereas perisomatic inhibitory currents in pyramidal cells are unaffected. At the beginning of CP55,940 superfusion on slices, a significant drop in oscillation power coincides with the reduced firing of FS BCs, while pyramidal cell spiking is still unchanged. Since CB_1Rs are predominantly, if not exclusively, located at axon terminals in the hippocampus, our data propose that the decrease in excitatory synaptic input upon activation of these receptors can result in fewer AP discharges with lower fidelity during synchronous network activities, which may account for the impairment of hippocampal oscillations observed after cannabinoid treatment.

III.1. Influencing gamma oscillations with different drugs have dissimilar effects reflecting distinct mechanisms for impairing rhythmicity

Our results clearly show that the excitatory synaptic inputs not only onto CA3 pyramidal cells but also onto FS BCs could be reduced by cannabinoids activating CB_1Rs. This finding seems to be in contrast to that published previously (Hoffman *et al.*, 2003), where evoked EPSCs recorded in CA1 interneurons located outside of the pyramidal cell layer were found to be insensitive to cannabinoid ligands. Since FS BCs can be predominantly found within the stratum pyramidale (Katsumaru *et al.*, 1988), it is likely that this GABAergic cell type was not among the interneurons tested by Hoffman and colleagues (Hoffman *et al.*, 2003).

In a previous report, we found that the mu-opioid agonist DAMGO could effectively diminish cholinergically-induced network oscillations in hippocampal slices (Gulyás *et al.*,

2010). Although both DAMGO and cannabinoids reduced the oscillation power, the cellular mechanisms underlying their effects were quite different. The activation of mu-opioid receptors located specifically at axon terminals of parvalbumin-containing interneurons suppressed GABA release (Drake & Milner, 2002; Glickfeld *et al.*, 2008; Gulyás *et al.*, 2010) and led to de-synchronization of neuronal firing without changing the mean discharge rate. Similarly, it was recently proposed that the agonists of H_3 histamine receptors could dampen gamma oscillations predominantly via the de-synchronization of firing of CA3 pyramidal cells with no effects on their spiking activity (Andersson *et al.*, 2010). In contrast, we found that the cannabinoid-induced decrease in the excitatory synaptic transmission predominantly onto FS BCs can already cause a significant reduction in their mean firing frequency. As a result, the magnitude of synchronous GABA release from FS BC axon terminals generating the field oscillation in CA3 is substantially depressed, producing smaller fluctuations in the field potentials (Oren *et al.*, 2010). However, the reduced discharge rate of pyramidal cells, producing even smaller excitatory drive onto FS BCs, may contribute to the full suppression of the oscillation power upon cannabinoid treatment. These results are consistent with the notion that the reduction of field oscillations, e.g. by anesthetics, may indicate the suppression of synaptic transmission (Destexhe *et al.*, 2003).

III.2. Role of excitatory synaptic transmission in the reduction of gamma oscillation power

Excitatory synaptic transmission is critical for carbachol-induced oscillations, since blocking AMPA receptors diminishes rhythmic activities (Fisahn *et al.*, 1998; Mann *et al.*, 2005). Furthermore, application of a selective AMPA receptor antagonist resulted in the hyperpolarization of the resting membrane potential of CA3 pyramidal cells, and abolished the rhythmic firing of FS BCs (Mann *et al.*, 2005), which has been shown to be driven by phasic excitatory input (Traub *et al.*, 2000; Oren *et al.*, 2006). The tonic depolarizing effect of AMPA receptor activation likely promotes pyramidal cell discharge, which is consistent with results indicating that slow, non-rhythmic excitatory input onto pyramidal cells during gamma oscillations may be enough to support the spiking of principal neurons synchronized by perisomatic inhibition (Fisahn *et al.*, 1998; Traub *et al.*, 2000; Mann *et al.*, 2005; Morita *et al.*, 2008). These observations together suggest that a partial reduction in excitatory synaptic

transmission, e.g. after cannabinoid treatment, can reduce the excitability of CA3 pyramidal cells in a recurrent network. The prediction that this will reduce the number of neurons firing synchronously during a gamma cycle is supported by our recordings and by modeling studies (Traub *et al.*, 2000; Morita *et al.*, 2008). The resulting smaller neuronal assembly will produce a lower excitatory drive onto FS BCs. This reduced phasic excitation from a smaller neuronal population together with the direct reduction of glutamate release onto FS BCs upon CB_1R activation is likely to be responsible for the full cannabinoid effect on gamma oscillations. Our observation that the significant suppression of the FS BC discharge rate was already accompanied by a drop in the oscillation power, while the pyramidal cell spiking was still unaltered, is in full agreement with a recent study proposing that the reduction of excitatory synaptic input solely onto FS BCs might be sufficient to suppress *in vitro* gamma oscillations (Fuchs *et al.*, 2007).

III.3. Selective reduction of intrahippocampal excitatory synaptic connections may contribute to cannabinoid-mediated weakening of gamma oscillation

In vivo studies uncovered that cannabinoids could effectively depress oscillatory activities in several frequency bands in the CA1 region of the hippocampus (Robbe *et al.*, 2006; Hajós *et al.*, 2008) and other cortical regions, but increase the synchronicity of thalamocortical oscillations (Sales-Carbonell *et al.*, 2013). At low doses, CP55,940 caused only de-synchronization of the firing of CA1 neurons without a significant change in their frequency, an effect that was already accomplished by the dampening of the rhythmic activities detected in local field potentials. At high doses, however, the firing rate was significantly suppressed (Robbe *et al.*, 2006). During exploratory behavior, when the theta rhythm dominates hippocampal field potentials, input from the entorhinal cortex might prevalently influence the firing of CA1 neurons (Buzsáki, 1989; Brun *et al.*, 2002). In contrast, their spiking during sharp wave-ripples, which characterize local field potentials in CA1 during consummatory behavior, is mainly controlled by excitation from CA3 (Buzsáki, 1989; Nakashiba *et al.*, 2009). Importantly, a recent *in vitro* study revealed that excitatory synaptic input from the entorhinal cortex onto CA1 pyramidal cells could be depressed only to a small extent upon CB_1R activation, in contrast to excitatory synaptic transmission originating from CA3, which was significantly reduced (Xu *et al.*, 2010). Taking into account

these results, we hypothesize that CP55,940 at low doses may not significantly attenuate the excitatory drive onto CA1 neurons from entorhinal cortex during theta rhythms, and thus the frequency of spiking would not be substantially changed, whereas the impairment in the temporal structure of the firing may be explained by the reduced excitation from CA3 (Jarsky *et al.*, 2005; Katz *et al.*, 2007). This proposal is supported by *in vivo* findings, showing that sharp wave-ripples in CA1 that are generated by the synchronous population discharge of CA3 pyramidal cells via Schaffer collaterals (Buzsáki *et al.*, 1992) are significantly suppressed after CP55,940 treatment (Robbe *et al.*, 2006). These observations are in line with our present results indicating that the reduction in synaptic excitation of CA3 pyramidal cells may underlie the cellular mechanisms of the CB_1R-dependent dampening of synchronous activities in hippocampal networks. Thus, cannabinoids could mainly alter intrahippocampal excitatory synaptic transmission, leading to impairment of oscillatory activities and memory formation (Hampson & Deadwyler, 1998; Robbe & Buzsáki, 2009).

IV. Functional implications

Our observations support the suggestions of recent studies that AACs and FS BCs may fulfill different roles in cortical computation (Zhu & Zhu, 2004; Bienvenu *et al.*, 2012; Massi *et al.*, 2012). AACs might rather convey information from the external world, while FS BCs should be the main generators of the intrinsic rhythm of several brain areas. These data presume that in a disease where the sensory gating is characteristically impaired, the two cell types might be involved differently. Therefore, in schizophrenic diseases, the malfunction of AACs may have a higher impact on poor filtering of irrelevant information. Indeed, it has been already shown that the ratio of VGAT1-positive cartridges selectively decreases among inhibitory terminals in tissues derived from schizophrenic patients (Woo *et al.*, 1998; Pierri *et al.*, 1999). Furthermore, treating monkeys with phencyclidine results a loss of PV-containing axo-axonic terminals (Morrow *et al.*, 2007). As the excitatory synaptic inputs onto PV+ cells are highly affected in schizophrenia (Inan *et al.*, 2013), distinguished investigations of the glutamatergic inputs onto AACs and FS BCs might confine our knowledge about the pathomechanisms underlying this disease.

Disruption of gamma oscillations is another symptom in schizophrenia, which might be related to the loss and failure of PV+ cell function. The effects of cannabinoids on

oscillations imply that the reduction of the synaptic excitation in FS BCs might have an impact on triggering schizophrenic symptoms by cannabis consumption. Accordingly, Hajós and coworkers (Hajós *et al.*, 2008) showed that auditory gating and neuronal synchrony was altered by CB_1R activation in the hippocampus and the entorhinal cortex. Moreover, as the blood (De Marchi *et al.*, 2003) or cerebrospinal (Leweke *et al.*, 1999) level of endocannabinoid molecules is elevated in schizophrenic patients independently of cannabis abuse, the endogenous activators of CB_1Rs may also contribute to the development of the disease e.g. by decreasing the power of gamma oscillations, resulting in cognitive deficits.

Despite the higher sensitivity of excitatory synaptic inputs onto FS BCs than pyramidal cells to exogenous cannabinoids, the induction threshold of LTD is higher in FS BCs compared to pyramidal cells. According to the lower levels of DGL-α in PV+ interneurons than pyramidal cells (Péterfi *et al.*, 2012), as a compensatory mechanism, it is susceptible that CB_1Rs at the excitatory synapses onto FS INs are more sensitive to their agonists than in the case of pyramidal cells. The differing efficiency of the inverse agonist AM251 in antagonizing the eCB-LTD in the two cell types might strengthen this suggestion.

The quantitative differences in the induction thresholds of endocannabinoid-mediated LTD suggest that different cell types may produce 2-AG during different network states. When excessive neuronal activity increases extracellular glutamate to sufficiently high levels for activation of perisynaptic group I mGluRs, 2-AG-signaling at the network level limits the spread of this pathological activity and protects against neuronal insult (Katona & Freund, 2008). Our results suggest that this circuit-breaker function switches on earlier in pyramidal cells than in GABAergic interneurons, and thereby may serve a role to prevent or delay the switch from normal to a pathological activity state (Monory *et al.*, 2006). As a consequence of these differences, there should be a time window when excitatory-excitatory connections are weakened, while excitatory-inhibitory interactions remain fully functional. During this period, the alteration in synaptic weights will enhance the dominance of synaptic inhibition in the network, which may help to reverse the high activity state to a lower one (Malva *et al.*, 2003). However, when synaptic excitation onto interneurons also becomes suppressed, network behavior might more easily shift to the pathological range (Piet *et al.*, 2011). Thus, cell type-specific regulation of retrograde 2-AG signaling may be a beneficial way to exploit this messenger system in a network state-dependent mode.

CONCLUSIONS

The main goal of the experiments shown in this thesis was to investigate the excitatory synaptic inputs onto PV+ interneurons in the CA3 and CA1 hippocampal regions.

Comparing the properties of excitatory synaptic inputs onto AACs and FS BCs in the CA3, we found that (1) FS BCs require lower stimulus intensity to generate AP than AACs, (2) FS BCs have higher sEPSC rate compared to AACs. (3) The density of excitatory synaptic inputs on the dendrites of the two cell types is similar, but (4) the dendrites of FS BCs are longer and more ramified in the strata radiatum and oriens. These data suggest that the two cell types receive excitatory synaptic inputs with distinct characteristics, which might underlie the different recruitment of AACs and FS BCs during network oscillations. As FS BCs are innervated by a higher number of CA3 pyramidal cells than AACs, the former cell type could be recruited more easily during oscillations and they can monitor more accurately the activity of excitatory cell assemblies.

We described a type of eCB-dependent LTD at excitatory synapses onto CA1 PV+ cells, which is (1) inducible by both post-pre pairing protocol and by pharmacological activation of $mGluR_{1/5}$. (2) The threshold of LTD induction in PV+ cells is significantly higher than in pyramidal cells, and (3) the induction of the two types of LTD share a similar signaling pathway involving $mGluR_5$, DGL-α and CB_1Rs. Thus, we provided physiological evidence that PV+ interneurons not only express DGL-α, the synthetizing enzyme of the main endocannabinoid, 2-AG, but under certain circumstances they are able to synthetize and release 2-AG. The lower levels of DGL-α in PV+ cells than in pyramidal cells could partly explain the higher threshold for LTD induction observed in PV+ interneurons.

Investigating the cellular mechanisms underlying the effects of CB_1R agonists on gamma oscillations, we uncovered that (1) carbachol-induced *in vitro* gamma oscillations are readily suppressed by CB_1R agonists. (2) Decreased peak oscillatory power is accompanied by reduced and less precise firing activity in CA3 pyramidal cells and FS BCs. (3) In the presence of carbachol, CB_1R activation suppresses excitatory synaptic transmission recorded in pyramidal cells and FS BCs, whereas inhibitory postsynaptic currents recorded in pyramidal cells are unaffected. (4) At the beginning of CB_1R agonist superfusion on slices, the suppression of excitatory synaptic inputs onto FS BCs occurs earlier than in pyramidal cells. In parallel, a significant drop in the firing of FS BCs can be observed, which coincides with the reduced oscillation power. Therefore, the weakening of excitatory synaptic inputs

onto FS BCs can be the primary cause of the suppression of gamma oscillations mediated by CB_1R agonists.

These findings might further our knowledge about the properties and physiological operation of excitatory synaptic inputs of PV+ cells, which could be highly affected in psychiatric diseases such as schizophrenia.

SUMMARY

The hippocampus is involved in several higher order cognitive functions, which are characterized with distinct oscillatory activities. The parvalbumin-expressing perisomatic region-targeting interneurons (PV+ cells) are key players in orchestrating synchronous network activities. The excitatory synaptic inputs of these cells are important in their recruitment during oscillations. Our aim was to investigate the properties of the excitatory synaptic inputs received by the PV+ cells.

The two types of PV+ cells, the axo-axonic cells and basket cells discharge differently during several network activities. Therefore, we examined whether any dissimilarity in their excitatory synaptic inputs might underlie the distinct recruitment. We compared the electrophysiological properties of glutamatergic inputs and the morphology of the dendritic trees of the two PV+ cells, and found that proximal parts of basket cells receive a higher number of excitatory synaptic inputs than axo-axonic cells, due to a more extensive arborization of their dendrites closer to the cell body.

Next, we asked whether the glutamatergic synapses onto PV+ cells are capable for undergoing long-term changes in their plasticity. We succeeded to induce long-term depression (LTD) at excitatory synaptic inputs onto PV+ cells by post-pre pairing of postsynaptic spiking and presynaptic stimulus, and by pharmacological activation of metabotropic glutamate receptors. The threshold for induction of LTD was higher in PV+ interneurons than in pyramidal cells. The molecular mechanism underlying this type of LTD was dependent on the release of the endocannabinoid 2-arachidonoyl glycerol.

Finally, we investigated the cellular mechanisms underlying the suppression of carbachol-induced gamma oscillations caused by CB_1 receptor agonists. In the hippocampal CA3, these compounds reduced the spiking activity of basket cells and principal cells in parallel with decreasing the power of the oscillations. CB_1 receptor agonists suppressed glutamatergic inputs onto both cell types, but unaffected inhibitory synaptic transmission in the presence of carbachol. Correlating the time courses of the observed effects of the CB_1 receptor agonists, our data suggested that the primary cause of the suppression of gamma oscillations was the weakening of excitatory synaptic inputs onto basket cells.

Thus, the function of PV+ cells in rhythm generation can be controlled by endogenous and exogenous cannabinoid ligands, which compounds may alter the cortical oscillations by reducing the spiking activities of these GABAergic interneurons.

ÖSSZEFOGLALÁS

A hippokampusz magasabbrendű kognitív folyamatokért felelős agyterület, ahol jellegzetes oszcillatorikus aktivitások figyelhetőek meg. A parvalbumint kifejező periszomatikus gátlósejtek (PV+ sejtek) fontos szervezői a hálózati aktivitásmintázatoknak. Serkentő szinaptikus bemeneteik jelentős szerepet töltenek be ezen gátlósejtek oszcillációk során megfigyelhető aktiválásában. Célunk a PV+ sejtekre érkező glutamáterg szinaptikus bemenetek vizsgálata volt.

A PV+ sejtek két típusa, az axo-axonikus sejtek és a kosársejtek különböző tüzelési mintázatokat mutatnak az oszcillációk során. Ezért megvizsgáltuk, hogy van-e olyan különbség a serkentő szinaptikus bemeneteikben, ami szerepet játszhat a két sejt eltérő aktiválódásában. Összehasonlítva a két típusú PV+ sejt glutamáterg bemeneteinek számos elektrofiziológiai tulajdonságát és dendritfájuk morfológiáját, megfigyeltük, hogy a kosársejtek proximálisan nagyobb mennyiségű serkentő szinaptikus bemenetet kapnak, mint az axo-axonikus sejtek, mert a kosársejtek dendritfájának szóma-közeli régiója kiterjedtebb és gazdagabban elágazik.

Ezután azt vizsgáltuk, hogy a PV+ sejtek glutamáterg bemenetei képesek-e hosszútávú plaszticitásra. Megfigyeltük, hogy a PV+ sejtek serkentő szinapszisainál indukálható volt hosszútávú depresszió (LTD) párosítási protokollal, és az I-es típusú metabotróp glutamát receptorok farmakológiai aktiválásával egyaránt. Az LTD indukciós küszöbe a PV+ sejtekben magasabb volt mint a piramissejtekben. Az LTD kialakulásának hátterében endokannabinoid-(2-arachidonil-glicerol) függő jelátviteli mechanizmus állt.

Végül azt tanulmányoztuk, hogy milyen sejtszintű mechanizmusokon keresztül csökkentik a CB_1 receptor agonisták a karbakol-indukált gamma oszcillációt. Kísérleteink azt mutatták, hogy a CB_1 receptor agonisták csökkentik a piramissejtek és a kosársejtek tüzelési gyakoriságát a gamma oszcilláció gyengülésével párhuzamosan. Az agonisták csökkentették mind a kosársejtek, mind a piramissejtek glutamáterg szinaptikus bemeneteinek nagyságát, a gátló szinaptikus transzmissziót viszont nem befolyásolták karbakol jelenlétében. A CB_1 receptor agonisták különböző hatásait időben korreláltatva megállapítottuk, hogy kosársejtek serkentő szinapszisainak csökkenő hatékonysága okozza elsősorban a gamma oszcillációk gyengülését.

Tehát ezen ritmusgenezisben kulcsszerepet játszó gátlósejtek működése befolyásolható mind endogén, mind exogén kannabinoid receptorligandumokkal, amelyek hatására jelentősen megváltoznak az agykérgi oszcillációk.

REFERENCES

Acsády, L., Arabadzisz, D. & Freund, T.F. (1996a) Correlated morphological and neurochemical features identify different subsets of vasoactive intestinal polypeptide-immunoreactive interneurons in rat hippocampus. *Neuroscience*, **73**, 299-315.

Acsády, L., Görcs, T.J. & Freund, T.F. (1996b) Different populations of vasoactive intestinal polypeptide-immunoreactive interneurons are specialized to control pyramidal cells or interneurons in the hippocampus. *Neuroscience*, **73**, 317-334.

Akbarian, S., Kim, J.J., Potkin, S.G., Hagman, J.O., Tafazzoli, A., Bunney, W.E., Jr. & Jones, E.G. (1995) Gene expression for glutamic acid decarboxylase is reduced without loss of neurons in prefrontal cortex of schizophrenics. *Archives of general psychiatry*, **52**, 258-266.

Alonso, A. & Kohler, C. (1982) Evidence for separate projections of hippocampal pyramidal and non-pyramidal neurons to different parts of the septum in the rat brain. *Neuroscience letters*, **31**, 209-214.

Andersen, M.R., Amaral D, Bliss T, O'Keefe J, eds (2007) *The Hippocampus Book: Oxford University Press, New York*

Andersen, P., Bliss, T.V. & Skrede, K.K. (1971) Lamellar organization of hippocampal pathways. *Experimental Brain Research*, **13**, 222-238.

Andersson, R., Lindskog, M. & Fisahn, A. (2010) Histamine H_3 receptor activation decreases kainate-induced hippocampal gamma oscillations *in vitro* by action potential desynchronization in pyramidal neurons. *Journal of Physiology*, **588**, 1241-1249.

Antal, M., Eyre, M., Finklea, B. & Nusser, Z. (2006) External tufted cells in the main olfactory bulb form two distinct subpopulations. *European Journal of Neuroscience*, **24**, 1124-1136.

Arion, D. & Lewis, D.A. (2011) Altered expression of regulators of the cortical chloride transporters NKCC1 and KCC2 in schizophrenia. *Archives of general psychiatry*, **68**, 21-31.

Ascoli, G.A., Alonso-Nanclares, L., Anderson, S.A., Barrionuevo, G., Benavides-Piccione, R., Burkhalter, A., Buzsáki, G., Cauli, B., Defelipe, J., Fairen, A., Feldmeyer, D., Fishell, G., Fregnac, Y., Freund, T.F., Gardner, D., Gardner, E.P., Goldberg, J.H., Helmstaedter, M., Hestrin, S., Karube, F., Kisvárday, Z.F., Lambolez, B., Lewis, D.A., Marin, O., Markram, H., Munoz, A., Packer, A., Petersen, C.C., Rockland, K.S., Rossier, J., Rudy, B., Somogyi, P., Staiger, J.F., Tamás, G., Thomson, A.M., Toledo-Rodriguez, M., Wang, Y., West, D.C. & Yuste, R. (2008) Petilla terminology: nomenclature of features of GABAergic interneurons of the cerebral cortex. *Nature reviews. Neuroscience*, **9**, 557-568.

Atallah, B.V. & Scanziani, M. (2009) Instantaneous modulation of gamma oscillation frequency by balancing excitation with inhibition. *Neuron*, **62**, 566-577.

Axmacher, N., Mormann, F., Fernandez, G., Elger, C.E. & Fell, J. (2006) Memory formation by neuronal synchronization. *Brain research reviews*, **52**, 170-182.

Banerjee, A., Meredith, R.M., Rodriguez-Moreno, A., Mierau, S.B., Auberson, Y.P. & Paulsen, O. (2009) Double dissociation of spike timing-dependent potentiation and depression by subunit-preferring NMDA receptor antagonists in mouse barrel cortex. *Cerebral Cortex*, **19**, 2959-2969.

Bartos, M., Vida, I., Frotscher, M., Geiger, J.R. & Jonas, P. (2001) Rapid signaling at inhibitory synapses in a dentate gyrus interneuron network. *The Journal of Neuroscience*, **21**, 2687-2698.

Bartos, M., Vida, I., Frotscher, M., Meyer, A., Monyer, H., Geiger, J.R. & Jonas, P. (2002) Fast synaptic inhibition promotes synchronized gamma oscillations in hippocampal interneuron networks. *PNAS*, **99**, 13222-13227.

Bartos, M., Vida, I. & Jonas, P. (2007) Synaptic mechanisms of synchronized gamma oscillations in inhibitory interneuron networks. *Nature reviews. Neuroscience*, **8**, 45-56.

Bashir, Z.I., Jane, D.E., Sunter, D.C., Watkins, J.C. & Collingridge, G.L. (1993) Metabotropic glutamate receptors contribute to the induction of long-term depression in the CA1 region of the hippocampus. *European journal of pharmacology*, **239**, 265-266.

Bear, M.F. (1995) Mechanism for a sliding synaptic modification threshold. *Neuron*, **15**, 1-4.

Beasley, C.L. & Reynolds, G.P. (1997) Parvalbumin-immunoreactive neurons are reduced in the prefrontal cortex of schizophrenics. *Schizophrenia research*, **24**, 349-355.

Behrens, M.M., Ali, S.S., Dao, D.N., Lucero, J., Shekhtman, G., Quick, K.L. & Dugan, L.L. (2007) Ketamine-induced loss of phenotype of fast-spiking interneurons is mediated by NADPH-oxidase. *Science*, **318**, 1645-1647.

Belforte, J.E., Zsíros, V., Sklar, E.R., Jiang, Z., Yu, G., Li, Y., Quinlan, E.M. & Nakazawa, K. (2010) Postnatal NMDA receptor ablation in corticolimbic interneurons confers schizophrenia-like phenotypes. *Nature Neuroscience*, **13**, 76-83.

Bender, V.A., Bender, K.J., Brasier, D.J. & Feldman, D.E. (2006) Two coincidence detectors for spike timing-dependent plasticity in somatosensory cortex. *The Journal of Neuroscience*, **26**, 4166-4177.

Beneyto, M., Abbott, A., Hashimoto, T. & Lewis, D.A. (2011) Lamina-specific alterations in cortical $GABA_A$ receptor subunit expression in schizophrenia. *Cerebral Cortex*, **21**, 999-1011.

Bienvenu, T.C., Busti, D., Magill, P.J., Ferraguti, F. & Capogna, M. (2012) Cell-type-specific recruitment of amygdala interneurons to hippocampal theta rhythm and noxious stimuli *in vivo*. *Neuron*, **74**, 1059-1074.

Bliss, T.V. & Lomo, T. (1973) Long-lasting potentiation of synaptic transmission in the dentate area of the anaesthetized rabbit following stimulation of the perforant path. *Journal of Physiology*, **232**, 331-356.

Boddeke, H.W., Best, R. & Boeijinga, P.H. (1997) Synchronous 20 Hz rhythmic activity in hippocampal networks induced by activation of metabotropic glutamate receptors *in vitro*. *Neuroscience*, **76**, 653-658.

Boiko, T., Vakulenko, M., Ewers, H., Yap, C.C., Norden, C. & Winckler, B. (2007) Ankyrin-dependent and -independent mechanisms orchestrate axonal compartmentalization of L1 family members neurofascin and L1/neuron-glia cell adhesion molecule. *The Journal of Neuroscience*, **27**, 590-603.

Bragin, A., Jandó, G., Nádasdy, Z., Hetke, J., Wise, K. & Buzsáki, G. (1995) Gamma (40-100 Hz) oscillation in the hippocampus of the behaving rat. *The Journal of Neuroscience*, **15**, 47-60.

Brun, V.H., Otnass, M.K., Molden, S., Steffenach, H.A., Witter, M.P., Moser, M.B. & Moser, E.I. (2002) Place cells and place recognition maintained by direct entorhinal-hippocampal circuitry. *Science*, **296**, 2243-2246.

Buhl, E.H., Han, Z.S., Lőrinczi, Z., Stezhka, V.V., Karnup, S.V. & Somogyi, P. (1994) Physiological properties of anatomically identified axo-axonic cells in the rat hippocampus. *Journal of neurophysiology*, **71**, 1289-1307.

Bullock, T.H., Buzsáki, G. & McClune, M.C. (1990) Coherence of compound field potentials reveals discontinuities in the CA1-subiculum of the hippocampus in freely-moving rats. *Neuroscience*, **38**, 609-619.

Buzsáki, G. (1986) Hippocampal sharp waves: their origin and significance. *Brain research*, **398**, 242-252.

Buzsáki, G. (1989) Two-stage model of memory trace formation: a role for "noisy" brain states. *Neuroscience*, **31**, 551-570.

Buzsáki, G., Buhl, D.L., Harris, K.D., Csicsvári, J., Czéh, B. & Morozov, A. (2003) Hippocampal network patterns of activity in the mouse. *Neuroscience*, **116**, 201-211.

Buzsáki, G. & Eidelberg, E. (1982) Direct afferent excitation and long-term potentiation of hippocampal interneurons. *Journal of neurophysiology*, **48**, 597-607.

Buzsáki, G., Horváth, Z., Urioste, R., Hetke, J. & Wise, K. (1992) High-frequency network oscillation in the hippocampus. *Science*, **256**, 1025-1027.

Buzsáki, G., Leung, L.W. & Vanderwolf, C.H. (1983) Cellular bases of hippocampal EEG in the behaving rat. *Brain research*, **287**, 139-171.

Buzsáki, G. & Wang, X.J. (2012) Mechanisms of gamma oscillations. *Annual review of neuroscience*, **35**, 203-225.

Campanac, E., Gasselin, C., Baude, A., Rama, S., Ankri, N. & Debanne, D. (2013) Enhanced intrinsic excitability in basket cells maintains excitatory-inhibitory balance in hippocampal circuits. *Neuron*, **77**, 712-722.

Cardin, J.A., Carlen, M., Meletis, K., Knoblich, U., Zhang, F., Deisseroth, K., Tsai, L.H. & Moore, C.I. (2009) Driving fast-spiking cells induces gamma rhythm and controls sensory responses. *Nature*, **459**, 663-667.

Carlen, M., Meletis, K., Siegle, J.H., Cardin, J.A., Futai, K., Vierling-Claassen, D., Ruhlmann, C., Jones, S.R., Deisseroth, K., Sheng, M., Moore, C.I. & Tsai, L.H. (2012) A critical role for NMDA receptors in parvalbumin interneurons for gamma rhythm induction and behavior. *Molecular psychiatry*, **17**, 537-548.

Cauli, B., Audinat, E., Lambolez, B., Angulo, M.C., Ropert, N., Tsuzuki, K., Hestrin, S. & Rossier, J. (1997) Molecular and physiological diversity of cortical nonpyramidal cells. *The Journal of Neuroscience*, **17**, 3894-3906.

Chamberland, S., Salesse, C., Topolnik, D. & Topolnik, L. (2010) Synapse-specific inhibitory control of hippocampal feedback inhibitory circuit. *Frontiers in cellular neuroscience*, **4**, 130.

Chapman, C.A. & Lacaille, J.C. (1999) Cholinergic induction of theta-frequency oscillations in hippocampal inhibitory interneurons and pacing of pyramidal cell firing. *The Journal of Neuroscience*, **19**, 8637-8645.

Chevaleyre, V. & Castillo, P.E. (2003) Heterosynaptic LTD of hippocampal GABAergic synapses: a novel role of endocannabinoids in regulating excitability. *Neuron*, **38**, 461-472.

Chevaleyre, V. & Siegelbaum, S.A. (2010) Strong CA2 pyramidal neuron synapses define a powerful disynaptic cortico-hippocampal loop. *Neuron*, **66**, 560-572.

Chiu, C.Q. & Castillo, P.E. (2008) Input-specific plasticity at excitatory synapses mediated by endocannabinoids in the dentate gyrus. *Neuropharmacology*, **54**, 68-78.

Cho, R.Y., Konecky, R.O. & Carter, C.S. (2006) Impairments in frontal cortical gamma synchrony and cognitive control in schizophrenia. *PNAS*, **103**, 19878-19883.

Chrobak, J.J. & Buzsáki, G. (1994) Selective activation of deep layer (V-VI) retrohippocampal cortical neurons during hippocampal sharp waves in the behaving rat. *The Journal of Neuroscience*, **14**, 6160-6170.

Chrobak, J.J. & Buzsáki, G. (1996) High-frequency oscillations in the output networks of the hippocampal-entorhinal axis of the freely behaving rat. *The Journal of Neuroscience*, **16**, 3056-3066.

Citri, A. & Malenka, R.C. (2008) Synaptic plasticity: multiple forms, functions, and mechanisms. *Neuropsychopharmacology*, **33**, 18-41.

Cobb, S.R., Buhl, E.H., Halasy, K., Paulsen, O. & Somogyi, P. (1995) Synchronization of neuronal activity in hippocampus by individual GABAergic interneurons. *Nature*, **378**, 75-78.

Colgin, L.L., Denninger, T., Fyhn, M., Hafting, T., Bonnevie, T., Jensen, O., Moser, M.B. & Moser, E.I. (2009) Frequency of gamma oscillations routes flow of information in the hippocampus. *Nature*, **462**, 353-357.

Colgin, L.L. & Moser, E.I. (2010) Gamma oscillations in the hippocampus. *Physiology (Bethesda, Md.)*, **25**, 319-329.

Collingridge, G.L., Peineau, S., Howland, J.G. & Wang, Y.T. (2010) Long-term depression in the CNS. *Nature reviews. Neuroscience*, **11**, 459-473.

Cope, D.W., Maccaferri, G., Marton, L.F., Roberts, J.D., Cobden, P.M. & Somogyi, P. (2002) Cholecystokinin-immunopositive basket and Schaffer collateral-associated interneurones target different domains of pyramidal cells in the CA1 area of the rat hippocampus. *Neuroscience*, **109**, 63-80.

Crozier, R.A., Wang, Y., Liu, C.H. & Bear, M.F. (2007) Deprivation-induced synaptic depression by distinct mechanisms in different layers of mouse visual cortex. *PNAS*, **104**, 1383-1388.

Csicsvári, J., Hirase, H., Czurkó, A., Mamiya, A. & Buzsáki, G. (1999) Fast network oscillations in the hippocampal CA1 region of the behaving rat. *The Journal of Neuroscience*, **19**, RC20.

Csicsvári, J., Hirase, H., Mamiya, A. & Buzsáki, G. (2000) Ensemble patterns of hippocampal CA3-CA1 neurons during sharp wave-associated population events. *Neuron*, **28**, 585-594.

Csicsvári, J., Jamieson, B., Wise, K.D. & Buzsáki, G. (2003) Mechanisms of gamma oscillations in the hippocampus of the behaving rat. *Neuron*, **37**, 311-322.

De Marchi, N., De Petrocellis, L., Orlando, P., Daniele, F., Fezza, F. & Di Marzo, V. (2003) Endocannabinoid signalling in the blood of patients with schizophrenia. *Lipids in health and disease*, **2**, 5.

Debanne, D., Gahwiler, B.H. & Thompson, S.M. (1994) Asynchronous pre- and postsynaptic activity induces associative long-term depression in area CA1 of the rat hippocampus *in vitro*. *PNAS*, **91**, 1148-1152.

Destexhe, A., Rudolph, M. & Pare, D. (2003) The high-conductance state of neocortical neurons *in vivo*. *Nature reviews. Neuroscience*, **4**, 739-751.

Diba, K. & Buzsáki, G. (2007) Forward and reverse hippocampal place-cell sequences during ripples. *Nature Neuroscience*, **10**, 1241-1242.

Doischer, D., Hosp, J.A., Yanagawa, Y., Obata, K., Jonas, P., Vida, I. & Bartos, M. (2008) Postnatal differentiation of basket cells from slow to fast signaling devices. *The Journal of Neuroscience*, **28**, 12956-12968.

Drake, C.T. & Milner, T.A. (2002) Mu opioid receptors are in discrete hippocampal interneuron subpopulations. *Hippocampus*, **12**, 119-136.

Dudek, S.M. & Bear, M.F. (1992) Homosynaptic long-term depression in area CA1 of hippocampus and effects of N-methyl-D-aspartate receptor blockade. *PNAS*, **89**, 4363-4367.

Dugladze, T., Schmitz, D., Whittington, M.A., Vida, I. & Gloveli, T. (2012) Segregation of axonal and somatic activity during fast network oscillations. *Science*, **336**, 1458-1461.

Dunwiddie, T. & Lynch, G. (1978) Long-term potentiation and depression of synaptic responses in the rat hippocampus: localization and frequency dependency. *Journal of Physiology*, **276**, 353-367.

Edwards, J.G., Gibson, H.E., Jensen, T., Nugent, F., Walther, C., Blickenstaff, J. & Kauer, J.A. (2012) A novel non-CB_1/$TRPV_1$ endocannabinoid-mediated mechanism depresses excitatory synapses on hippocampal CA1 interneurons. *Hippocampus*, **22**, 209-221.

Ellender, T.J., Nissen, W., Colgin, L.L., Mann, E.O. & Paulsen, O. (2010) Priming of hippocampal population bursts by individual perisomatic-targeting interneurons. *The Journal of Neuroscience*, **30**, 5979-5991.

Ellender, T.J. & Paulsen, O. (2010) The many tunes of perisomatic targeting interneurons in the hippocampal network. *Frontiers in cellular neuroscience*, **4**.

Feldman, D.E. (2009) Synaptic mechanisms for plasticity in neocortex. *Annual review of neuroscience*, **32**, 33-55.

Ferraguti, F., Klausberger, T., Cobden, P., Baude, A., Roberts, J.D., Szűcs, P., Kinoshita, A., Shigemoto, R., Somogyi, P. & Dalezios, Y. (2005) Metabotropic glutamate receptor 8-expressing nerve terminals target subsets of GABAergic neurons in the hippocampus. *The Journal of Neuroscience*, **25**, 10520-10536.

Fisahn, A., Contractor, A., Traub, R.D., Buhl, E.H., Heinemann, S.F. & McBain, C.J. (2004) Distinct roles for the kainate receptor subunits GluR5 and GluR6 in kainate-induced hippocampal gamma oscillations. *The Journal of Neuroscience*, **24**, 9658-9668.

Fisahn, A., Pike, F.G., Buhl, E.H. & Paulsen, O. (1998) Cholinergic induction of network oscillations at 40 Hz in the hippocampus *in vitro*. *Nature*, **394**, 186-189.

Fox, S.E. (1989) Membrane potential and impedance changes in hippocampal pyramidal cells during theta rhythm. *Experimental Brain Research*, **77**, 283-294.

Freedman, R., Adler, L.E., Myles-Worsley, M., Nagamoto, H.T., Miller, C., Kisley, M., McRae, K., Cawthra, E. & Waldo, M. (1996) Inhibitory gating of an evoked response

to repeated auditory stimuli in schizophrenic and normal subjects. Human recordings, computer simulation, and an animal model. *Archives of general psychiatry*, **53**, 1114-1121.

Fremeau, R.T., Jr., Kam, K., Qureshi, T., Johnson, J., Copenhagen, D.R., Storm-Mathisen, J., Chaudhry, F.A., Nicoll, R.A. & Edwards, R.H. (2004) Vesicular glutamate transporters 1 and 2 target to functionally distinct synaptic release sites. *Science*, **304**, 1815-1819.

Freund, T.F. (2003) Interneuron Diversity series: Rhythm and mood in perisomatic inhibition. *Trends in neurosciences*, **26**, 489-495.

Freund, T.F. & Antal, M. (1988) GABA-containing neurons in the septum control inhibitory interneurons in the hippocampus. *Nature*, **336**, 170-173.

Freund, T.F. & Buzsáki, G. (1996) Interneurons of the hippocampus. *Hippocampus*, **6**, 347-470.

Freund, T.F., Gulyás, A.I., Acsády, L., Görcs, T. & Tóth, K. (1990) Serotonergic control of the hippocampus via local inhibitory interneurons. *PNAS*, **87**, 8501-8505.

Freund, T.F. & Katona, I. (2007) Perisomatic inhibition. *Neuron*, **56**, 33-42.

Fricker, D., Verheugen, J.A. & Miles, R. (1999) Cell-attached measurements of the firing threshold of rat hippocampal neurones. *Journal of Physiology*, **517 (Pt 3)**, 791-804.

Frotscher, M., Seress, L., Schwerdtfeger, W.K. & Buhl, E. (1991) The mossy cells of the fascia dentata: a comparative study of their fine structure and synaptic connections in rodents and primates. *Journal of Comparative Neurology*, **312**, 145-163.

Fuchs, E.C., Zivkovic, A.R., Cunningham, M.O., Middleton, S., Lebeau, F.E., Bannerman, D.M., Rozov, A., Whittington, M.A., Traub, R.D., Rawlins, J.N. & Monyer, H. (2007) Recruitment of parvalbumin-positive interneurons determines hippocampal function and associated behavior. *Neuron*, **53**, 591-604.

Fuentealba, P., Tomioka, R., Dalezios, Y., Marton, L.F., Studer, M., Rockland, K., Klausberger, T. & Somogyi, P. (2008) Rhythmically active enkephalin-expressing GABAergic cells in the CA1 area of the hippocampus project to the subiculum and preferentially innervate interneurons. *The Journal of Neuroscience*, **28**, 10017-10022.

Fukuda, T. & Kosaka, T. (2000) Gap junctions linking the dendritic network of GABAergic interneurons in the hippocampus. *The Journal of Neuroscience*, **20**, 1519-1528.

Fukudome, Y., Ohno-Shosaku, T., Matsui, M., Omori, Y., Fukaya, M., Tsubokawa, H., Taketo, M.M., Watanabe, M., Manabe, T. & Kano, M. (2004) Two distinct classes of muscarinic action on hippocampal inhibitory synapses: M2-mediated direct suppression and M1/M3-mediated indirect suppression through endocannabinoid signalling. *European Journal of Neuroscience*, **19**, 2682-2692.

Fung, S.J., Webster, M.J., Sivagnanasundaram, S., Duncan, C., Elashoff, M. & Weickert, C.S. (2010) Expression of interneuron markers in the dorsolateral prefrontal cortex of the developing human and in schizophrenia. *The American journal of psychiatry*, **167**, 1479-1488.

Galarreta, M. & Hestrin, S. (1999) A network of fast-spiking cells in the neocortex connected by electrical synapses. *Nature*, **402**, 72-75.

Galarreta, M. & Hestrin, S. (2001) Spike transmission and synchrony detection in networks of GABAergic interneurons. *Science*, **292**, 2295-2299.

Galván, E.J., Calixto, E. & Barrionuevo, G. (2008) Bidirectional Hebbian plasticity at hippocampal mossy fiber synapses on CA3 interneurons. *The Journal of Neuroscience*, **28**, 14042-14055.

Ganter, P., Szűcs, P., Paulsen, O. & Somogyi, P. (2004) Properties of horizontal axo-axonic cells in stratum oriens of the hippocampal CA1 area of rats *in vitro*. *Hippocampus*, **14**, 232-243.

Geiger, J.R., Lübke, J., Roth, A., Frotscher, M. & Jonas, P. (1997) Submillisecond AMPA receptor-mediated signaling at a principal neuron-interneuron synapse. *Neuron*, **18**, 1009-1023.

Geiger, J.R., Melcher, T., Koh, D.S., Sakmann, B., Seeburg, P.H., Jonas, P. & Monyer, H. (1995) Relative abundance of subunit mRNAs determines gating and Ca^{2+} permeability of AMPA receptors in principal neurons and interneurons in rat CNS. *Neuron*, **15**, 193-204.

Gerdeman, G.L., Ronesi, J. & Lovinger, D.M. (2002) Postsynaptic endocannabinoid release is critical to long-term depression in the striatum. *Nature Neuroscience*, **5**, 446-451.

Gibson, H.E., Edwards, J.G., Page, R.S., Van Hook, M.J. & Kauer, J.A. (2008) $TRPV_1$ channels mediate long-term depression at synapses on hippocampal interneurons. *Neuron*, **57**, 746-759.

Glausier, J.R. & Lewis, D.A. (2011) Selective pyramidal cell reduction of GABA(A) receptor alpha1 subunit messenger RNA expression in schizophrenia. *Neuropsychopharmacology*, **36**, 2103-2110.

Glickfeld, L.L., Atallah, B.V. & Scanziani, M. (2008) Complementary modulation of somatic inhibition by opioids and cannabinoids. *The Journal of Neuroscience*, **28**, 1824-1832.

Glickfeld, L.L., Roberts, J.D., Somogyi, P. & Scanziani, M. (2009) Interneurons hyperpolarize pyramidal cells along their entire somatodendritic axis. *Nature Neuroscience*, **12**, 21-23.

Glickfeld, L.L. & Scanziani, M. (2006) Distinct timing in the activity of cannabinoid-sensitive and cannabinoid-insensitive basket cells. *Nature Neuroscience*, **9**, 807-815.

Gloveli, T., Dugladze, T., Rotstein, H.G., Traub, R.D., Monyer, H., Heinemann, U., Whittington, M.A. & Kopell, N.J. (2005) Orthogonal arrangement of rhythm-generating microcircuits in the hippocampus. *PNAS*, **102**, 13295-13300.

Goldberg, E.M., Jeong, H.Y., Kruglikov, I., Tremblay, R., Lazarenko, R.M. & Rudy, B. (2011) Rapid developmental maturation of neocortical FS cell intrinsic excitability. *Cerebral Cortex*, **21**, 666-682.

Goldberg, J.H., Tamás, G. & Yuste, R. (2003) Ca^{2+} imaging of mouse neocortical interneurone dendrites: I_a-type K^+ channels control action potential backpropagation. *Journal of Physiology*, **551**, 49-65.

Grubb, M.S. & Burrone, J. (2010) Activity-dependent relocation of the axon initial segment fine-tunes neuronal excitability. *Nature*, **465**, 1070-1074.

Gulyás, A.I., Hájos, N. & Freund, T.F. (1996) Interneurons containing calretinin are specialized to control other interneurons in the rat hippocampus. *The Journal of Neuroscience*, **16**, 3397-3411.

Gulyás, A.I., Hájos, N., Katona, I. & Freund, T.F. (2003) Interneurons are the local targets of hippocampal inhibitory cells which project to the medial septum. *European Journal of Neuroscience*, **17**, 1861-1872.

Gulyás, A.I., Miles, R., Hájos, N. & Freund, T.F. (1993a) Precision and variability in postsynaptic target selection of inhibitory cells in the hippocampal CA3 region. *European Journal of Neuroscience*, **5**, 1729-1751.

Gulyás, A.I., Miles, R., Sík, A., Tóth, K., Tamamaki, N. & Freund, T.F. (1993b) Hippocampal pyramidal cells excite inhibitory neurons through a single release site. *Nature*, **366**, 683-687.

Gulyás, A.I., Szabó, G.G., Ulbert, I., Holderith, N., Monyer, H., Erdélyi, F., Szabó, G., Freund, T.F. & Hájos, N. (2010) Parvalbumin-containing fast-spiking basket cells generate the field potential oscillations induced by cholinergic receptor activation in the hippocampus. *The Journal of Neuroscience*, **30**, 15134-15145.

Hajós, M., Hoffmann, W.E. & Kocsis, B. (2008) Activation of cannabinoid-1 receptors disrupts sensory gating and neuronal oscillation: relevance to schizophrenia. *Biological psychiatry*, **63**, 1075-1083.

Hájos, N. & Freund, T.F. (2002) Pharmacological separation of cannabinoid sensitive receptors on hippocampal excitatory and inhibitory fibers. *Neuropharmacology*, **43**, 503-510.

Hájos, N., Katona, I., Naiem, S.S., MacKie, K., Ledent, C., Mody, I. & Freund, T.F. (2000) Cannabinoids inhibit hippocampal GABAergic transmission and network oscillations. *European Journal of Neuroscience*, **12**, 3239-3249.

Hájos, N. & Mody, I. (1997) Synaptic communication among hippocampal interneurons: properties of spontaneous IPSCs in morphologically identified cells. *The Journal of Neuroscience*, **17**, 8427-8442.

Hájos, N. & Mody, I. (2009) Establishing a physiological environment for visualized *in vitro* brain slice recordings by increasing oxygen supply and modifying aCSF content. *The Journal of Neuroscience Methods*, **183**, 107-113.

Hájos, N., Pálhalmi, J., Mann, E.O., Németh, B., Paulsen, O. & Freund, T.F. (2004) Spike timing of distinct types of GABAergic interneuron during hippocampal gamma oscillations *in vitro*. *The Journal of Neuroscience*, **24**, 9127-9137.

Hájos, N. & Paulsen, O. (2009) Network mechanisms of gamma oscillations in the CA3 region of the hippocampus. *Neural networks*, **22**, 1113-1119.

Halasy, K., Buhl, E.H., Lőrinczi, Z., Tamás, G. & Somogyi, P. (1996) Synaptic target selectivity and input of GABAergic basket and bistratified interneurons in the CA1 area of the rat hippocampus. *Hippocampus*, **6**, 306-329.

Hampson, R.E. & Deadwyler, S.A. (1998) Role of cannabinoid receptors in memory storage. *Neurobiology of disease*, **5**, 474-482.

Han, J., Kesner, P., Metna-Laurent, M., Duan, T., Xu, L., Georges, F., Koehl, M., Abrous, D.N., Mendizabal-Zubiaga, J., Grandes, P., Liu, Q., Bai, G., Wang, W., Xiong, L., Ren, W., Marsicano, G. & Zhang, X. (2012) Acute cannabinoids impair working memory through astroglial CB_1 receptor modulation of hippocampal LTD. *Cell*, **148**, 1039-1050.

Hangya, B., Borhegyi, Z., Szilágyi, N., Freund, T.F. & Varga, V. (2009) GABAergic neurons of the medial septum lead the hippocampal network during theta activity. *The Journal of Neuroscience*, **29**, 8094-8102.

Hashimoto, T., Arion, D., Unger, T., Maldonado-Aviles, J.G., Morris, H.M., Volk, D.W., Mirnics, K. & Lewis, D.A. (2008a) Alterations in GABA-related transcriptome in the dorsolateral prefrontal cortex of subjects with schizophrenia. *Molecular psychiatry*, **13**, 147-161.

Hashimoto, T., Bazmi, H.H., Mirnics, K., Wu, Q., Sampson, A.R. & Lewis, D.A. (2008b) Conserved regional patterns of GABA-related transcript expression in the neocortex of subjects with schizophrenia. *The American journal of psychiatry*, **165**, 479-489.

Hashimoto, T., Volk, D.W., Eggan, S.M., Mirnics, K., Pierri, J.N., Sun, Z., Sampson, A.R. & Lewis, D.A. (2003) Gene expression deficits in a subclass of GABA neurons in the prefrontal cortex of subjects with schizophrenia. *The Journal of Neuroscience*, **23**, 6315-6326.

Hefft, S. & Jonas, P. (2005) Asynchronous GABA release generates long-lasting inhibition at a hippocampal interneuron-principal neuron synapse. *Nature Neuroscience*, **8**, 1319-1328.

Heifets, B.D. & Castillo, P.E. (2009) Endocannabinoid signaling and long-term synaptic plasticity. *Annual review of physiology*, **71**, 283-306.

Hoffman, A.F., Riegel, A.C. & Lupica, C.R. (2003) Functional localization of cannabinoid receptors and endogenous cannabinoid production in distinct neuron populations of the hippocampus. *European Journal of Neuroscience*, **18**, 524-534.

Hofmann, M.E., Nahir, B. & Frazier, C.J. (2008) Excitatory afferents to CA3 pyramidal cells display differential sensitivity to CB_1 dependent inhibition of synaptic transmission. *Neuropharmacology*, **55**, 1140-1146.

Hölscher, C., Anwyl, R. & Rowan, M.J. (1997) Stimulation on the positive phase of hippocampal theta rhythm induces long-term potentiation that can Be depotentiated by stimulation on the negative phase in area CA1 *in vivo*. *The Journal of Neuroscience*, **17**, 6470-6477.

Hu, H., Martina, M. & Jonas, P. (2010) Dendritic mechanisms underlying rapid synaptic activation of fast-spiking hippocampal interneurons. *Science*, **327**, 52-58.

Huber, K.M., Roder, J.C. & Bear, M.F. (2001) Chemical induction of $mGluR_5$- and protein synthesis--dependent long-term depression in hippocampal area CA1. *Journal of neurophysiology*, **86**, 321-325.

Huerta, P.T. & Lisman, J.E. (1995) Bidirectional synaptic plasticity induced by a single burst during cholinergic theta oscillation in CA1 *in vitro*. *Neuron*, **15**, 1053-1063.

Inan, M., Petros, T.J. & Anderson, S.A. (2013) Losing your inhibition: linking cortical GABAergic interneurons to schizophrenia. *Neurobiology of disease*, **53**, 36-48.

Ito, M. & Kano, M. (1982) Long-lasting depression of parallel fiber-Purkinje cell transmission induced by conjunctive stimulation of parallel fibers and climbing fibers in the cerebellar cortex. *Neuroscience letters*, **33**, 253-258.

Izumi, Y. & Zorumski, C.F. (2012) NMDA receptors, $mGluR_5$, and endocannabinoids are involved in a cascade leading to hippocampal long-term depression. *Neuropsychopharmacology*, **37**, 609-617.

Jackson, M.E., Homayoun, H. & Moghaddam, B. (2004) NMDA receptor hypofunction produces concomitant firing rate potentiation and burst activity reduction in the prefrontal cortex. *PNAS*, **101**, 8467-8472.

Jarsky, T., Roxin, A., Kath, W.L. & Spruston, N. (2005) Conditional dendritic spike propagation following distal synaptic activation of hippocampal CA1 pyramidal neurons. *Nature Neuroscience*, **8**, 1667-1676.

Javitt, D.C. (1987) Negative schizophrenic symptomatology and the PCP (phencyclidine) model of schizophrenia. *The Hillside journal of clinical psychiatry*, **9**, 12-35.

Javitt, D.C. (2009) Sensory processing in schizophrenia: neither simple nor intact. *Schizophrenia bulletin*, **35**, 1059-1064.

Jenkins, S.M. & Bennett, V. (2001) Ankyrin-G coordinates assembly of the spectrin-based membrane skeleton, voltage-gated sodium channels, and L1 CAMs at Purkinje neuron initial segments. *The Journal of Cell Biology*, **155**, 739-746.

Jinno, S., Klausberger, T., Marton, L.F., Dalezios, Y., Roberts, J.D., Fuentealba, P., Bushong, E.A., Henze, D., Buzsáki, G. & Somogyi, P. (2007) Neuronal diversity in GABAergic long-range projections from the hippocampus. *The Journal of Neuroscience*, **27**, 8790-8804.

Joho, R.H., Ho, C.S. & Marks, G.A. (1999) Increased gamma- and decreased delta-oscillations in a mouse deficient for a potassium channel expressed in fast-spiking interneurons. *Journal of neurophysiology*, **82**, 1855-1864.

Jonas, P., Bischofberger, J., Fricker, D. & Miles, R. (2004) Interneuron Diversity series: Fast in, fast out--temporal and spatial signal processing in hippocampal interneurons. *Trends in neurosciences*, **27**, 30-40.

Jonas, P., Racca, C., Sakmann, B., Seeburg, P.H. & Monyer, H. (1994) Differences in Ca^{2+} permeability of AMPA-type glutamate receptor channels in neocortical neurons caused by differential GluR-B subunit expression. *Neuron*, **12**, 1281-1289.

Jung, K.M., Astarita, G., Zhu, C., Wallace, M., Mackie, K. & Piomelli, D. (2007) A key role for diacylglycerol lipase-alpha in metabotropic glutamate receptor-dependent endocannabinoid mobilization. *Molecular pharmacology*, **72**, 612-621.

Jung, K.M., Mangieri, R., Stapleton, C., Kim, J., Fegley, D., Wallace, M., Mackie, K. & Piomelli, D. (2005) Stimulation of endocannabinoid formation in brain slice cultures through activation of group I metabotropic glutamate receptors. *Molecular pharmacology*, **68**, 1196-1202.

Kamondi, A., Acsády, L., Wang, X.J. & Buzsáki, G. (1998) Theta oscillations in somata and dendrites of hippocampal pyramidal cells *in vivo*: activity-dependent phase-precession of action potentials. *Hippocampus*, **8**, 244-261.

Kaneko, T. & Fujiyama, F. (2002) Complementary distribution of vesicular glutamate transporters in the central nervous system. *Neuroscience Research*, **42**, 243-250.

Kano, M., Ohno-Shosaku, T., Hashimotodani, Y., Uchigashima, M. & Watanabe, M. (2009) Endocannabinoid-mediated control of synaptic transmission. *Physiological reviews*, **89**, 309-380.

Katona, I. & Freund, T.F. (2008) Endocannabinoid signaling as a synaptic circuit breaker in neurological disease. *Nature medicine*, **14**, 923-930.

Katona, I. & Freund, T.F. (2012) Multiple functions of endocannabinoid signaling in the brain. *Annual review of neuroscience*, **35**, 529-558.

Katona, I., Sperlágh, B., Sík, A., Kőfalvi, A., Vizi, E.S., Mackie, K. & Freund, T.F. (1999) Presynaptically located CB_1 cannabinoid receptors regulate GABA release from axon

terminals of specific hippocampal interneurons. *The Journal of Neuroscience*, **19**, 4544-4558.

Katona, I., Urbán, G.M., Wallace, M., Ledent, C., Jung, K.M., Piomelli, D., Mackie, K. & Freund, T.F. (2006) Molecular composition of the endocannabinoid system at glutamatergic synapses. *The Journal of Neuroscience*, **26**, 5628-5637.

Katsumaru, H., Kosaka, T., Heizmann, C.W. & Hama, K. (1988) Immunocytochemical study of GABAergic neurons containing the calcium-binding protein parvalbumin in the rat hippocampus. *Experimental Brain Research*, **72**, 347-362.

Katz, Y., Kath, W.L., Spruston, N. & Hasselmo, M.E. (2007) Coincidence detection of place and temporal context in a network model of spiking hippocampal neurons. *PLoS computational biology*, **3**, e234.

Kawaguchi, Y. (1995) Physiological subgroups of nonpyramidal cells with specific morphological characteristics in layer II/III of rat frontal cortex. *The Journal of Neuroscience*, **15**, 2638-2655.

Kawaguchi, Y. & Kubota, Y. (1997) GABAergic cell subtypes and their synaptic connections in rat frontal cortex. *Cerebral Cortex*, **7**, 476-486.

Kawamura, Y., Fukaya, M., Maejima, T., Yoshida, T., Miura, E., Watanabe, M., Ohno-Shosaku, T. & Kano, M. (2006) The CB_1 cannabinoid receptor is the major cannabinoid receptor at excitatory presynaptic sites in the hippocampus and cerebellum. *The Journal of Neuroscience*, **26**, 2991-3001.

Kellogg, R., Mackie, K. & Straiker, A. (2009) Cannabinoid CB_1 receptor-dependent long-term depression in autaptic excitatory neurons. *Journal of neurophysiology*, **102**, 1160-1171.

Kheirbek, M.A., Drew, L.J., Burghardt, N.S., Costantini, D.O., Tannenholz, L., Ahmari, S.E., Zeng, H., Fenton, A.A. & Hen, R. (2013) Differential control of learning and anxiety along the dorsoventral axis of the dentate gyrus. *Neuron*, **77**, 955-968.

Khirug, S., Yamada, J., Afzalov, R., Voipio, J., Khiroug, L. & Kaila, K. (2008) GABAergic depolarization of the axon initial segment in cortical principal neurons is caused by the Na-K-2Cl cotransporter NKCC1. *The Journal of Neuroscience*, **28**, 4635-4639.

Kinney, J.W., Davis, C.N., Tabarean, I., Conti, B., Bartfai, T. & Behrens, M.M. (2006) A specific role for NR2A-containing NMDA receptors in the maintenance of parvalbumin and GAD67 immunoreactivity in cultured interneurons. *The Journal of Neuroscience*, **26**, 1604-1615.

Klausberger, T. (2009) GABAergic interneurons targeting dendrites of pyramidal cells in the CA1 area of the hippocampus. *European Journal of Neuroscience*, **30**, 947-957.

Klausberger, T., Magill, P.J., Márton, L.F., Roberts, J.D., Cobden, P.M., Buzsáki, G. & Somogyi, P. (2003) Brain-state- and cell-type-specific firing of hippocampal interneurons *in vivo*. *Nature*, **421**, 844-848.

Klausberger, T., Márton, L.F., Baude, A., Roberts, J.D., Magill, P.J. & Somogyi, P. (2004) Spike timing of dendrite-targeting bistratified cells during hippocampal network oscillations *in vivo*. *Nature Neuroscience*, **7**, 41-47.

Klausberger, T., Márton, L.F., O'Neill, J., Huck, J.H., Dalezios, Y., Fuentealba, P., Suen, W.Y., Papp, E., Kaneko, T., Watanabe, M., Csicsvári, J. & Somogyi, P. (2005) Complementary roles of cholecystokinin- and parvalbumin-expressing GABAergic neurons in hippocampal network oscillations. *The Journal of Neuroscience*, **25**, 9782-9793.

Klausberger, T. & Somogyi, P. (2008) Neuronal diversity and temporal dynamics: the unity of hippocampal circuit operations. *Science*, **321**, 53-57.

Konradi, C., Yang, C.K., Zimmerman, E.I., Lohmann, K.M., Gresch, P., Pantazopoulos, H., Berretta, S. & Heckers, S. (2011) Hippocampal interneurons are abnormal in schizophrenia. *Schizophrenia research*, **131**, 165-173.

Korotkova, T., Fuchs, E.C., Ponomarenko, A., von Engelhardt, J. & Monyer, H. (2010) NMDA receptor ablation on parvalbumin-positive interneurons impairs hippocampal synchrony, spatial representations, and working memory. *Neuron*, **68**, 557-569.

Kramis, R., Vanderwolf, C.H. & Bland, B.H. (1975) Two types of hippocampal rhythmical slow activity in both the rabbit and the rat: relations to behavior and effects of atropine, diethyl ether, urethane, and pentobarbital. *Experimental neurology*, **49**, 58-85.

Krystal, J.H., Karper, L.P., Seibyl, J.P., Freeman, G.K., Delaney, R., Bremner, J.D., Heninger, G.R., Bowers, M.B., Jr. & Charney, D.S. (1994) Subanesthetic effects of the noncompetitive NMDA antagonist, ketamine, in humans. Psychotomimetic, perceptual, cognitive, and neuroendocrine responses. *Archives of general psychiatry*, **51**, 199-214.

Kuba, H., Oichi, Y. & Ohmori, H. (2010) Presynaptic activity regulates Na^+ channel distribution at the axon initial segment. *Nature*, **465**, 1075-1078.

Kubota, Y., Hatada, S., Kondo, S., Karube, F. & Kawaguchi, Y. (2007) Neocortical inhibitory terminals innervate dendritic spines targeted by thalamocortical afferents. *The Journal of Neuroscience*, **27**, 1139-1150.

Kullmann, D.M. & Lamsa, K.P. (2011) LTP and LTD in cortical GABAergic interneurons: emerging rules and roles. *Neuropharmacology*, **60**, 712-719.

Laezza, F. & Dingledine, R. (2011) Induction and expression rules of synaptic plasticity in hippocampal interneurons. *Neuropharmacology*, **60**, 720-729.

Laezza, F., Doherty, J.J. & Dingledine, R. (1999) Long-term depression in hippocampal interneurons: joint requirement for pre- and postsynaptic events. *Science*, **285**, 1411-1414.

Lafourcade, M., Elezgarai, I., Mato, S., Bakiri, Y., Grandes, P. & Manzoni, O.J. (2007) Molecular components and functions of the endocannabinoid system in mouse prefrontal cortex. *PloS one*, **2**, e709.

Lamsa, K., Heeroma, J.H. & Kullmann, D.M. (2005) Hebbian LTP in feed-forward inhibitory interneurons and the temporal fidelity of input discrimination. *Nature Neuroscience*, **8**, 916-924.

Lamsa, K.P., Heeroma, J.H., Somogyi, P., Rusakov, D.A. & Kullmann, D.M. (2007) Anti-Hebbian long-term potentiation in the hippocampal feedback inhibitory circuit. *Science*, **315**, 1262-1266.

Lamsa, K.P., Kullmann, D.M. & Woodin, M.A. (2010) Spike-timing dependent plasticity in inhibitory circuits. *Frontiers in synaptic neuroscience*, **2**, 8.

Lanté, F., Cavalier, M., Cohen-Solal, C., Guiramand, J. & Vignes, M. (2006) Developmental switch from LTD to LTP in low frequency-induced plasticity. *Hippocampus*, **16**, 981-989.

Lapointe, V., Morin, F., Ratte, S., Croce, A., Conquet, F. & Lacaille, J.C. (2004) Synapse-specific $mGluR_1$-dependent long-term potentiation in interneurones regulates mouse hippocampal inhibition. *Journal of Physiology*, **555**, 125-135.

Lapray, D., Lasztóczi, B., Lagler, M., Viney, T.J., Katona, L., Valenti, O., Hartwich, K., Borhegyi, Z., Somogyi, P. & Klausberger, T. (2012) Behavior-dependent specialization of identified hippocampal interneurons. *Nature Neuroscience*, **15**, 1265-1271.

Lasztóczi, B., Tukker, J.J., Somogyi, P. & Klausberger, T. (2011) Terminal field and firing selectivity of cholecystokinin-expressing interneurons in the hippocampal CA3 area. *The Journal of Neuroscience*, **31**, 18073-18093.

Law, A.J., Lipska, B.K., Weickert, C.S., Hyde, T.M., Straub, R.E., Hashimoto, R., Harrison, P.J., Kleinman, J.E. & Weinberger, D.R. (2006) Neuregulin 1 transcripts are differentially expressed in schizophrenia and regulated by 5' SNPs associated with the disease. *PNAS*, **103**, 6747-6752.

Le Duigou, C., Holden, T. & Kullmann, D.M. (2011) Short- and long-term depression at glutamatergic synapses on hippocampal interneurons by group I mGluR activation. *Neuropharmacology*, **60**, 748-756.

Lee, M.G., Chrobak, J.J., Sík, A., Wiley, R.G. & Buzsáki, G. (1994) Hippocampal theta activity following selective lesion of the septal cholinergic system. *Neuroscience*, **62**, 1033-1047.

Leung, L.S. (1980) Behavior-dependent evoked potentials in the hippocampal CA1 region of the rat. I. Correlation with behavior and EEG. *Brain research*, **198**, 95-117.

Leung, L.S. & Yim, C.Y. (1986) Intracellular records of theta rhythm in hippocampal CA1 cells of the rat. *Brain research*, **367**, 323-327.

Leung, L.W. & Yim, C.Y. (1991) Intrinsic membrane potential oscillations in hippocampal neurons *in vitro*. *Brain research*, **553**, 261-274.

Leweke, F.M., Giuffrida, A., Wurster, U., Emrich, H.M. & Piomelli, D. (1999) Elevated endogenous cannabinoids in schizophrenia. *Neuroreport*, **10**, 1665-1669.

Lewis, D.A., Curley, A.A., Glausier, J.R. & Volk, D.W. (2012) Cortical parvalbumin interneurons and cognitive dysfunction in schizophrenia. *Trends in neurosciences*, **35**, 57-67.

Li, X.G., Somogyi, P., Tepper, J.M. & Buzsáki, G. (1992) Axonal and dendritic arborization of an intracellularly labeled chandelier cell in the CA1 region of rat hippocampus. *Experimental Brain Research*, **90**, 519-525.

Li, X.G., Somogyi, P., Ylinen, A. & Buzsáki, G. (1994) The hippocampal CA3 network: an *in vivo* intracellular labeling study. *Journal of Comparative Neurology*, **339**, 181-208.

Lien, C.C. & Jonas, P. (2003) Kv3 potassium conductance is necessary and kinetically optimized for high-frequency action potential generation in hippocampal interneurons. *The Journal of Neuroscience*, **23**, 2058-2068.

Lisman, J.E. & Idiart, M.A. (1995) Storage of 7 +/- 2 short-term memories in oscillatory subcycles. *Science*, **267**, 1512-1515.

Lodge, D. & Anis, N.A. (1982) Effects of phencyclidine on excitatory amino acid activation of spinal interneurones in the cat. *European journal of pharmacology*, **77**, 203-204.

Lu, J.T., Li, C.Y., Zhao, J.P., Poo, M.M. & Zhang, X.H. (2007) Spike-timing-dependent plasticity of neocortical excitatory synapses on inhibitory interneurons depends on target cell type. *The Journal of Neuroscience*, **27**, 9711-9720.

Luján, R., Nusser, Z., Roberts, J.D., Shigemoto, R. & Somogyi, P. (1996) Perisynaptic location of metabotropic glutamate receptors $mGluR_1$ and $mGluR_5$ on dendrites and dendritic spines in the rat hippocampus. *European Journal of Neuroscience*, **8**, 1488-1500.

Maglóczky, Z., Acsády, L. & Freund, T.F. (1994) Principal cells are the postsynaptic targets of supramammillary afferents in the hippocampus of the rat. *Hippocampus*, **4**, 322-334.

Maier, N., Guldenagel, M., Sohl, G., Siegmund, H., Willecke, K. & Draguhn, A. (2002) Reduction of high-frequency network oscillations (ripples) and pathological network discharges in hippocampal slices from connexin 36-deficient mice. *Journal of Physiology*, **541**, 521-528.

Malenka, R.C. & Bear, M.F. (2004) LTP and LTD: an embarrassment of riches. *Neuron*, **44**, 5-21.

Malva, J.O., Silva, A.P. & Cunha, R.A. (2003) Presynaptic modulation controlling neuronal excitability and epileptogenesis: role of kainate, adenosine and neuropeptide Y receptors. *Neurochemical research*, **28**, 1501-1515.

Mann, E.O., Suckling, J.M., Hájos, N., Greenfield, S.A. & Paulsen, O. (2005) Perisomatic feedback inhibition underlies cholinergically induced fast network oscillations in the rat hippocampus *in vitro*. *Neuron*, **45**, 105-117.

Marrosu, F., Portas, C., Mascia, M.S., Casu, M.A., Fa, M., Giagheddu, M., Imperato, A. & Gessa, G.L. (1995) Microdialysis measurement of cortical and hippocampal acetylcholine release during sleep-wake cycle in freely moving cats. *Brain research*, **671**, 329-332.

Marsicano, G., Wotjak, C.T., Azad, S.C., Bisogno, T., Rammes, G., Cascio, M.G., Hermann, H., Tang, J., Hofmann, C., Zieglgansberger, W., Di Marzo, V. & Lutz, B. (2002) The endogenous cannabinoid system controls extinction of aversive memories. *Nature*, **418**, 530-534.

Massi, L., Lagler, M., Hartwich, K., Borhegyi, Z., Somogyi, P. & Klausberger, T. (2012) Temporal Dynamics of Parvalbumin-Expressing Axo-axonic and Basket Cells in the Rat Medial Prefrontal Cortex *In Vivo*. *The Journal of Neuroscience*, **32**, 16496-16502.

McBain, C.J., DiChiara, T.J. & Kauer, J.A. (1994) Activation of metabotropic glutamate receptors differentially affects two classes of hippocampal interneurons and potentiates excitatory synaptic transmission. *The Journal of Neuroscience*, **14**, 4433-4445.

McBain, C.J., Freund, T.F. & Mody, I. (1999) Glutamatergic synapses onto hippocampal interneurons: precision timing without lasting plasticity. *Trends in neurosciences*, **22**, 228-235.

McMahon, L.L. & Kauer, J.A. (1997a) Hippocampal interneurons are excited via serotonin-gated ion channels. *Journal of neurophysiology*, **78**, 2493-2502.

McMahon, L.L. & Kauer, J.A. (1997b) Hippocampal interneurons express a novel form of synaptic plasticity. *Neuron*, **18**, 295-305.

Melzer, S., Michael, M., Caputi, A., Eliava, M., Fuchs, E.C., Whittington, M.A. & Monyer, H. (2012) Long-range-projecting GABAergic neurons modulate inhibition in hippocampus and entorhinal cortex. *Science*, **335**, 1506-1510.

Meyer, A.H., Katona, I., Blatow, M., Rozov, A. & Monyer, H. (2002) *In vivo* labeling of parvalbumin-positive interneurons and analysis of electrical coupling in identified neurons. *The Journal of Neuroscience*, **22**, 7055-7064.

Miettinen, R. & Freund, T.F. (1992) Convergence and segregation of septal and median raphe inputs onto different subsets of hippocampal inhibitory interneurons. *Brain research*, **594**, 263-272.

Miles, R. (1990) Synaptic excitation of inhibitory cells by single CA3 hippocampal pyramidal cells of the guinea-pig *in vitro*. *Journal of Physiology*, **428**, 61-77.

Miles, R. & Wong, R.K. (1983) Single neurones can initiate synchronized population discharge in the hippocampus. *Nature*, **306**, 371-373.

Min, R. & Nevian, T. (2012) Astrocyte signaling controls spike timing-dependent depression at neocortical synapses. *Nature Neuroscience*, **15**, 746-753.

Minzenberg, M.J., Firl, A.J., Yoon, J.H., Gomes, G.C., Reinking, C. & Carter, C.S. (2010) Gamma oscillatory power is impaired during cognitive control independent of medication status in first-episode schizophrenia. *Neuropsychopharmacology*, **35**, 2590-2599.

Misner, D.L. & Sullivan, J.M. (1999) Mechanism of cannabinoid effects on long-term potentiation and depression in hippocampal CA1 neurons. *The Journal of Neuroscience*, **19**, 6795-6805.

Monory, K., Massa, F., Egertova, M., Eder, M., Blaudzun, H., Westenbroek, R., Kelsch, W., Jacob, W., Marsch, R., Ekker, M., Long, J., Rubenstein, J.L., Goebbels, S., Nave, K.A., During, M., Klugmann, M., Wolfel, B., Dodt, H.U., Zieglgansberger, W., Wotjak, C.T., Mackie, K., Elphick, M.R., Marsicano, G. & Lutz, B. (2006) The endocannabinoid system controls key epileptogenic circuits in the hippocampus. *Neuron*, **51**, 455-466.

Morita, K., Kalra, R., Aihara, K. & Robinson, H.P. (2008) Recurrent synaptic input and the timing of gamma-frequency-modulated firing of pyramidal cells during neocortical "UP" states. *The Journal of Neuroscience*, **28**, 1871-1881.

Morrow, B.A., Elsworth, J.D. & Roth, R.H. (2007) Repeated phencyclidine in monkeys results in loss of parvalbumin-containing axo-axonic projections in the prefrontal cortex. *Psychopharmacology*, **192**, 283-290.

Mulkey, R.M. & Malenka, R.C. (1992) Mechanisms underlying induction of homosynaptic long-term depression in area CA1 of the hippocampus. *Neuron*, **9**, 967-975.

Müller, W. & Misgeld, U. (1986) Slow cholinergic excitation of guinea pig hippocampal neurons is mediated by two muscarinic receptor subtypes. *Neuroscience letters*, **67**, 107-112.

Nádasdy, Z., Hirase, H., Czurkó, A., Csicsvári, J. & Buzsáki, G. (1999) Replay and time compression of recurring spike sequences in the hippocampus. *The Journal of Neuroscience*, **19**, 9497-9507.

Nakashiba, T., Buhl, D.L., McHugh, T.J. & Tonegawa, S. (2009) Hippocampal CA3 output is crucial for ripple-associated reactivation and consolidation of memory. *Neuron*, **62**, 781-787.

Nakazawa, K., Zsíros, V., Jiang, Z., Nakao, K., Kolata, S., Zhang, S. & Belforte, J.E. (2012) GABAergic interneuron origin of schizophrenia pathophysiology. *Neuropharmacology*, **62**, 1574-1583.

Navarrete, M. & Araque, A. (2010) Endocannabinoids potentiate synaptic transmission through stimulation of astrocytes. *Neuron*, **68**, 113-126.

Neher, E. (1998) Vesicle pools and Ca^{2+} microdomains: new tools for understanding their roles in neurotransmitter release. *Neuron*, **20**, 389-399.

Neu, A., Földy, C. & Soltész, I. (2007) Postsynaptic origin of CB_1-dependent tonic inhibition of GABA release at cholecystokinin-positive basket cell to pyramidal cell synapses in the CA1 region of the rat hippocampus. *Journal of Physiology*, **578**, 233-247.

Nevian, T. & Sakmann, B. (2006) Spine Ca^{2+} signaling in spike-timing-dependent plasticity. *The Journal of Neuroscience*, **26**, 11001-11013.

Nicoll, R.A., Kauer, J.A. & Malenka, R.C. (1988) The current excitement in long-term potentiation. *Neuron*, **1**, 97-103.

Nicoll, R.A. & Malenka, R.C. (1995) Contrasting properties of two forms of long-term potentiation in the hippocampus. *Nature*, **377**, 115-118.

Niehusmann, P., Seifert, G., Clark, K., Atas, H.C., Herpfer, I., Fiebich, B., Bischofberger, J. & Normann, C. (2010) Coincidence detection and stress modulation of spike time-dependent long-term depression in the hippocampus. *The Journal of Neuroscience*, **30**, 6225-6235.

Nissen, W., Szabó, A., Somogyi, J., Somogyi, P. & Lamsa, K.P. (2010) Cell type-specific long-term plasticity at glutamatergic synapses onto hippocampal interneurons expressing either parvalbumin or CB_1 cannabinoid receptor. *The Journal of Neuroscience*, **30**, 1337-1347.

Nosyreva, E.D. & Huber, K.M. (2005) Developmental switch in synaptic mechanisms of hippocampal metabotropic glutamate receptor-dependent long-term depression. *The Journal of Neuroscience*, **25**, 2992-3001.

Nörenberg, A., Hu, H., Vida, I., Bartos, M. & Jonas, P. (2010) Distinct nonuniform cable properties optimize rapid and efficient activation of fast-spiking GABAergic interneurons. *PNAS*, **107**, 894-899.

O'Keefe, J. & Dostrovsky, J. (1971) The hippocampus as a spatial map. Preliminary evidence from unit activity in the freely-moving rat. *Brain research*, **34**, 171-175.

O'Keefe, J. & Recce, M.L. (1993) Phase relationship between hippocampal place units and the EEG theta rhythm. *Hippocampus*, **3**, 317-330.

Ohno-Shosaku, T., Maejima, T. & Kano, M. (2001) Endogenous cannabinoids mediate retrograde signals from depolarized postsynaptic neurons to presynaptic terminals. *Neuron*, **29**, 729-738.

Ohno-Shosaku, T., Tsubokawa, H., Mizushima, I., Yoneda, N., Zimmer, A. & Kano, M. (2002) Presynaptic cannabinoid sensitivity is a major determinant of depolarization-induced retrograde suppression at hippocampal synapses. *The Journal of Neuroscience*, **22**, 3864-3872.

Oláh, S., Füle, M., Komlósi, G., Varga, C., Báldi, R., Barzó, P. & Tamás, G. (2009) Regulation of cortical microcircuits by unitary GABA-mediated volume transmission. *Nature*, **461**, 1278-1281.

Oren, I., Hájos, N. & Paulsen, O. (2010) Identification of the current generator underlying cholinergically induced gamma frequency field potential oscillations in the hippocampal CA3 region. *Journal of Physiology*, **588**, 785-797.

Oren, I., Mann, E.O., Paulsen, O. & Hájos, N. (2006) Synaptic currents in anatomically identified CA3 neurons during hippocampal gamma oscillations *in vitro*. *The Journal of Neuroscience*, **26**, 9923-9934.

Oren, I., Nissen, W., Kullmann, D.M., Somogyi, P. & Lamsa, K.P. (2009) Role of ionotropic glutamate receptors in long-term potentiation in rat hippocampal CA1 oriens-lacunosum moleculare interneurons. *The Journal of Neuroscience*, **29**, 939-950.

Oren, I. & Paulsen, O. (2010) Currents in space: understanding inhibitory field potentials. *Journal of Physiology*, **588**, 2015-2016.

Palmer, M.J., Irving, A.J., Seabrook, G.R., Jane, D.E. & Collingridge, G.L. (1997) The group I mGlu receptor agonist DHPG induces a novel form of LTD in the CA1 region of the hippocampus. *Neuropharmacology*, **36**, 1517-1532.

Panula, P., Pirvola, U., Auvinen, S. & Airaksinen, M.S. (1989) Histamine-immunoreactive nerve fibers in the rat brain. *Neuroscience*, **28**, 585-610.

Patenaude, C., Chapman, C.A., Bertrand, S., Congar, P. & Lacaille, J.C. (2003) $GABA_B$ receptor- and metabotropic glutamate receptor-dependent cooperative long-term potentiation of rat hippocampal $GABA_A$ synaptic transmission. *Journal of Physiology*, **553**, 155-167.

Pawelzik, H., Hughes, D.I. & Thomson, A.M. (2002) Physiological and morphological diversity of immunocytochemically defined parvalbumin- and cholecystokinin-positive interneurones in CA1 of the adult rat hippocampus. *Journal of Comparative Neurology*, **443**, 346-367.

Pelkey, K.A., Lavezzari, G., Racca, C., Roche, K.W. & McBain, C.J. (2005) $mGluR_7$ is a metaplastic switch controlling bidirectional plasticity of feedforward inhibition. *Neuron*, **46**, 89-102.

Péterfi, Z., Urbán, G.M., Papp, O.I., Németh, B., Monyer, H., Szabó, G., Erdélyi, F., Mackie, K., Freund, T.F., Hájos, N. & Katona, I. (2012) Endocannabinoid-mediated long-term depression of afferent excitatory synapses in hippocampal pyramidal cells and GABAergic interneurons. *The Journal of Neuroscience*, **32**, 14448-14463.

Petsche, H., Stumpf, C. & Gogolak, G. (1962) [The significance of the rabbit's septum as a relay station between the midbrain and the hippocampus. I. The control of hippocampus arousal activity by the septum cells]. *Electroencephalography and clinical neurophysiology*, **14**, 202-211.

Pierri, J.N., Chaudry, A.S., Woo, T.U. & Lewis, D.A. (1999) Alterations in chandelier neuron axon terminals in the prefrontal cortex of schizophrenic subjects. *The American journal of psychiatry*, **156**, 1709-1719.

Piet, R., Garenne, A., Farrugia, F., Le Masson, G., Marsicano, G., Chavis, P. & Manzoni, O.J. (2011) State-dependent, bidirectional modulation of neural network activity by endocannabinoids. *The Journal of Neuroscience*, **31**, 16591-16596.

Price, C.J., Cauli, B., Kovács, E.R., Kulik, A., Lambolez, B., Shigemoto, R. & Capogna, M. (2005) Neurogliaform neurons form a novel inhibitory network in the hippocampal CA1 area. *The Journal of Neuroscience*, **25**, 6775-6786.

Rácz, A., Ponomarenko, A.A., Fuchs, E.C. & Monyer, H. (2009) Augmented hippocampal ripple oscillations in mice with reduced fast excitation onto parvalbumin-positive cells. *The Journal of Neuroscience*, **29**, 2563-2568.

Rao, S.G., Williams, G.V. & Goldman-Rakic, P.S. (2000) Destruction and creation of spatial tuning by disinhibition: GABA(A) blockade of prefrontal cortical neurons engaged by working memory. *The Journal of Neuroscience*, **20**, 485-494.

Richter, K., Langnaese, K., Kreutz, M.R., Olias, G., Zhai, R., Scheich, H., Garner, C.C. & Gundelfinger, E.D. (1999) Presynaptic cytomatrix protein bassoon is localized at both excitatory and inhibitory synapses of rat brain. *Journal of Comparative Neurology*, **408**, 437-448.

Robbe, D. & Buzsáki, G. (2009) Alteration of theta timescale dynamics of hippocampal place cells by a cannabinoid is associated with memory impairment. *The Journal of Neuroscience*, **29**, 12597-12605.

Robbe, D., Kopf, M., Remaury, A., Bockaert, J. & Manzoni, O.J. (2002) Endogenous cannabinoids mediate long-term synaptic depression in the nucleus accumbens. *PNAS*, **99**, 8384-8388.

Robbe, D., Montgomery, S.M., Thome, A., Rueda-Orozco, P.E., McNaughton, B.L. & Buzsáki, G. (2006) Cannabinoids reveal importance of spike timing coordination in hippocampal function. *Nature Neuroscience*, **9**, 1526-1533.

Rodriguez-Moreno, A. & Paulsen, O. (2008) Spike timing-dependent long-term depression requires presynaptic NMDA receptors. *Nature Neuroscience*, **11**, 744-745.

Rouach, N. & Nicoll, R.A. (2003) Endocannabinoids contribute to short-term but not long-term mGluR-induced depression in the hippocampus. *European Journal of Neuroscience*, **18**, 1017-1020.

Sales-Carbonell, C., Rueda-Orozco, P.E., Soria-Gomez, E., Buzsáki, G., Marsicano, G. & Robbe, D. (2013) Striatal GABAergic and cortical glutamatergic neurons mediate contrasting effects of cannabinoids on cortical network synchrony. *PNAS*, **110**, 719-724.

Senior, T.J., Huxter, J.R., Allen, K., O'Neill, J. & Csicsvári, J. (2008) Gamma oscillatory firing reveals distinct populations of pyramidal cells in the CA1 region of the hippocampus. *The Journal of Neuroscience*, **28**, 2274-2286.

Sík, A., Penttonen, M., Ylinen, A. & Buzsáki, G. (1995) Hippocampal CA1 interneurons: an *in vivo* intracellular labeling study. *The Journal of Neuroscience*, **15**, 6651-6665.

Sík, A., Tamamaki, N. & Freund, T.F. (1993) Complete axon arborization of a single CA3 pyramidal cell in the rat hippocampus, and its relationship with postsynaptic parvalbumin-containing interneurons. *European Journal of Neuroscience*, **5**, 1719-1728.

Sík, A., Ylinen, A., Penttonen, M. & Buzsáki, G. (1994) Inhibitory CA1-CA3-hilar region feedback in the hippocampus. *Science*, **265**, 1722-1724.

Singer, W. (1993) Synchronization of cortical activity and its putative role in information processing and learning. *Annual review of physiology*, **55**, 349-374.

Sjostrom, P.J., Turrigiano, G.G. & Nelson, S.B. (2003) Neocortical LTD via coincident activation of presynaptic NMDA and cannabinoid receptors. *Neuron*, **39**, 641-654.

Skaggs, W.E. & McNaughton, B.L. (1996) Replay of neuronal firing sequences in rat hippocampus during sleep following spatial experience. *Science*, **271**, 1870-1873.

Skaggs, W.E., McNaughton, B.L., Wilson, M.A. & Barnes, C.A. (1996) Theta phase precession in hippocampal neuronal populations and the compression of temporal sequences. *Hippocampus*, **6**, 149-172.

Sohal, V.S., Zhang, F., Yizhar, O. & Deisseroth, K. (2009) Parvalbumin neurons and gamma rhythms enhance cortical circuit performance. *Nature*, **459**, 698-702.

Somogyi, P. (1977) A specific 'axo-axonal' interneuron in the visual cortex of the rat. *Brain research*, **136**, 345-350.

Somogyi, P., Kisvárday, Z.F., Martin, K.A. & Whitteridge, D. (1983) Synaptic connections of morphologically identified and physiologically characterized large basket cells in the striate cortex of cat. *Neuroscience*, **10**, 261-294.

Soussi, R., Zhang, N., Tahtakran, S., Houser, C.R. & Esclapez, M. (2010) Heterogeneity of the supramammillary-hippocampal pathways: evidence for a unique GABAergic neurotransmitter phenotype and regional differences. *European Journal of Neuroscience*, **32**, 771-785.

Stewart, M. & Fox, S.E. (1990) Do septal neurons pace the hippocampal theta rhythm? *Trends in neurosciences*, **13**, 163-168.

Strata, F. (1998) Intrinsic oscillations in CA3 hippocampal pyramids: physiological relevance to theta rhythm generation. *Hippocampus*, **8**, 666-679.

Suzuki, Y., Jodo, E., Takeuchi, S., Niwa, S. & Kayama, Y. (2002) Acute administration of phencyclidine induces tonic activation of medial prefrontal cortex neurons in freely moving rats. *Neuroscience*, **114**, 769-779.

Szabadics, J., Varga, C., Molnár, G., Oláh, S., Barzó, P. & Tamás, G. (2006) Excitatory effect of GABAergic axo-axonic cells in cortical microcircuits. *Science*, **311**, 233-235.

Szabó, G.G., Holderith, N., Gulyás, A.I., Freund, T.F. & Hájos, N. (2010) Distinct synaptic properties of perisomatic inhibitory cell types and their different modulation by cholinergic receptor activation in the CA3 region of the mouse hippocampus. *European Journal of Neuroscience*, **31**, 2234-2246.

Tamás, G., Buhl, E.H., Lőrincz, A. & Somogyi, P. (2000) Proximally targeted GABAergic synapses and gap junctions synchronize cortical interneurons. *Nature Neuroscience*, **3**, 366-371.

Tamás, G., Lőrincz, A., Simon, A. & Szabadics, J. (2003) Identified sources and targets of slow inhibition in the neocortex. *Science*, **299**, 1902-1905.

Tamminga, C.A. (1998) Schizophrenia and glutamatergic transmission. *Critical reviews in neurobiology*, **12**, 21-36.

Tanimura, A., Yamazaki, M., Hashimotodani, Y., Uchigashima, M., Kawata, S., Abe, M., Kita, Y., Hashimoto, K., Shimizu, T., Watanabe, M., Sakimura, K. & Kano, M. (2010) The endocannabinoid 2-arachidonoylglycerol produced by diacylglycerol lipase alpha mediates retrograde suppression of synaptic transmission. *Neuron*, **65**, 320-327.

tom Dieck, S., Sanmarti-Vila, L., Langnaese, K., Richter, K., Kindler, S., Soyke, A., Wex, H., Smalla, K.H., Kampf, U., Franzer, J.T., Stumm, M., Garner, C.C. & Gundelfinger, E.D. (1998) Bassoon, a novel zinc-finger CAG/glutamine-repeat protein selectively localized at the active zone of presynaptic nerve terminals. *The Journal of Cell Biology*, **142**, 499-509.

Topolnik, L., Azzi, M., Morin, F., Kougioumoutzakis, A. & Lacaille, J.C. (2006) $mGluR_{1/5}$ subtype-specific calcium signalling and induction of long-term potentiation in rat hippocampal oriens/alveus interneurones. *Journal of Physiology*, **575**, 115-131.

Tóth, K., Borhegyi, Z. & Freund, T.F. (1993) Postsynaptic targets of GABAergic hippocampal neurons in the medial septum-diagonal band of broca complex. *The Journal of Neuroscience*, **13**, 3712-3724.

Tóth, K. & Freund, T.F. (1992) Calbindin D28k-containing nonpyramidal cells in the rat hippocampus: their immunoreactivity for GABA and projection to the medial septum. *Neuroscience*, **49**, 793-805.

Traub, R.D., Bibbig, A., Fisahn, A., LeBeau, F.E., Whittington, M.A. & Buhl, E.H. (2000) A model of gamma-frequency network oscillations induced in the rat CA3 region by carbachol *in vitro*. *European Journal of Neuroscience*, **12**, 4093-4106.

Traub, R.D., Whittington, M.A., Colling, S.B., Buzsáki, G. & Jefferys, J.G. (1996) Analysis of gamma rhythms in the rat hippocampus *in vitro* and *in vivo*. *Journal of Physiology*, **493 (Pt 2)**, 471-484.

Tukker, J.J., Fuentealba, P., Hartwich, K., Somogyi, P. & Klausberger, T. (2007) Cell type-specific tuning of hippocampal interneuron firing during gamma oscillations *in vivo*. *The Journal of Neuroscience*, **27**, 8184-8189.

Tukker, J.J., Lasztóczi, B., Katona, L., Roberts, J.D., Pissadaki, E.K., Dalezios, Y., Márton, L., Zhang, L., Klausberger, T. & Somogyi, P. (2013) Distinct Dendritic Arborization and *In Vivo* Firing Patterns of Parvalbumin-Expressing Basket Cells in the Hippocampal Area CA3. *The Journal of Neuroscience*, **33**, 6809-6825.

Uhlhaas, P.J. & Singer, W. (2010) Abnormal neural oscillations and synchrony in schizophrenia. *Nature reviews. Neuroscience*, **11**, 100-113.

Vanderwolf, C.H. (1969) Hippocampal electrical activity and voluntary movement in the rat. *Electroencephalography and clinical neurophysiology*, **26**, 407-418.

Varga, C., Golshani, P. & Soltész, I. (2012) Frequency-invariant temporal ordering of interneuronal discharges during hippocampal oscillations in awake mice. *PNAS*, **109**, E2726-2734.

Varga, V., Losonczy, A., Zemelman, B.V., Borhegyi, Z., Nyíri, G., Domonkos, A., Hangya, B., Holderith, N., Magee, J.C. & Freund, T.F. (2009) Fast synaptic subcortical control of hippocampal circuits. *Science*, **326**, 449-453.

Verheugen, J.A., Fricker, D. & Miles, R. (1999) Noninvasive measurements of the membrane potential and GABAergic action in hippocampal interneurons. *The Journal of Neuroscience*, **19**, 2546-2555.

von der Malsburg, C. (1995) Binding in models of perception and brain function. *Current opinion in neurobiology*, **5**, 520-526.

Vreugdenhil, M., Jefferys, J.G., Celio, M.R. & Schwaller, B. (2003) Parvalbumin-deficiency facilitates repetitive IPSCs and gamma oscillations in the hippocampus. *Journal of neurophysiology*, **89**, 1414-1422.

Wang, H.X. & Gao, W.J. (2012) Prolonged exposure to NMDAR antagonist induces cell-type specific changes of glutamatergic receptors in rat prefrontal cortex. *Neuropharmacology*, **62**, 1808-1822.

Wang, X.J. & Buzsáki, G. (1996) Gamma oscillation by synaptic inhibition in a hippocampal interneuronal network model. *The Journal of Neuroscience*, **16**, 6402-6413.

Whittington, M.A., Traub, R.D. & Jefferys, J.G. (1995) Synchronized oscillations in interneuron networks driven by metabotropic glutamate receptor activation. *Nature*, **373**, 612-615.

Wilson, R.I. & Nicoll, R.A. (2001) Endogenous cannabinoids mediate retrograde signalling at hippocampal synapses. *Nature*, **410**, 588-592.

Winson, J. (1974) Patterns of hippocampal theta rhythm in the freely moving rat. *Electroencephalography and clinical neurophysiology*, **36**, 291-301.

Woo, T.U., Whitehead, R.E., Melchitzky, D.S. & Lewis, D.A. (1998) A subclass of prefrontal gamma-aminobutyric acid axon terminals are selectively altered in schizophrenia. *PNAS*, **95**, 5341-5346.

Woodruff, A., Xu, Q., Anderson, S.A. & Yuste, R. (2009) Depolarizing effect of neocortical chandelier neurons. *Frontiers in Neural Circuits*, **3**, 15.

Woodruff, A.R., McGarry, L.M., Vogels, T.P., Inan, M., Anderson, S.A. & Yuste, R. (2011) State-dependent function of neocortical chandelier cells. *The Journal of Neuroscience*, **31**, 17872-17886.

Wouterlood, F.G., Saldana, E. & Witter, M.P. (1990) Projection from the nucleus reuniens thalami to the hippocampal region: light and electron microscopic tracing study in the rat with the anterograde tracer Phaseolus vulgaris-leucoagglutinin. *Journal of Comparative Neurology*, **296**, 179-203.

Wulff, P., Ponomarenko, A.A., Bartos, M., Korotkova, T.M., Fuchs, E.C., Bahner, F., Both, M., Tort, A.B., Kopell, N.J., Wisden, W. & Monyer, H. (2009) Hippocampal theta rhythm and its coupling with gamma oscillations require fast inhibition onto parvalbumin-positive interneurons. *PNAS*, **106**, 3561-3566.

Xu, J.Y., Chen, R., Zhang, J. & Chen, C. (2010) Endocannabinoids differentially modulate synaptic plasticity in rat hippocampal CA1 pyramidal neurons. *PloS one*, **5**, e10306.

Xu, X. & Callaway, E.M. (2009) Laminar specificity of functional input to distinct types of inhibitory cortical neurons. *The Journal of Neuroscience*, **29**, 70-85.

Yasuda, H., Huang, Y. & Tsumoto, T. (2008) Regulation of excitability and plasticity by endocannabinoids and PKA in developing hippocampus. *PNAS*, **105**, 3106-3111.

Ylinen, A., Bragin, A., Nádasdy, Z., Jandó, G., Szabó, I., Sík, A. & Buzsáki, G. (1995) Sharp wave-associated high-frequency oscillation (200 Hz) in the intact hippocampus: network and intracellular mechanisms. *The Journal of Neuroscience*, **15**, 30-46.

Yoshida, T., Fukaya, M., Uchigashima, M., Miura, E., Kamiya, H., Kano, M. & Watanabe, M. (2006) Localization of diacylglycerol lipase-alpha around postsynaptic spine suggests close proximity between production site of an endocannabinoid, 2-arachidonoyl-glycerol, and presynaptic cannabinoid CB_1 receptor. *The Journal of Neuroscience*, **26**, 4740-4751.

Zemankovics, R., Káli, S., Paulsen, O., Freund, T.F. & Hájos, N. (2010) Differences in subthreshold resonance of hippocampal pyramidal cells and interneurons: the role of h-current and passive membrane characteristics. *Journal of Physiology*, **588**, 2109-2132.

Zhu, Y. & Zhu, J.J. (2004) Rapid arrival and integration of ascending sensory information in layer 1 nonpyramidal neurons and tuft dendrites of layer 5 pyramidal neurons of the neocortex. *The Journal of Neuroscience*, **24**, 1272-1279.

Zimmer, A., Zimmer, A.M., Hohmann, A.G., Herkenham, M. & Bonner, T.I. (1999) Increased mortality, hypoactivity, and hypoalgesia in cannabinoid CB_1 receptor knockout mice. *PNAS*, **96**, 5780-5785.

LIST OF PUBLICATIONS

Publications related to the dissertation

Papp OI, Karlócai MR, Tóth EI, Freund TF and Hájos N. 2013. Different input and output properties characterize parvalbumin-positive basket and axo-axonic cells in the hippocampal CA3 subfield. Hippocampus

Holderith N, Németh B, **Papp OI**, Veres JM, Nagy GA, Hájos N. 2011. Cannabinoids attenuate hippocampal gamma oscillations by suppressing excitatory synaptic input onto CA3 pyramidal neurons and fast spiking basket cells. Journal of Physiology 589:4921-34.

Péterfi Z, Urbán GM, **Papp OI**, Németh B, Monyer H, Szabó G, Erdélyi F, Mackie K, Freund TF, Hájos N and Katona I. 2012. Endocannabinoid-mediated long-term depression of afferent excitatory synapses in hippocampal pyramidal cells and GABAergic interneurons. The Journal of Neuroscience 32:14448-63.

Other publications

Hájos N, Holderith N, Németh B, **Papp OI**, Szabó GG, Zemankovics R, Freund TF, Haller J. The effects of an Echinacea preparation on synaptic transmission and the firing properties of CA1 pyramidal cells in the hippocampus. Phytotherapy Research 2012 Mar; 26 (3):354-62.

ACKNOWLEDGEMENTS

I wish to thank my supervisor, Dr. Norbert Hájos for the excellent education, guidance and encouragement during my PhD years. I feel very lucky to have such strict, reliable and precise boss possessing a huge amount of knowledge and conceptions.

I would like to thank to Prof. Tamás Freund the possibility to work in the Institute of Experimental Medicine and his continuous support during my PhD years.

I owe my deepest gratitude to Judit Veres, Dr. Noémi Holderith and Dr. István Katona, who spent their time to read the thesis and provided advices to improve the quality of my artwork. For these people, I would like to thank the lot of stimulating discussions spiced with their enthusiasm for science, which inspired me very much.

I am grateful to Dr. Szabolcs Káli and Dr. Attila Gulyás for analysis programs and helpful discussions.

I express my gratitude to present and former members of the Laboratory of Network Neurophysiology for their everyday support in my work. Special thanks for Dr. Rita Zemankovics, Dr. Gergely Szabó, Dr. Boglárka Barsy, Judit Veres and Zsolt Kohus for the inspiring discussions and the joyful atmosphere we shared in the lab.

I am very grateful to Erzsébet Gregori for her excellent technical assistance.

I would like to thank my family and friends for their support during all times.